The FhaB Prodomain of *Bordetella* Affects the Biogenesis of Filamentous Hemagglutinin, Influencing *Bordetella* Virulence

Christopher Robert Noël

A dissertation submitted to the faculty of the University of North Carolina at Chapel Hill in partial fulfillment of the requirements for the degree of Doctor of Philosophy in the Department of Microbiology and Immunology.

Chapel Hill
2012

Approved by:

Peggy A. Cotter, Ph.D.

Edward J. Collins, Ph.D.

Miriam Braunstein, Ph.D.

Thomas H. Kawula, Ph.D.

Anthony R. Richardson, Ph.D.

Abstract

CHRISTOPHER ROBERT NOËL: The FhaB Prodomain of *Bordetella* Affects the Biogenesis of Filamentous Hemagglutinin, Influencing *Bordetella* Virulence
(Under the direction of Peggy Ann Cotter, Ph.D.)

Two-partner secretion (TPS) systems use β-barrel proteins of the Omp85-TpsB superfamily to transport large exoproteins across the outer membranes of Gram-negative bacteria. The *Bordetella* FHA/FhaC proteins are prototypical of TPS systems in which the exoprotein contains a large C-terminal prodomain that is removed during translocation. Although it is known that the FhaB prodomain is required for FHA function *in vivo*, its role in FHA maturation has remained mysterious. We show here that the FhaB prodomain is required for the extracellularly located mature C-terminal domain (MCD) of FHA to achieve its proper conformation. We show that the C-terminus of the prodomain is retained intracellularly and that sequences within the N-terminus of the prodomain are required for this intracellular localization. We also identify the MCD and prodomain N-terminus (PNT) as determinants of mature FHA release efficiency. Finally, we characterize subdomains at the C-terminus of the prodomain and their effects on FHA biogenesis and *Bordetella* virulence. Our data support a model in which the intracellularly located prodomain affects the final conformation of the extracellularly located MCD.

To my mother and father, without whom I cannot fathom having reached this point. Your love, encouragement and sacrifice have shaped me as a scientist and a person. Thank you.

Acknowledgments

The following work is the summation of years of work. This journey has had its triumphs and struggles, both personal and professional. Through it all, though, I have benefitted from a strong academic network without which this work would not be possible. First and foremost, I would like to thank my advisor, Dr. Peggy Cotter. Thank you for inviting me into your lab and your life. I quickly realized just how important the FHA project is to you and I am honored to have been trusted with such a significant portion of it. I would additionally like to thank the Department of Microbiology and Immunology, from my dissertation committee to the administrative staff to my post-doctoral and graduate friends. Ours is a rich scientific community and I am gratefully to have been a part of it. Finally, I would like to thank Dr. Javin Oza, who is not only a source of scientific inspiration and guidance, but is also my best friend.

Copyright Permission

Individual Contributions

The experiments shown in Figure 8 were performed by Dr. Joseph Mazar. The experiment shown in Figure 9 was performed by Dr. Jessica A. Sexton, Dr. Joseph Mazar, and myself. The experiments shown in Figures 13, 14, and 16 were performed by Dr. Jeffrey A. Melvin. The experiments shown in Figures 18, 19, 25, 26 and 27 were performed by Dr. Jeffrey A. Melvin and myself. The experiments shown in Figures 21 and 22 were performed by Kurtis Host and Dr. Jeffrey A. Melvin. Histology was provided by Histology Core Facility in the UNC School of Medicine. Mircroscopy is courtesy of Dr. William E. Goldman.

Table of Contents

List of Tables

Table

List of Figures

Figure

Chapter I – Introduction

Type 5 Secretion Systems of Gram-negative bacteria

Protein secretion – the trafficking of protein from the cytoplasm of the cell to the cell surface – is ubiquitous to all forms of life (Yen et al., 2002; Henderson et al., 2004; Albers et al., 2006; Scott and Barnett, 2006; Braakman and Bulleid, 2011). Gram-negative bacteria have evolved numerous methods to secrete polypeptides. One of these methods, the Type 5 Secretion System (T5SS), is used to secrete particularly large proteins. The Type 5 secreted exoproteins, many of which are virulence factors, can function as adhesins, cytolysins, proteases, or contact-dependent inhibitors of growth (Cotter et al., 1998; Aoki et al., 2005; Hertle, 2005; St Geme and Yeo, 2009). The T5SS also stands out for its mechanistic simplicity, seemingly requiring only a small set of proteins (two to three) for secretion (Henderson et al., 2004; Jacob-Dubuisson et al., 2004; Leo et al., 2012). Based on specific features of the various secretion systems encompassed, T5SS can be divided into different families of secretion pathways that likely employ conserved mechanics to secrete protein. These families consist of classical autotransporters, trimeric autotransporters, intimins/invasins, and two-partner secretion (Figure 1).

Figure 1

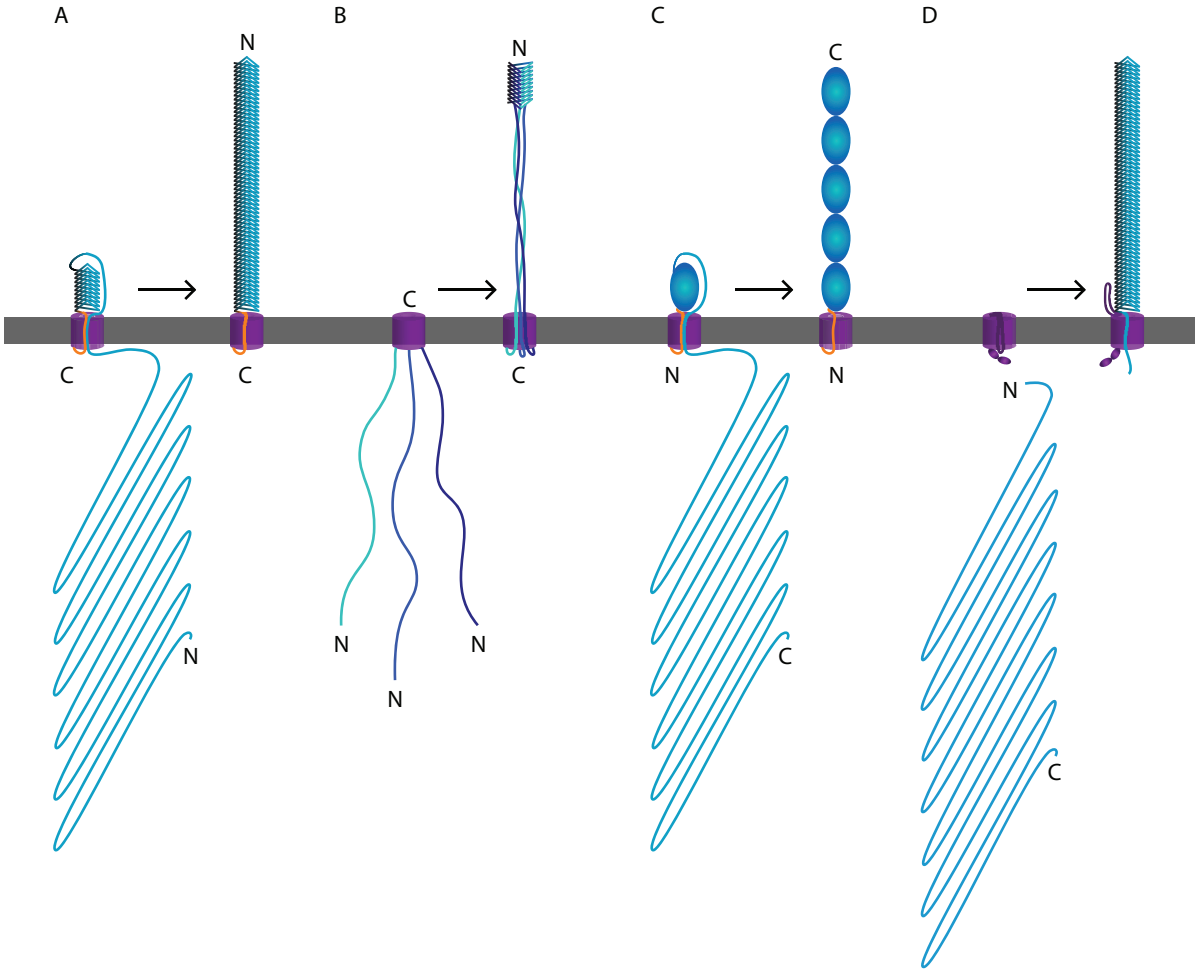

The T5SS consists of four families

A. Classical autotransporters (ATs). ATs use a C-terminal transporter domain (purple) and a central autochaperone (orange) to secrete an N-terminal passenger domain (blue).
B. Trimeric autotransporters (TATs). TATs use a homo-trimeric transporter domain (purple) to secrete three passenger domains (shades of blue) to the extracellular space, where they homo-trimerize.
C. Intimins/Invasins. Proteins of this family use an N-terminal transporter domain (purple) and a central autochaperone (orange) to secrete a C-terminal passenger domain (blue).
D. Two-partner secretion (TPS). TPS systems use a TpsB transporter protein (purple) to secrete a TpsA protein (blue). Topology varies within TPS and, therefore, is not labeled in the secreted form.

N-terminal extensions of signal peptides in T5SS

A unique characteristic of some T5SS proteins is the presence of N-terminal extensions on their signal peptides (Lambert-Buisine et al., 1998; Sijbrandi et al., 2003; Chevalier et al., 2004; Szabady et al., 2005; Desvaux et al., 2007; Hiss and Schneider, 2009). Although N-terminal extensions are broadly represented across a variety of T5SS proteins, the function of these extensions remains unknown. Sijbrani *et al.* reported that an autotransporter containing an N-terminal extension is targeted to the general secretory system (Sec) in a co-translational, signal recognition particle-dependent manner, but they did not demonstrate that the N-terminal extension specifically plays any role in this targeting (Sijbrandi et al., 2003). Conversely, work by Chevalier *et al.* and Desvaux *et al.* suggests that the N-terminal extension directs post-translational, SecAB-dependent targeting to the SecYEG complex (Chevalier et al., 2004; Desvaux et al., 2007). Their separate works also indicate that the N-terminal extension delays translocation across the inner membrane by Sec. Szabady *et al.* showed that N-terminal extensions may act *in cis* post-translocationally to affect the folding of the polypeptides to which they are attached (Szabady et al., 2005)**.** To summarize, N-terminal extensions do not appear to direct co- versus post-translational secretion, but may rather be involved in regulating the rate and dynamics of secretion. This hypothesis of secretion regulation is particularly attractive as the theme of secretion regulation is a common one throughout this dissertation.

Classical Autotransporters

Classical autotransporters (ATs) are translated as a single polypeptide. They have an N-terminal signal peptide that, in some proteins, contains an N-terminal extension (Sijbrandi et al., 2003; Szabady et al., 2005; Desvaux et al., 2007; Hiss and Schneider, 2009). C-terminal to the signal peptide is the AT passenger domain, which ultimately adopts a β-helical fold and bears the functional domain of the AT (Emsley et al., 1996; Dautin and Bernstein, 2007; Khan et al., 2011; van Ulsen, 2011; Leyton et al., 2012). The C-terminus of the AT folds into an integral outer membrane β-barrel that is used to translocate the passenger domain into the extracellular space. An autochaperone domain and α-helical linker connect the passenger domain to the β-barrel domain and have been implicated in nucleating β-helical folding of the passenger domain in the extracellular space (Oliver et al., 2003; Jacob-Dubuisson et al., 2004; Ieva et al., 2008; Peterson et al., 2010; Leyton et al., 2012). An attractive hypothesis is that as the C-terminal β-helical portion of the passenger domain folds, it serves as a Brownian ratchet that drives secretion of N-terminal sequences of the passenger domain.

One of the outstanding challenges of AT research is to fully understand the mechanics of passenger domain secretion. Two models exist to explain how the passenger domain transits from the periplasm to the extracellular space. One states that the passenger domain transits as a hairpin through the pore of the β-barrel domain, with translocation proceeding in a C- to N-terminal manner (Junker et al.,

2006; Dautin and Bernstein, 2007; Leyton et al., 2012). Kinetic studies indicate that the C-terminal portion of the passenger domain reaches the extracellular space first and provides the energetics of extracellular folding of the upstream passenger domain (Junker et al., 2009; Renn et al., 2012).

A second model of AT secretion states that AT proteins are not truly self-sufficient for extracellular localization, but rather that they require the assistance of the Bam complex to translocate the passenger domain across the outer membrane. According to this model, the passenger domain does not transit through the β-barrel domain pore, but associates with the Bam complex in the outer membrane (Skillman et al., 2005; Dautin and Bernstein, 2007; Ieva and Bernstein, 2009; Leyton et al., 2012). This model postulates that upon association with the Bam complex, the Bam complex 'flips' a partially folded passenger domain across the outer membrane, where it subsequently folds into a β-helix. Indeed, the *E. coli* AT has been shown to complex with BamA of the Bam complex (Ieva and Bernstein, 2009).

These two models are not mutually exclusive, though. It is feasible that ATs are translocated to the extracellular space (either through the β-domain pore or the Bam complex) in a C- to N-terminal vectorial manner that is dependent on the activity of the Bam complex – a model that has recently gained traction (Peterson et al., 2010). Once AT passenger domains are surface exposed they perform a variety of functions, serving in adhesion, proteolysis, motility, enterotoxicity, immune evasion, or lipolysis (Henderson et al., 2004; Klemm et al., 2006).

Trimeric Autotransporters

Trimeric autotransporters (TATs), so named due to their homo-trimerization in the outer membrane, are another family of T5SS. TATs begin with an N-terminal signal peptide that sometimes contains an N-terminal extension (Leo et al., 2012), which is followed by the passenger domain. As in classical ATs, the passenger domain contains the functional and structural portion of the TAT (Cotter et al., 2005; Łyskowski et al., 2011; Leo et al., 2012). Unlike classical ATs, however, the passenger domain of an individual TAT polypeptide contains only one-third of the fully functional passenger domain and the passenger domains of three polypeptides co-localize as a homo-trimer at the cell surface, assembling into a coiled coil to establish an elongated shaft with an N-terminal functional domain (Łyskowski et al., 2011; Leo et al., 2012). The C-terminal domain of TAT polypeptides is the β-barrel – specifically one third of the final barrel. Like the passenger domain, the individual TAT proteins' β-barrel domains trimerize to assembly a complete integral outer membrane β-barrel (Cotter et al., 2005; Leo et al., 2012). It is via this homo-trimeric β-barrel that the three passenger domains are thought to reach the cell surface, although it is not known whether they translocate across the outer membrane concurrently or individually. As with classical ATs, there is evidence that the Bam complex is involved in TAT passenger domain secretion (Lehr et al., 2010). Once folded on the cell surface, all TATs that have been studied so far appear to function as adhesins (Cotter et al., 2005; Łyskowski et al., 2011).

Intimins and Invasins

A third class of T5SS is intimins/invasins. Intimin is used by enterpathogenic *E. coli* and enterohemorrhagic *E. coli* to bind a translocated intimin receptor (Tir) that is delivered to host cells by the bacterial Type 3 Secretion System (Nougayrède et al., 2003; Niemann et al., 2004; Leo et al., 2012). Invasin is used by *Y. pseduotuberculosis* and *Y. enterocolitica* to bind integrins of host cells (Isberg and Barnes, 2001; Niemann et al., 2004; Leo et al., 2012). Consistent with classical ATs, secretion of intimins/invasins has been demonstrated to require periplasmic chaperones and the Bam complex (Bodelón et al., 2009). The standout feature of these proteins is their domain organization. While classical and trimeric ATs have N-terminal passenger domains and a C-terminal β-barrel domain, intimins/invasins have an N-terminal β-barrel domain and a C-terminal passenger domain. This results in a C-terminus that is distal from the cell surface (Leong et al., 1990; Batchelor et al., 2000), having likely crossed the outer membrane through the β-barrel domain as a hairpin that folds in an N- to C-terminal order (Adams et al., 2005; Tsai et al., 2010). Furthermore, intimins/invasins are distinct from ATs in that their extracellular shaft is composed of a series of immunoglobulin-like domains, rather than a β-helix (Hamburger et al., 1999; Kelly et al., 1999; Niemann et al., 2004). Proteins of the intimin/invasin family of T5SS are commonly thought to be adhesins – understandable since their namesake proteins function in adherence. BipA of *Bordetella*, however, also belongs to the intimin/invasin family, but does not

appear to function in adherence *in vitro* or persistence *in vivo* (Stockbauer et al., 2001), suggesting that intimin/invasin-like proteins may have additional functions.

Overview of Two-Partner Secretion

In the case of the Two-Partner Secretion (TPS) pathway, two proteins are involved in surface localization, generically referred to as TpsA and TpsB proteins (Jacob-Dubuisson et al., 2004; Newman and Stathopoulos, 2004; Mazar and Cotter, 2007). TpsA proteins most closely parallel the passenger domains of ATs. They have an N-terminal signal peptide that may or may not include an N-terminal extension (Chevalier et al., 2004). C-terminal to the signal peptide is the "Two-Partner Secretion domain" (TPS domain), a hallmark feature of TpsA proteins that is involved in translocation of the TpsA protein across the outer membrane (Jacob-Dubuisson et al., 2004). Beyond the TPS domain, TpsA polypeptide content varies, however structure prediction programs suggest a great deal of β-helical structure (Makhov et al., 1994; Kajava et al., 2001; Clantin et al., 2004). The second protein involved in TPS, the TpsB protein, is an integral outer membrane β-barrel transporter, reminiscent of the C-terminal β-domain of ATs (Jacob-Dubuisson et al., 2004; Mazar and Cotter, 2007). The TpsB protein is required to translocate the TpsA protein across the outer membrane. Once it emerges into the extracellular space, the TPS domain of the TpsA protein begins to fold into a β-helix (Clantin et al., 2004; Jacob-Dubuisson et al., 2004), and in doing so is thought to nucleate further β-helical folding of downstream TpsA polypeptide as translocation proceeds. Upon

secretion, TpsA proteins can serve as adhesins, cytolysins, regulators of host response, or contact-dependent growth inhibitors (St Geme et al., 1993; Cotter et al., 1998; Aoki et al., 2005; Hertle, 2005; Henderson et al., 2012).

TpsB proteins

The TPS pathways employ an integral outer membrane protein to secrete cognate TpsA proteins. The translocator proteins, generically referred to as TpsB proteins, belong to the Omp85 superfamily (Genevrois et al., 2003; Voulhoux et al., 2003; Gentle et al., 2004; Voulhoux and Tommassen, 2004; Gentle et al., 2005; Werner and Misra, 2005). Present in mitochondria, chloroplasts and Gram-negative bacteria, Omp85-like proteins are the most widely distributed class of outer membrane proteins across nature (Yen et al., 2002). Proteins belonging to the Omp85 superfamily can have between one to five N-terminal polypeptide transport associated (POTRA) domains. These domains typically consist of a conserved βααββ secondary structure arranged into a globular conformation, despite limited conservation of amino acids sequences, even amongst POTRA domains within the same protein (Sanchez-Pulido et al., 2003; Clantin et al., 2007; Kim et al., 2007).

TpsB proteins contain an N-terminal signal peptide, which is followed by two POTRA domains. POTRA domains of TpsB proteins are periplasmic and are required for translocation of TpsA proteins across the outer membrane (Delattre et al., 2011). The current model postulates that they serve as the first point of contact

between TpsA and TpsB proteins and initiate secretion of the TpsA protein (Hodak et al., 2006; Mazar and Cotter, 2007; Delattre et al., 2011). Following the POTRA domains is the ~300 aa β-barrel domain (Surana et al., 2006; Clantin et al., 2007; Méli et al., 2009). Topological studies of a handful of β-barrel domains suggest that TpsB proteins vary widely in their structure (Könninger et al., 1999; Guedin et al., 2000; Surana et al., 2006). The crystal structure of FhaC, a TpsB protein, from *B. pertussis* has been solved (Clantin et al., 2007) and potentially reveals a great deal about TpsB proteins as a whole. The FhaC β-barrel consists of 16 anti-parallel β-strands with both the N- and C- termini facing into the periplasm (Figure 2). The β-strands are connected by a series of short periplasmic turns and longer extracellular loops. Loop 6 (L6) occupies the FhaC pore in the crystal structure with the tip of the loop reaching the periplasm. The tip of the loop contains a VRGY motif that is conserved throughout the Omp85 superfamily (Gentle et al., 2005; Moslavac et al., 2005; Clantin et al., 2007; Delattre et al., 2010). Studies of *B. pertussis* FhaC in *E. coli* indicate that this motif is required for secretion of a polypeptide corresponding to the N-terminal 80 kDa of FhaB (named FHA44) at a step of the secretion subsequent to interaction between the TPS domain and POTRA domain (Delattre et al., 2010). FhaC additionally contains an α-helix (H1) N-terminal to the POTRA domains that occupies the FhaC pore alongside L6 (Clantin et al., 2007). The function of H1 is unknown, however its removal from FhaC does not affect secretion of FHA44 by FhaC (Guedin et al., 2000; Méli et al., 2006). This α-helix is predicted to occur in some additional, but not all, TpsB proteins (Méli et al., 2009).

Figure 2

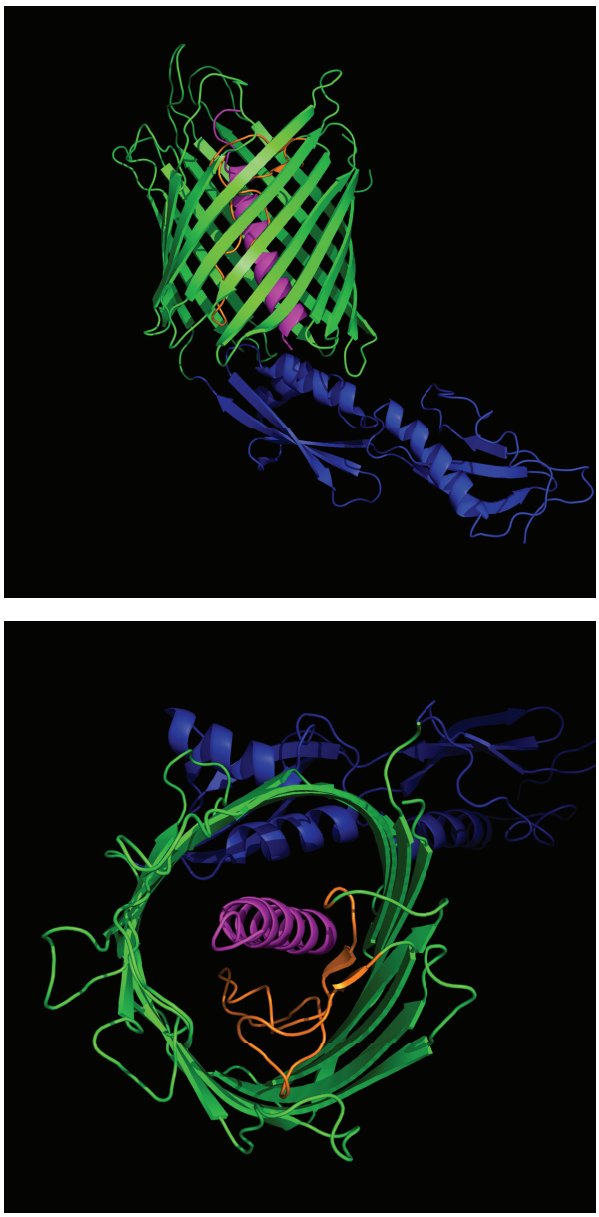

Structure of FhaC

At the top is a side view of the ribbon strucute of FhaC. Helix 1 (magenta) is shown occupying the FhaC pore. POTRA domains (blue) face into the *Bordetella* periplasm. The FhaC β-barrel (green) is integrated into the *Bordetella* outer membrane. Loop 6 of FhaC (orange) co-occupies the FhaC pore. At the bottom is an overhead view of the ribbon structure of FhaC, included to better show helix 1 and loop 6 occupying the FhaC pore. Images generated in PyMOL.

Phylogentic categorization of TPS systems into subfamilies

Exoproteins and transporters belonging to the TPS family can be categorized into subfamilies based on multiple criteria. One method of categorization is phylogenetic analysis of the TPS domains of TpsA proteins. As previously mentioned, the TPS domain is a hallmark of the TPS system, necessary for secretion of TpsA proteins across the outer membrane. A summarized phylogenetic tree was generated by using ClustalW (Figure 3). ClustalW alignment of previously characterized TpsA proteins and analysis of their phylogenetic tree reveals that these proteins arrange into four subfamilies best represented by FhaB, HMW1A, ShlA and CdiA (Jacob-Dubuisson et al., 2001; Clantin et al., 2004; Choi et al., 2007; Mazar and Cotter, 2007). While the FhaB, ShlA and CdiA subfamilies show high similarity across their TPS domains, the HMW1A subfamily differs across most of the domain. The non-HMW1A TPS domains contain less conserved (LC) and conserved (C) subdomains, with subdomains arranged LC1, C1, LC2, and C2 (Clantin et al., 2004). It is thought that the LC subdomains confer TpsA/TpsB specificity while the C subdomains are necessary for secretion mechanics regardless of TPS subfamily (Hodak et al., 2006). The C1 subdomain stands out because it contains two motifs – NPNL and NPNGI – that are required for TpsA secretion in most TPS subfamilies (Schönherr et al., 1993; Jacob-Dubuisson et al., 1997; Brillard et al., 2002; Ward et al., 2003; Choi et al., 2007). While the HMW1A TPS domain also contains – and requires – an NPNGI motif (St Geme and Grass, 1998), it and members of the HMW1A subfamily lack the NPNL motif. Rather, a

Figure 3

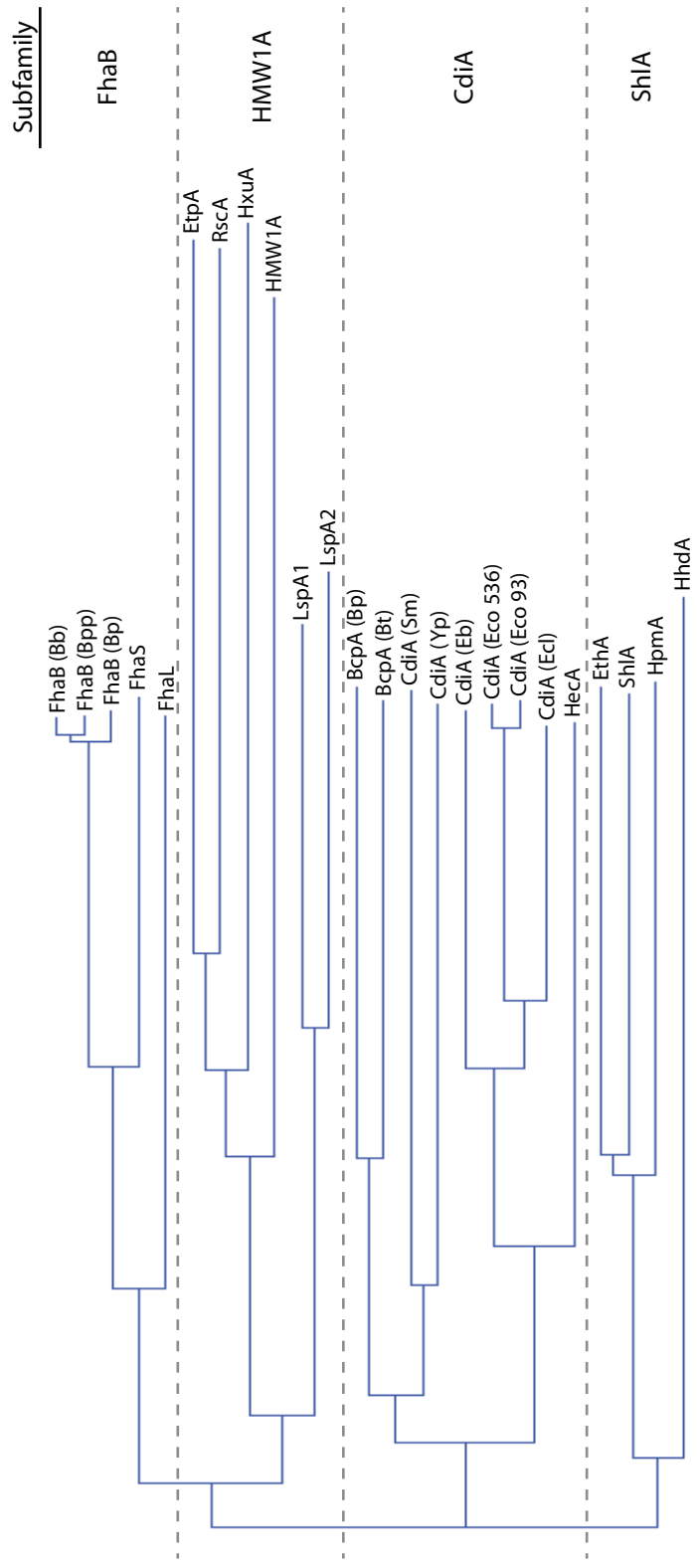

Phylogenetic analysis of TpsA sequences shows distinct subfamilies

ClustalW analysis of the TPS domains of characterized TpsA proteins yields a phylogenetic tree that categorizes TpsA proteins into subfamilies. The best-studied representatives of these subfamilies are FhaB, HMW1A, CdiA, and ShlA. LspA1 and LspA2 do not strongly categorize with any subfamily and may represent a fifth subfamily. FhaB is produced by *B. bronchiseptica* (Bb), *B. parapertussis* (Bpp), and *B. pertussis* (Bp). BcpA is produced by *B. pseudomallei* (Bp) and *B. thailandensis* (Bt). CdiA is produced by *S. maltophilia* (Sm), *Y. pestis* (Yp), *E. billingiae* (Eb), *E. coli* 536 (Eco 536), *E. coli* 93 (Eco 93), and *E. cloacae* (Ecl).

downstream NTNG motif may contribute to the ability of the TPS domain to mediate HMW1A secretion (Grass and St Geme, 2000). LspA1 and LspA2 categorize with the HMW1A subfamily based on their TPS domain, though LspB does not phylogenetically categorize with HMW1B (described below).

The basis for TpsA/TpsB specificity likely has as much to do with sequences in TpsB proteins' POTRA domains as it does with sequences in TpsA proteins' TPS domains. Indeed, ClustalW analyses of full-length TpsB proteins (Figure 4A) and just their POTRA domains (Figure 4B) reveal that these proteins categorize similarly to the TPS domains of their respective TpsA proteins (Jacob-Dubuisson et al., 2004; Choi et al., 2007; Jacob-Dubuisson et al., 2009). This phylogenetic correlation between TPS domains and POTRA domains strongly suggests that TpsA/TpsB interactions are specific within a subfamily, if not strictly to the cognate protein. As previously mentioned, phylogenetic characterization of LspB is inconsistent with the characterization of LspA1 and LspA2, making it difficult to assign LspAB to a TPS subfamily. Experimental evidence corroborates the idea of TpsA/TpsB specificity. It has previously been reported that TpsA/TpsB specificity is fairly strict. When expressed in *E. coli*, HpmB of *P. mirabilis* is incompatible with secretion of FHA44 (Jacob-Dubuisson et al., 1997). Likewise, FhaC is incompatible with secretion of full-length HpmA, but ShlB of *S. marcescens* is capable of secreting HpmA. Though FhaC is not able to secrete cytolysins of the ShlA subfamily, it is able to secrete both FhaB and FhaS (FhaS will be explained in greater detail on page 40) of *Bordetella* (Julio and Cotter, 2005). LspB of *H. ducreyi* is similarly able to secrete both LspA1

Figure 4

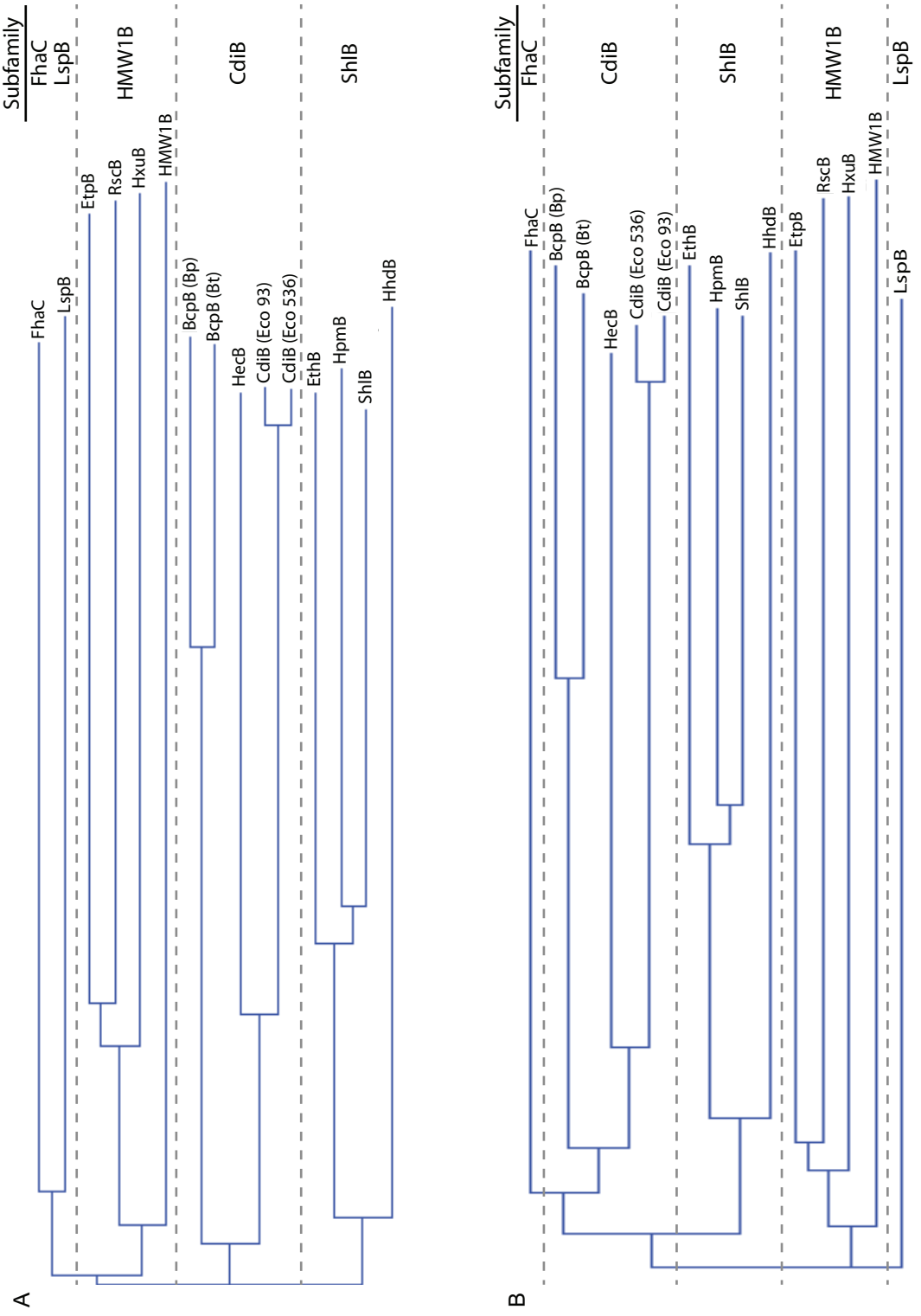
A
Subfamily
FhaC
LspB
HMW1B
CdiB
ShlB
FhaC
LspB
EtpB
RscB
HxuB
HMW1B
BcpB (Bp)
BcpB (Bt)
HecB
CdiB (Eco 93)
CdiB (Eco 536)
EthB
HpmB
ShlB
HhdB
B
Subfamily
FhaC
CdiB
ShlB
HMW1B
LspB
FhaC
BcpB (Bp)
BcpB (Bt)
HecB
CdiB (Eco 536)
CdiB (Eco 93)
EthB
HpmB
ShlB
HhdB
EtpB
RscB
HxuB
HMW1B
LspB

Figure 4

TpsB proteins can be phylogenetically categorized into subfamilies based on their complete peptide and POTRA domain sequences

A. ClustalW analysis of the full sequence of characterized TpsB proteins yields a phylogenetic tree that categorizes TpsB proteins into subfamilies. The best-studied representatives of these subfamilies are FhaC, HMW1B, CdiB, and ShlB. LspB and does not strongly categorize with any subfamily and may represent a fifth subfamily. B. ClustalW analysis of the POTRA domains of the proteins examined in Figure 4A yields a phylogenetic tree that categorizes TpsB proteins into subfamilies similarly to Figure 4A.

and LspA2, two TpsA proteins of *H. ducreyi* that share 86% identity (Ward et al., 1998; 2004). In the case of nontypeable *H. influenzae*, two TpsB proteins – HMW1B and HMW2B – are functionally interchangeable for the secretion of HMW1A and HMW2A when expressed in *E. coli* (St Geme and Grass, 1998).

Functional categorization of TPS system subfamilies

TPS systems can also be categorized based on functional properties of prototypical members of each subfamily (Table 1), providing a basis for functional predictions of uncharacterized TpsA proteins based on their subfamily categorization. FhaB is an adherence factor and has been shown to be immuno-suppressive (Urisu et al., 1986; Locht et al., 1993; Cotter et al., 1998; McGuirk and Mills, 2000; Julio et al., 2009; Henderson et al., 2012). HMW1A, although belonging to a different subfamily, is also involved in adhesion (St Geme et al., 1993; St Geme, 1994). Members of the CdiA subfamily, best characterized in *Burkholderia* spp., *D. dadantii*, and a specific strain of *E. coli*, are involved in contact-dependent growth inhibition (Aoki et al., 2005; 2010; Anderson et al., 2012). Members of the ShlA subfamily are cytolysins (Poole et al., 1988; Hertle et al., 1999).

Topological categorization of TPS system subfamilies

TPS may be further categorized by extracellular topology. FHA (the mature form of FhaB) has its N-terminus associated with the *Bordetella* outer membrane

(Mazar and Cotter, 2007). The C-terminus of the protein is distal from the cell surface, likely enabling the adhesive C-terminus to reach out from the bacteria (Julio et al., 2009). Although also an adhesin, HMW1A can be distinguished from FHA by an opposite orientation, with its C-terminus associated with the *H. influenzae* outer membrane and the N-terminus sticking out (Grass and St Geme, 2000; Dawid et al., 2001; Buscher et al., 2006). Less is known about CdiA and ShlA subfamily topologies. Both are speculated to have C-termini that face out, based on their C-terminal functional domains (Hertle, 2005; Aoki et al., 2010; Hayes et al., 2010).

Categorization of TPS system subfamilies based on presence of pro-regions

Finally, TPS can be classified based on the presence of pro-regions. FhaB has an ~1200 aa “prodomain” at its C-terminus (Delisse-Gathoye et al., 1990; Mazar and Cotter, 2006). The FhaB prodomain has previously been reported to be required for FHA-dependent adherence of *Bordetella* to mammalian cells *in vitro* and tracheal colonization *in vivo* (Mazar and Cotter, 2006). In HMW1A, an ~370 aa N-terminal “pro-piece” that contains the TPS domain is cleaved during the secretion process (Grass and St Geme, 2000; Yeo et al., 2007). The HMW1A pro-piece contains the TPS domain, but additional functions are unknown. Proteins belonging to the CdiA and ShlA subfamilies do not appear to have pro-regions.

Table 1 - Categorization of TpsA proteins by function, topology and pro-region

TPS Subfamily	Function	Topology	Pro-Region
FhaB	Adhesion/Immunomodulation	C-terminus Out	C-terminal
HMW1A	Adhesion	N-terminus Out	N-terminal
CdiA	Contact-Dependent Growth Inhibition	C-terminus Out	None
ShlA	Cytolysin	C-terminus Out	None

Bordetella bronchiseptica FHA biogenesis

The *fhaB* open reading frame is 11,130 bp in *B. bronchiseptica*, our model organism for FHA studies. While TPS loci are typically arranged 5'-*tpsB-tpsA*-3', the *fha* locus is arranged 5'-*fhaB-fimA-fimB-fimC-fimD-fhaC*-3' (Locht et al., 1992; Cotter et al., 1998), with genes encoding components of fimbria biogenesis being located between *fhaB* and *fhaC* (Locht et al., 1992; Cotter et al., 1998). The locus is found next to the genes encoding the BvgAS two-component system, with the *fhaB* and *bvgAS* genes diverging. Expression of *fhaB* is regulated by BvgAS, with BvgS serving as the sensor-kinase and BvgA serving as the response regulator (Weiss et al., 1983; Miller et al., 1989; Cotter and Miller, 1994; Uhl and Miller, 1996; Jones et al., 2005). A low amount of phosphorylated BvgA is sufficient to initiate transcription of *fhaB* (Boucher et al., 1997; 2001).

The translated FhaB preproprotein (Figure 5) contains a 72 aa N-terminal signal peptide that contains an N-terminal extension of 22 aa (Lambert-Buisine et al., 1998; Chevalier et al., 2004). C-terminal to the signal peptide is the ~250 aa TPS domain, which is required for secretion of FhaB across the outer membrane (Renauld-Mongenie et al., 1996; Clantin et al., 2004; Jacob-Dubuisson et al., 2004). C-terminal to the TPS domain is an ~1600 aa stretch of residues that become the β-helical shaft of the mature protein (Makhov et al., 1994; Kajava et al., 2001; Clantin et al., 2004). The β-helix consists of two well defined repeat regions, R1 and R2, with repeats that differ in both sequence and predicted structure (Kajava et al., 2001; Kajava and Steven, 2006). FhaB of *B. bronchiseptica* ($FhaB_{Bb}$) contains 45 copies of the R1 repeat and 13 copies of the R2 repeat. Separating these regions is a so-called carbohydrate recognition domain that contains an RGD motif and is predicted to form a β-helix of less-conserved repeats than the R1 or R2 regions (Relman et al., 1989; 1990; Saukkonen et al., 1991; Prasad et al., 1993; Kajava et al., 2001). The stretch of polypeptide that will ultimately become the mature C-terminal domain (MCD) follows the β-helix (Makhov et al., 1994; Mazar and Cotter, 2006). Electron microscopy of negatively stained FHA molecules indicates that this domain is globular, although detail on the structure is lacking (Makhov et al., 1994). C-teriminal to the MCD is an ~1200 aa prodomain (Delisse-Gathoye et al., 1990; Mazar and Cotter, 2006). Towards the C-terminus of the prodomain is an ~200 aa proline-rich region of unknown importance (Locht et al., 1992; 1993).

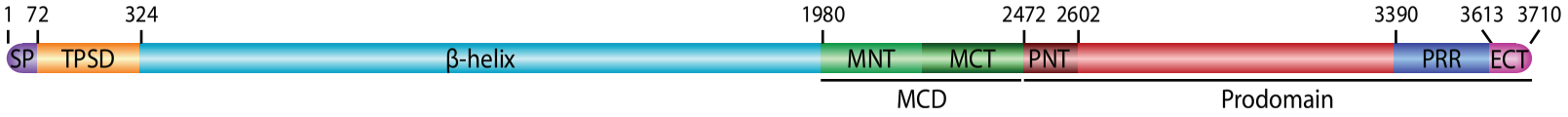

Domain layout of the FhaB preproprotein

The FhaB preproprotein consists of (N- to C-terminally) a signal peptide (purple), a TPS domain (TPSD, orange), a β-helical region (light blue), a mature C-terminal domain (MCD) that can be divided into an MCD N-terminus (MNT, light green) and a MCD C-terminus (MCT, dark green), and a prodomain (red) that can be divided into a prodomain N-terminus (PNT, dark red), a proline-rich region (PRR, dark blue), and an extreme C-terminus (ECT, magenta).

The signal peptide targets nascent FhaB preproprotein to the general secretory system, which translocates the polypeptide across the inner membrane (Jacob-Dubuisson et al., 2004). Localization to the Sec system appears to be mediated by SecAB, suggesting that periplasmic translocation of FhaB occurs post-translationally (Chevalier et al., 2004). Little is known about FhaB's existence in the periplasm. When FHA44 (the N-terminal 80 kDa of FhaB) and FhaC are expressed in *E. coli*, FHA44 is unable to be recovered from the periplasm (Guedin et al., 1998), suggesting that FhaB begins transit through FhaC immediately upon exposure of the TPS domain to the POTRA domains. Furthermore, Guedin *et al.* showed that FHA44 synthesized prior to FhaC expression cannot be released into the supernatant by live cells, though subcellular localization of FHA44 was not performed to determine the integrity of pre-*fhaC*-induction FHA44. It is likely that the FHA44 synthesized prior to *fhaC* expression was degraded, as FhaB is not detected in *B. bronchiseptica* whole cell lysates when FhaC is disrupted, suggesting that it is degraded in response to lack of secretion (Julio and Cotter, 2005). Collectively, these observations support a model for periplasmic transit of FhaB in which translocation across the inner and outer membrane is coupled and FhaB does not spend time in a soluble, periplasmic state. Alternatively, FhaB may be completely translocated into periplasm prior to recognition of the TPS domain by FhaC. Regardless of the model of periplasmic transit, recent studies have identified periplasmic chaperones that may be involved in ensuring that FhaB reaches FhaC (Hodak et al., 2008; Baud et al., 2009; 2011). These proteins may keep periplasmic FhaB unfolded while it transits across the outer membrane, suggesting that FhaB spends some appreciable

amount of time in the periplasm before extracellular translocation. These chaperones may also prevent aggregation of FhaB in the periplasm.

The interaction between FhaB and FhaC is hypothesized to initiate translocation of FhaB across the outer membrane. The N-terminal TPS domain of the FhaB proprotein associates with the periplasmic POTRA domains of FhaC (Hodak et al., 2006) *in vitro*, suggesting that it also does so *in vivo* (Figure 6A). The TPS domain must be unfolded for this interaction. Far Western blotting demonstrated that the N-terminal 30 kDa of FHA (Fha30) only associates with FhaC when Fha30 is unfolded (Hodak et al., 2006). Pull-down assays confirmed that Fha30 in its native fold is unable to bind FhaC. Hodak *et al.* also conducted a systematic analysis of molecular determinants of the TPS domain for association with POTRA domains and secretion of Fha30, concluding that residues in the C1 and C2 subdomains were critical for these processes. Similarly, a systematic analysis of FhaC's two POTRA domains was performed, revealing residues required for recognition and secretion of the TPS domain by FhaC (Delattre et al., 2011). The current model of FhaB secretion is that this TPS-POTRA association causes conformational shifts in FhaC that expel H1 and L6, and in doing so clear the FhaC channel for FhaB secretion. The FhaC pore is 16 Å wide, though its occupation by H1 and L6 leaves even less room for FhaB secretion (Clantin et al., 2007). Given the 40 Å width of folded FHA's β-helix (Makhov et al., 1994), FhaB must transit the pore in an unfolded state (regardless of H1 and L6 occupation of the FhaC pore).

Figure 6

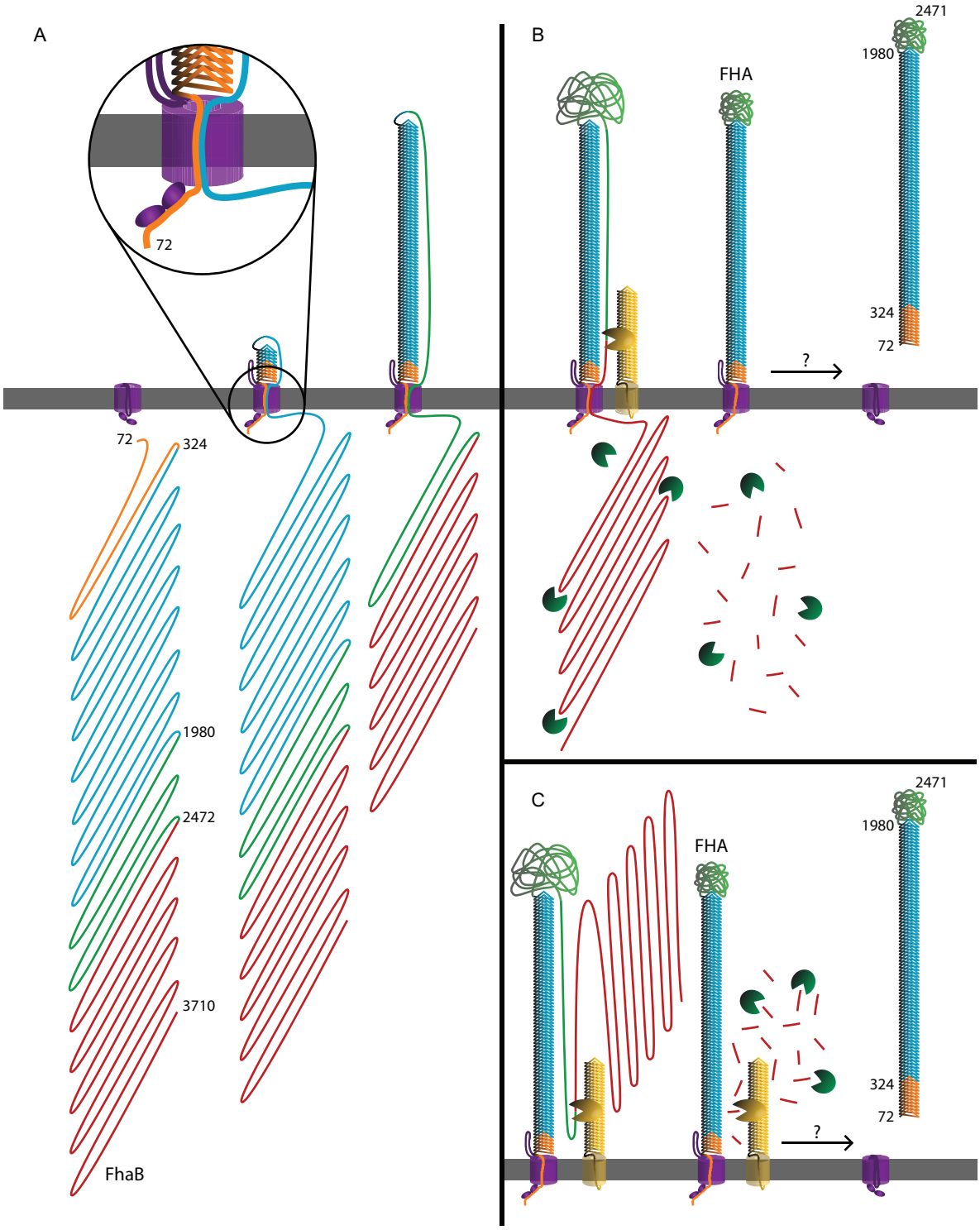
A
72
72
324
1980
2472
3710
FhaB
B
FHA
2471
1980
324
72
?
C
FHA
2471
1980
324
72
?

Figure 6

Model of the FhaB/FhaC Two-Partner Secretion (TPS) system

A. FhaB translocation across the *Bordetella* outer membrane. The FhaB preproprotein (labeled) is exported into the periplasm by the general secretory system (not shown). It is not known if the entire polypeptide is translocated into the periplasm before translocation through FhaC occurs. In this figure, the peptidoglycan layer and cytoplasmic membrane are not shown for simplicity. Also note that this figure was drawn to scale, as best as possible. Residue numbers of the FhaB proprotein are indicated. The FhaB TPS domain (orange) interacts with FhaC (purple) to initiate outer membrane translocation of FhaB as a hairpin. Upon extracellular exposure, the C-terminal portion of the TPS domain folds into a β-helix, nucleating folding of the β-helical shaft (blue) in an N- to C-terminal direction. At this point, FHA biogenesis could proceed by two routes, depending on the localization of the prodomain. The TPS domain remains associated with FHA after FHA release.
B. Possibility that the prodomain remains intracellular. After the MCD (light green) has reached the cell surface, SphB1 (yellow) and an unidentified protease (dark green) cleave the intracellular prodomain (red) from FhaB and the prodomain is rapidly degraded. Mature FHA (labeled) can be either surface-associated or released. The mechanism for release is unknown.
C. Possibility that the prodomain reaches the extracellular space. In this scenario, prodomain cleavage and degradation would both occur extracellularly.

Chimeric fusions of FHA44 and the globular B subunit of cholera toxin, CtxB, in *E. coli* indicate that the fusion protein is unable to be secreted when it is folded (Guedin et al., 1998). Only when the CtxB domain was unable to form intramolecular disulfide bonds was the chimeric protein able to be secreted. FhaB likely secretes through FhaC as an extended hairpin (Mazar and Cotter, 2006), with the N-terminus remaining associated with the POTRA domains while the downstream polypeptide transits through the pore of FhaC completely unfolded and as a hairpin (Figure 6A). Indeed, experimental evidence as to the topology of FHA demonstrates that the hairpin model of secretion is correct (Mazar and Cotter, 2006).

During hairpin secretion of FhaB, the C-terminus of the TPS domain is the first portion of the protein to emerge into the extracellular space. The model states that upon emerging into the extracellular milieu, the TPS domain folds into a right-handed β-helix (Kajava et al., 2001; Clantin et al., 2004) (Figure 6A). The source of energy to initiate secretion is unknown, as the periplasm has no ATP to drive secretion. It is thought that such folding nucleates the β-helical folding of C-terminal polypeptide as it crosses the outer membrane, thereby assembling an ~350 Å β-helical shaft that extends away from the cell surface (Makhov et al., 1994; Kajava et al., 2001). The free energy provided by β-helical folding is hypothesized to pull the polypeptides of the MCD across the outer membrane (Mazar and Cotter, 2006). Complete folding of the β-helix is believed to draw the MCD into the extracellular space, where it is believed to fold into its functional conformation. After folding is complete, the FhaB proprotein is cleaved to generate mature FHA (Figure 6A). The

current model postulates that SphB1, a subtilisin-like autotransporter, is involved in cleavage of FhaB (Coutte et al., 2001; 2003). Although deletion of *sphB1* in *B. pertussis* and *B. bronchiseptica* results in reduced processing of FhaB, SphB1 has not been shown to cleave FhaB directly (Coutte et al., 2001; Mazar and Cotter, 2006). Furthermore, since deletion of *sphB1* does not completely prevent maturation, it is clear that one or more SphB1-independent maturation determinants exist. The identities and mechanisms of these molecules, however, remain unknown. Cleavage of ~375 kDa FhaB results in separation of ~250 kDa mature FHA from the C-terminal ~130 kDa prodomain. The prodomain is not immuno-detected as a stable, standalone polypeptide in *Bordetella* whole-cell lysates or supernatants, indicating that once it is cleaved from FhaB, it is quickly degraded (Delisse-Gathoye et al., 1990; Mazar and Cotter, 2006) (Figure 6A). When grown overnight in Stainer-Scholte media, *Bordetella* can both retain FHA on the outer membrane surface and release FHA into the media (Renauld-Mongenie et al., 1996) (Figure 6A). The mechanism regulating FHA retention is unknown, as are the *in vivo* functions of the surface-associated versus released forms of FHA.

FHA function

Although FHA is one of the primary components of acellular pertussis vaccines (Sato and Sato, 1999), an understanding of its role in virulence and host response is still incomplete. *In vitro* studies reveal a role for FHA in adherence to a variety of cell lines including lung epithelial cells and macrophages (Urisu et al.,

1986; Tuomanen et al., 1988; Relman et al., 1989; 1990; Aricò et al., 1993; Locht et al., 1993; Cotter et al., 1998; Ishibashi et al., 2001). The VLA-5 receptor of mammalian cells and the CR3 and LRI/IAP receptors of macrophages have been proposed to be the receptors of FHA, with adhesion being mediated by an RGD motif found in the carbohydrate recognition domain of FHA (Relman et al., 1990; Ishibashi et al., 1994; 2001). *In vivo* studies indicate that FHA is required for colonization of the lower respiratory tract and persistence in the lungs (Cotter et al., 1998; Inatsuka et al., 2005; Julio et al., 2009). Contrary to previous reports that emphasize the importance of the RGD motif, *in vivo* studies indicate that the RGD does not contribute to FHA-dependent pathogenesis (Julio et al., 2009). Rather, Julio *et al.* demonstrated that it is the MCD of FHA that is the primary determinant of FHA-mediated adherence *in vitro* and virulence *in vivo*. Furthermore, the FhaB prodomain affects FHA-dependent virulence, as prodomain truncations render *B. bronchiseptica* unable to adhere to lung epithelial cells or colonize the trachea of rats (Mazar and Cotter, 2006).

FHA also exhibits immuno-modulatory properties. *B. bronchiseptica* in which *fhaB* has been deleted causes a hyper-inflammatory immune response in mouse lungs, much to the detriment of *Bordetella* persistence (Inatsuka et al., 2005). Specifically, FHA appears to regulate an IL-17-mediated immune response in mice, as deletion of *fhaB* results in an early influx of IL-17-postive neutrophils, macrophages and $CD4^+$ T cells (Henderson et al., 2012). As mentioned earlier, FHA is both surface-associated and released. Whether either or both of these forms are

functional *in vivo*, and precisely what those functions are, remain among the greatest challenges to understanding the role of FHA in virulence. *In vitro* studies suggest that the released form of FHA may affect cell signaling to down-regulate IL-12 production in macrophages (McGuirk and Mills, 2000). Purified FHA has also been implicated in affecting NF-κB and interferon responses *in vitro* (Abramson et al., 2008; Dieterich and Relman, 2011).

FHA in Bordetella pertussis

B. pertussis is a human-specific pathogen and *B. pertussis* research is hampered due to the lack of a good animal model of infection. *B. bronchiseptica* infects a broad range of mammalian hosts, and *in vivo* work done using *B. bronchiseptica* is conducted in hopes that it will translate well into our understanding of *B. pertussis* virulence. In the case of FHA specifically, $FhaB_{Bb}$ and the FhaB of *B. pertussis* ($FhaB_{Bp}$) are functionally interchangeable (Julio et al., 2009), validating studies of FhaB in *B. bronchiseptica*. Although functionally interchangeable, there are a handful of differences between the two proteins. Alignment of amino acid sequence of $FhaB_{Bb}$ and $FhaB_{Bp}$ reveals that $FhaB_{Bp}$ has fewer repeats in the R1 region of the β-helix – 39 compared to 45 for $FhaB_{Bb}$ (Kajava et al., 2001). The MCDs of $FhaB_{Bb}$ and $FhaB_{Bp}$ are ~93.5% identical, likely accounting in large part for functional interchangeability of the two proteins. The prodomains of the two proteins are also very highly conserved. Two regions differ between the *B. bronchiseptica* and *B. pertussis* prodomains – both in the proline-rich region. The first difference is

residues 3442-3454 of *B. bronchiseptica*, which share little similarity to their corresponding region of the *B. pertussis* FhaB prodomain (3330-3342 of *B. pertussis*). The second difference is a $(PA)_6(PK)_4$ motif towards the end of the *B. bronchiseptica* PRR that is instead a $(PK)_5$ motif in *B. pertussis*. $FhaB_{Bp}$ undergoes maturation proteolysis to a greater extent than $FhaB_{Bb}$ (Mazar and Cotter, 2006). As previously mentioned, SphB1 is one of the proteases implicated in FhaB maturation cleavage and $FhaB_{Bb}$ and $FhaB_{Bp}$ differ in their SphB1-dependent cleavage. Generally speaking, FhaB is processed into four isoforms, with the three smaller isoforms (FHA, FHA_1, and FHA_2) being cleaved in the same site in *B. bronchiseptica* and *B. pertussis* (Mazar and Cotter, 2006). The cleavage site of the larger isoform, however, differs between the two strains. The cleavage site of the largest *B. pertussis* isoform, FHA*, is located C-terminal that of *B. bronchiseptica*, FHA′ (Mazar and Cotter, 2006). When $FhaB_{Bb}$ is expressed in *B. pertussis*, SphB1-dependent cleavage of $FhaB_{Bb}$ occurs at the same sites as it does in *B. bronchiseptica* (Julio et al., 2009), indicating that the site of maturation cleavage is determined by the peptide sequence rather than the strain background. In *B. pertussis*, SphB1-dependent FhaB maturation yields virtually no full-length $FhaB_{Bp}$ in whole-cell lysates. SphB1-dependent processing is less efficient in *B. bronchiseptica*, where appreciable levels of full-length $FhaB_{Bb}$ detected in whole-cell lysates (Mazar and Cotter, 2006). When $FhaB_{Bb}$ is expressed in *B. pertussis*, full-length $FhaB_{Bb}$ is detected at a level that is in between that of $FhaB_{Bp}$ in *B. pertussis* and $FhaB_{Bb}$ in *B. bronchiseptica* (Julio et al., 2009). Furthermore, *B. pertussis* releases much more FHA than *B. bronchiseptica* (Jacob-Dubuisson et al., 2000; Mazar and Cotter, 2006;

Julio et al., 2009). Similar to the case of SphB1-dependent processing, *B. pertussis* producing $FhaB_{Bb}$ releases mature FHA_{Bb} at a level in between FHA_{Bp} in *B. pertussis* and FHA_{Bb} in *B. bronchiseptica* (Julio et al., 2009). Collectively, the data presented by Julio *et al.* indicates that both strain background and polypeptide sequence are determinants of FhaB processing thoroughness and FHA release levels.

FhaB homologues in Bordetella

FhaB is not the only TPS system present in *Bordetella*. Two FHA-like proteins, FhaS and FhaL, are also encoded in the genome of *B. bronchiseptica* and *B. pertussis*. FhaL has not been functionally or molecularly characterized, but some work has been done to characterize FhaS. Expression of the *fhaS* gene is under the control of the BvgAS two-component regulatory system, though maximal expression does not appear to be regulated by phosphorylated BvgA in the same manner by which *fhaB* expression is regulated (Julio and Cotter, 2005). A standout difference between $FhaS_{Bb}$ and $FhaB_{Bb}$ is the absence of a 28 residues towards the C-terminus of the MCD in FhaS. *B. bronchiseptica* in which these 28 residues are deleted from FhaB is able to adhere to L2 and macrophage-like cells, but is unable to colonize the trachea of rats (Julio et al., 2009). Furthermore, this deletion mutant induces a hyper-inflammatory response in the lungs of infected mice. Additionally, the FhaS prodomain is missing the proline-rich region found in FhaB. Functionally, FhaS remains largely mysterious. Deletion of *fhaS* from *B. bronchiseptica* does not result in defective adherence to L2 and BEAS-2B cells (Julio and Cotter, 2005). The Δ*fhaS*

strain also appears to have no defect in tracheal colonization of rats. When rats are co-infected with wild-type *B. bronchiseptica* and the *fhaS* strain, however, the number of CFUs recovered for the mutant strain is lower than those of the wild-type strain, indicating that FhaS does indeed contribute to bacterial fitness *in vivo* in a manner that cannot be complemented by wild-type *Bordetella* in a wild-type/Δ*fhaS* co-infection.

Outstanding Questions

An initial impression of FHA might be that it is a fairly straightforward protein – a very long β-helical shaft with a distal adhesive tip. These impressions are indeed consistent with data collected on FHA, but they overlook a prominent feature of FhaB – its ~130 kDa prodomain. Since it was first described as a part of the FhaB proprotein, researchers have hypothesized that it functions as an intramolecular chaperone, keeping FhaB in an unfolded state in order to prevent aggregation and keep FhaB secretion-competent (Delisse-Gathoye et al., 1990). Mazar and Cotter, however, demonstrated that FhaB could be secreted by strains that contained a variety of FhaB prodomain truncations (Mazar and Cotter, 2006), indicating that the prodomain did not chaperone the proprotein the FhaC. Even so, truncations of the prodomain resulted in adherence defects *in vitro* and colonization defects *in vivo*, showing that the prodomain serves a critical role in FHA functionality. What that role is, though, remains unknown. Furthermore, although previous models of FhaB secretion indicate that the prodomain remains in an intracellular compartment

(Figure 6B), its fate is unknown and it may very well function in the extracellular space (Figure 6C).

In addition to its enormous size, a standout feature of the FhaB prodomain is a ~200 aa proline-rich region at the prodomain C-terminus (Locht et al., 1992; 1993). For a subdomain of such unusually high proline content, it is surprising that no research has been performed to reveal its contribution to FHA biogenesis and function. Of further interest is what other subdomains exist within the ~1200 aa prodomain, and what their contributions are.

Chapter II – The FhaB prodomain affects the conformation of the MCD

Bioinformatic analysis of the FhaB prodomain

A PSI-BLAST search using the entire *B. bronchiseptica* FhaB prodomain as query revealed substantial similarity over the entire length of the prodomain (E-values ≤ e-30) with other FHA-related proteins in *Bordetella* species as well as a few related proteins in *Pasteurella multocida, Haemophilus ducreyi, Citrobacter rodentium* and *Erwinia billingiae.* Strikingly, however, hundreds of predicted TpsA proteins, many of which are known to belong to the FHA subfamily, were identified with significant similarity (alignment scores between 80 and 200) to residues 2472-2601 of the FhaB prodomain, which we are now calling the prodomain N-terminus (PNT). ClustalW analysis revealed ~50% similarity overall among the proteins identified in our analysis (Figure 7). No similarity with other proteins above the threshold level set by PSI-BLAST was identified for regions of the FhaB prodomain C-terminal to the PNT. We did, however, notice a proline-rich region near the C-terminus of the prodomain by simple visual examination of the amino acid sequence. This proline-rich region has been noted previously (Antoine and Locht, 1992; Locht et al., 1992) and, curiously, a putative FHA orthologue in *Bordetella avium* contains a region with even more prolines near its C-terminus. There are no reports of functional characterization for any sequences with which similarity with the

Figure 7

The FhaB prodomain comprises distinct subdomains

At the top is a schematic of *B. bronchiseptica* FhaB showing domain locations. At the bottom, WebLogo 3.1 display of homology shared amongst TpsA proteins to the ~125 aa *B. bronchiseptica* FhaB prodomain N-terminus (PNT). The species (and accessions) included in the ClustalW alignment are *A. radiobacter* (YP_002542793.1), *B. bronchiseptica* (NP_889529.1), *B. grahamii* (YP_002971785.1), *B. henselae* (YP_033492.1), *B. parapertussis* (NP_885212.1), *B. pertussis* (NP_880571.1), *E. billingiae* (YP_003741557.1), *E. cancerogenous* (ZP_05970215.2), *E. coli* UTI 89 (YP_543880.1), *F. gonidiaformans* (ZP_05631037.1), *F. nucleatum* (NP_602617.1), *F. varium* (ZP_04859779.1), *H. ducreyi* (NP_873911.1), *H. somnus* (YP_001784809.1), *L. hofstadii* (ZP_05902926.1), *P. dagmatis* (ZP_0592026.1), *P. fluorescens* (YP_257313.1), *P. multocida* (NP_244996.1), *P. vagans* (YP_003931455.1), *R. leguminosarum* (YP_002278042.1), *Shigella* sp. D9 (ZP_05433039.1), *S. aggregata* (ZP_01545092.1), *S. termitidus* (YP_003310063.1), *V. cholerae* (ZP_01955515.1), *V. coralliilyticus* (ZP_05888559.1), *V. mimicus* (ZP_05718784.1), *X. oryzae* (YP_001915776.1), *Y. frederiksenii* (ZP_046344430.1), *Y. intermedia* (ZP_04636695.1), *Y kristensenii* (ZP_04622797.1)

prodomain was identified.

The conformation of purified MCD is affected by the prodomain

Because the prodomain is required for FHA function *in vivo* (Mazar and Cotter, 2006) and there is evidence that the MCD is an important functional domain (Julio et al., 2009; Henderson et al., 2012), we hypothesized that the FhaB prodomain is required for the MCD to attain its proper conformation. To test this hypothesis, two *B. pertussis* strains were constructed that produce FhaB proteins containing hexahistidine (His_6) insertions immediately C-terminal to Q72 (the N-terminal amino acid of mature FHA) and tobacco etch virus (TEV) protease cleavage sites at the junction between the β-helical shaft and the MCD. One strain (BPSMAQ) produced full-length FhaB and the other (BPSMAQT-N) contained a stop codon in *fhaB* 48 codons 3′ to the region encoding the primary SphB1-dependent cleavage site (Figure 8A – note that residue numbering of the schematic corresponds to *B. pertussis* FhaB, not *B. bronchiseptica* FhaB). We used *B. pertussis* strain BPSM for these experiments because it releases substantially more FHA into culture supernatants than *B. bronchiseptica* strain RB50, facilitating our ability to recover a sufficient amount of protein with minimal manipulation (Jacob-Dubuisson et al., 2000; Mazar and Cotter, 2006). The presence of the His_6 tag and the TEV protease cleavage site did not affect the ability of otherwise wild-type FHA to function as an adhesin *in vitro* (Figure 8B). Bacteria were grown under *fhaB*-inducing conditions, and culture supernatants were collected under native conditions and incubated with

Figure 8

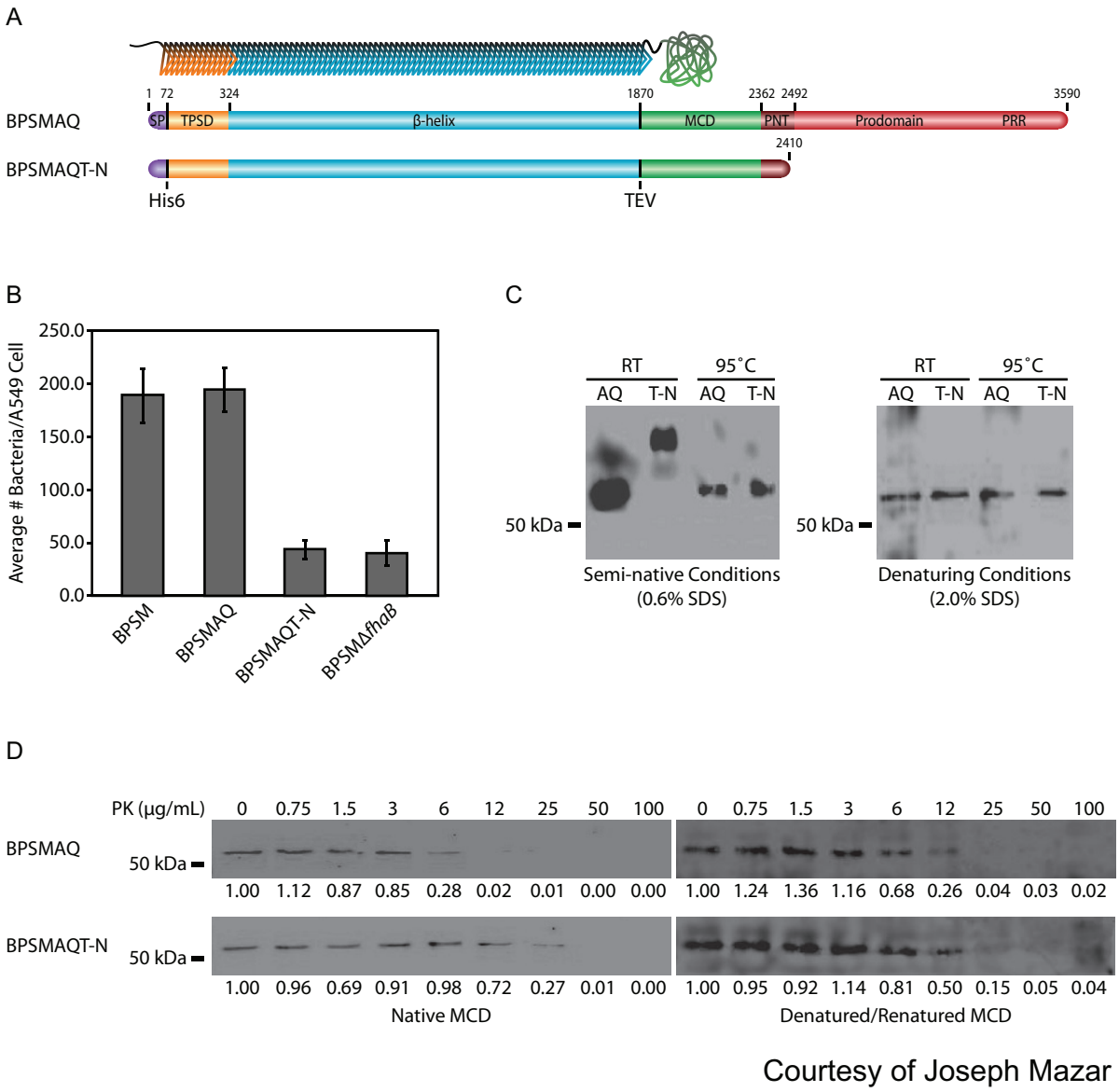

Courtesy of Joseph Mazar

Figure 8

The FhaB prodomain affects the conformation of the MCD

A. At top is an illustration of mature FHA with an N-terminal hexahistidine tag and a TEV protease cleavage site upstream of the MCD. Below are schematics of the *B. pertussis* FhaB proteins as initially synthesized. From left, the domains illustrated are the signal peptide (purple), the TPS domain (orange), the β-helical shaft (light blue), the MCD (green), the PNT (dark red), and the remainder of the prodomain (red). The hexahistidine tag is located between the signal peptide and the TPS domain. The TEV protease cleavage site is located between the β-helix and the MCD. The approximate site of SphB1-dependent cleavage is noted. The proline-rich region (PRR) of the prodomain is also noted. Residue numbering is based on the *B. pertussis* FhaB protein.
B. The strains were tested to determine if the hexahistidine tag and TEV protease site altered FHA-mediated adherence to A549 human lung epithelial cells. BPSMAQ adhered in a manner indistinguishable from wild-type *B. pertussis*, while BPSMAQT-N adhered as inefficiently as an fhaB deletion strain.
C. Anti-MCD immunoblot of purified MCD polypeptides. Semi-native gel analysis indicated altered mobility of the MCD derived from the prodomain-truncated (T-N) FhaB compared with the MCD derived from full-length (AQ) FhaB. When denatured by either heat or chemical denaturation, the MCDs of both proteins migrate identically.
D. Western blot of MCD polypeptides after proteinase-K treatment. Purified MCDs were tested for sensitivity to proteinase-K. Samples were incubated with increasing concentrations of proteinase-K, separated by SDS-PAGE, and detected with anti-MCD antibody. Additionally, samples were denatured/renatured prior to analysis of proteinase-K sensitivity. Densitometry values proportionate to the undigested sample of each Western blot are listed below the blots.

nickel-chelating resin, which was then washed and incubated with AcTEV protease to release the MCD from FHA. The MCD polypeptides were resolved on a semi-native polyacrylamide gel (0.6% SDS).

Samples were then transferred to a nitrocellulose membrane and probed with anti-MCD antibody. The MCD polypeptides recovered from the BPSMAQ and BPSMAQT-N strains under native conditions migrated with different mobilities on the semi-native gel, but they migrated with the same mobility after heat denaturation (Figure 8C). The MCD polypeptides migrated with the same mobility regardless of pre-heating when separated by standard, denaturing, SDS-PAGE (2.0% SDS). These results suggest that the presence of the prodomain in the nascent FhaB polypeptide affects the conformation of the MCD in mature FHA.

We also treated the native MCD polypeptides with increasing concentrations of proteinase-K and resolved them by SDS-PAGE. While the MCD from BPSMAQ (which produces full-length FhaB) was completely digested by 12 μg/mL of proteinase-K, 50 μg/mL of proteinase-K was required to completely degrade the MCD from BPSMAQT-N (Figure 8D). As a control, the MCDs from both strains were boiled to denature the proteins, then allowed to renature, and were then incubated with proteinase-K. After being subjected to denaturing and renaturing conditions *in vitro,* both MCD polypeptides were completely degraded by 25 μg/mL proteinase-K, suggesting that the conformations of the *in vitro* renatured proteins were the same (but different from those of the naturally folded polypeptides, which were digested by

either 25 or 50 μg/mL proteinase-K). Together, these data indicate that the conformation of the MCD that forms after translocation to the bacterial surface differs depending on whether the initially synthesized FhaB protein contains the C-terminal prodomain.

The conformation of the MCD of mature FHA is affected by the prodomain

As an additional approach to probe the conformation of the MCD, we performed cysteine-accessibility experiments, taking advantage of the fact that FHA contains no cysteine residues. We constructed a series of *B. bronchiseptica* strains – in both wild-type (WT) and prodomain-truncated (ΔPD) backgrounds – in which a single codon in the MCD-encoding region of *fhaB* was changed to a cysteine codon (Figure 9A), with substitutions regularly spaced ~50 aa apart. (We used *B. bronchiseptica* for these experiments so that the mutant strains could subsequently be compared with wild-type bacteria for their ability to establish respiratory infections in natural-host animal models.) The strains shown in Figure 9 are those that grew and adhered to L2 rat lung epithelial cells in a manner indistinguishable from wild-type *B. bronchiseptica* (data not shown) and they released FHA as efficiently as wild-type bacteria. Culture supernatants were concentrated under native conditions and incubated with DyLight 680 Maleimide, which forms a covalent bond with the sulfhydryl group on cysteine residues. Samples were then separated by SDS-PAGE, transferred to a nitrocellulose membrane, and probed with an antibody that recognizes a central region of FHA [the carbohydrate recognition domain (CRD)] to

Figure 9

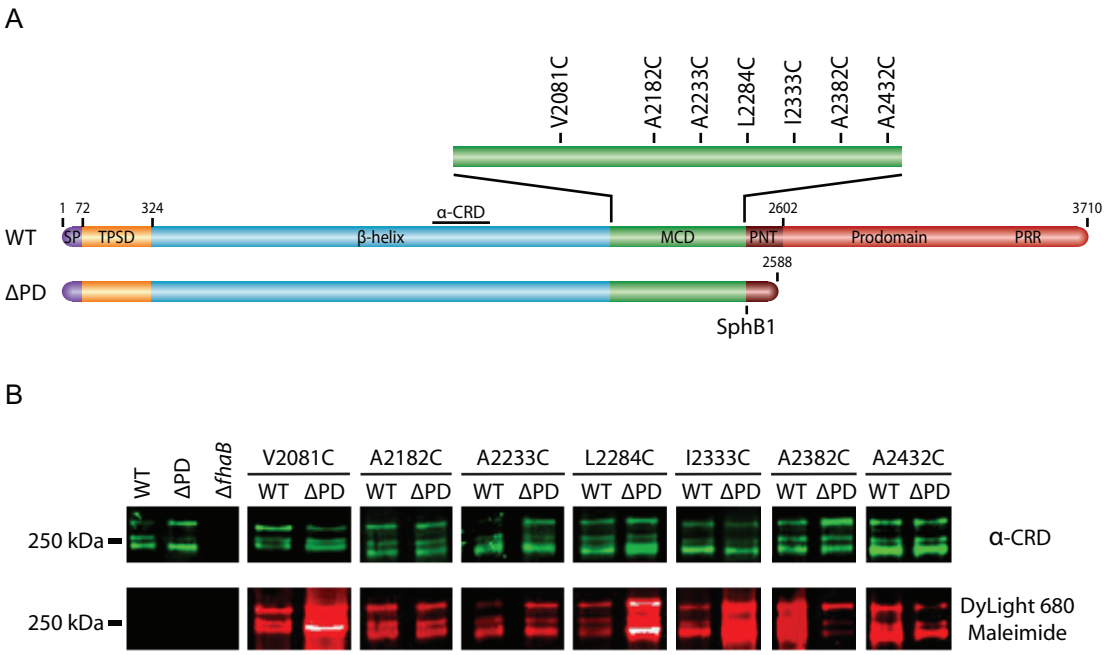

The FhaB prodomain affects the surface-accessibility of MCD residues

A. Schematic of *B. bronchiseptica* FhaB cysteine-substitution proteins. Single cysteine residues were substituted into wild-type (WT) and prodomain-truncated (DPD) proteins.
B. Cysteine-accessibility immunoblot of FHA recovered under native conditions from culture supernatants. The Western blots were immuno-stained with an anti-CRD antibody (green) and displayed four isoforms of mature, released FHA. Native FHA

determine the relative amounts of FHA contained in each sample. The anti-CRD antibody was detected with anti-chicken antibody conjugated to a near-infrared dye that fluoresces at 800 nm, shown in green in Figure 9B. The fluorophore of the DyLight 680 Maleimide fluoresces at 680 nm, shown in red in Figure 9B. For the A2382C substitution, and to a lesser extent, the A2432C substitution, FHA produced in the wild-type strain displayed greater DyLight-dependent fluorescence than FHA produced in the ΔPD strain, indicating that these cysteines were more accessible in the FHA produced by the wild-type strain than in the FHA produced by the ΔPD strain (Figure 9B). Conversely, for the V2081C, L2284C and I2233C substitutions, FHA produced by the wild-type strain displayed weaker fluorescence than FHA produced by the ΔPD strain. These data indicate that the accessibility of the cysteine residues differed depending on whether FhaB contained an intact prodomain and therefore provide further support for the conclusion that the prodomain affects the conformation of the MCD.

Chapter III – The FhaB prodomain mediates its own intracellular localization

The C-terminus of the prodomain remains in an intracellular compartment

We envisaged three mechanisms by which the FhaB prodomain could affect the conformation of the MCD on mature FHA: (i) the prodomain could function as a scaffold or 'foldase' for the MCD, analogous to the prodomains of many secreted proteases of Gram-positive bacteria (Shinde and Thomas, 2011); (ii) the prodomain could remain in an intracellular compartment, functioning as a tether to constrain the possible conformations that the MCD can sample before attaining a stably folded state; (iii) the prodomain could control the rate of translocation of the MCD to the cell surface and that controlled translocation could be required for proper folding (e.g. perhaps the N-terminal region needs to fold first, followed by the C-terminal region). In the first mechanism, the entire prodomain would be translocated to the cell surface before subsequent maturation (assuming that a fully folded MCD cannot be translocated through FhaC) while in the second and third mechanisms, the C-terminus of the prodomain would remain in an intracellular compartment. We therefore sought to determine the location of the prodomain during maturation of FHA. We were specifically interested in determining the location of the C-terminus of the prodomain before cleavage of FhaB to form FHA.

We first constructed a *B. bronchiseptica* strain (CTHA) producing FhaB with a hemagglutinin (HA) epitope seven residues N-terminal to the C-terminus of FhaB (Figure 10A). Immunoblot analysis indicated that the HA epitope disrupted the stability of full-length FhaB [no full-length FhaB protein was detected in this strain by either the anti-MCD or anti-HA antibodies (Figure 10B)], rendering the strain unsuitable for localization studies. We therefore constructed a *B. bronchiseptica* strain (HAPRR) producing FhaB with an HA epitope after residue 3265, just N-terminal to the proline-rich region in the FhaB prodomain (Figure 10A). This epitope did not affect secretion, maturation or release of FhaB, as the proportion of FhaB and FHA polypeptides was indistinguishable between this strain and wild-type bacteria (Figure 10B). Moreover, preliminary data suggest this strain is indistinguishable from wild-type *B. bronchiseptica* in its ability to cause respiratory infection in mice (our unpublished results).

To determine if the prodomain remains in an intracellular location, the HAPRR strain was grown under FHA-inducing conditions, cells were harvested by centrifugation and suspended in buffer with 1 μg/mL proteinase-K to cleave surface-exposed proteins, washed to remove extra-cellular protein fragments, then whole-cell lysates (whole-cell lysates) were prepared and analyzed by immunoblot (Figure 11B. Note that the left and right panels in Figure 11B are the same immunoblot. The intensity of the red channel was increased in the panel on the right to facilitate visualization of polypeptides detected by the anti-HA antibody. Similar manipulation of the green channel did not reveal any additional bands). In the untreated sample,

Figure 10

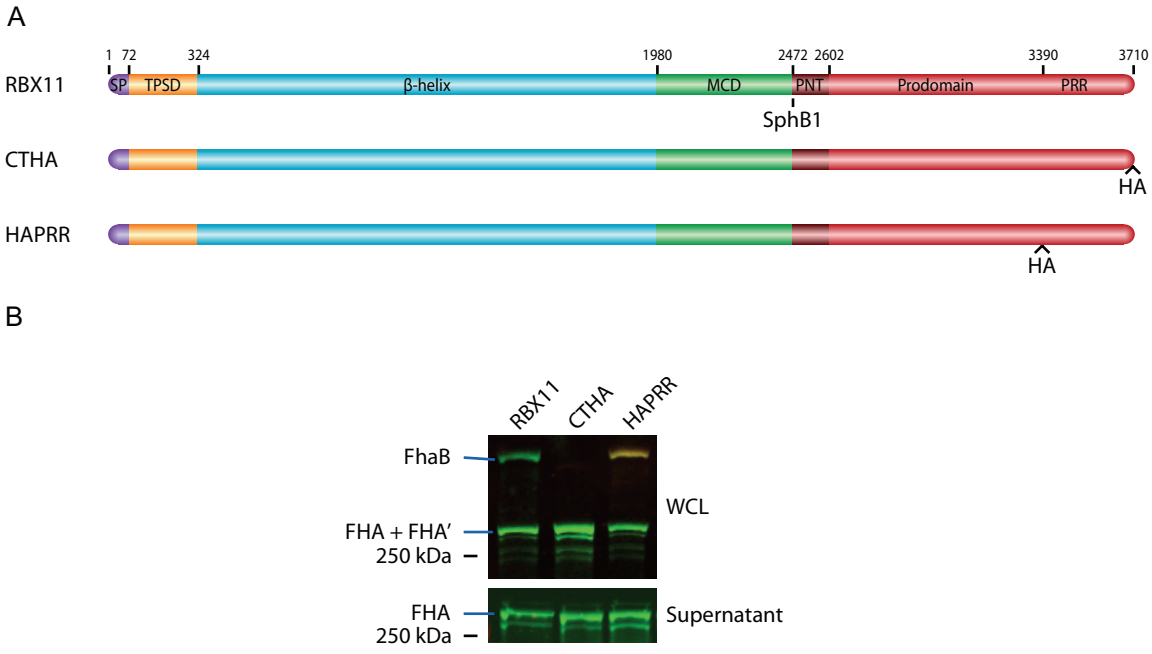

Insertion of an HA epitope tag before the FhaB proline-rich region (PRR) does not affect FHA maturation or function

A. Schematic of FhaB proteins used in experiment. Domain layout is the same as that of Figure 4. The PRR in front of which the HA tag was introduced is labeled for the HAPRR strain.
B. Anti-MCD (green) and anti-HA (red) immunoblot of whole-cell lysates and concentrated supernatants. Introducing an HA tag at the C-terminus of FhaB causes instability of full-length FhaB. Moving the epitope upstream of the PRR does not affect the integrity or maturation of full-length FhaB. FHA release into the supernatants is unaffected by either location of the HA tag.

Figure 11

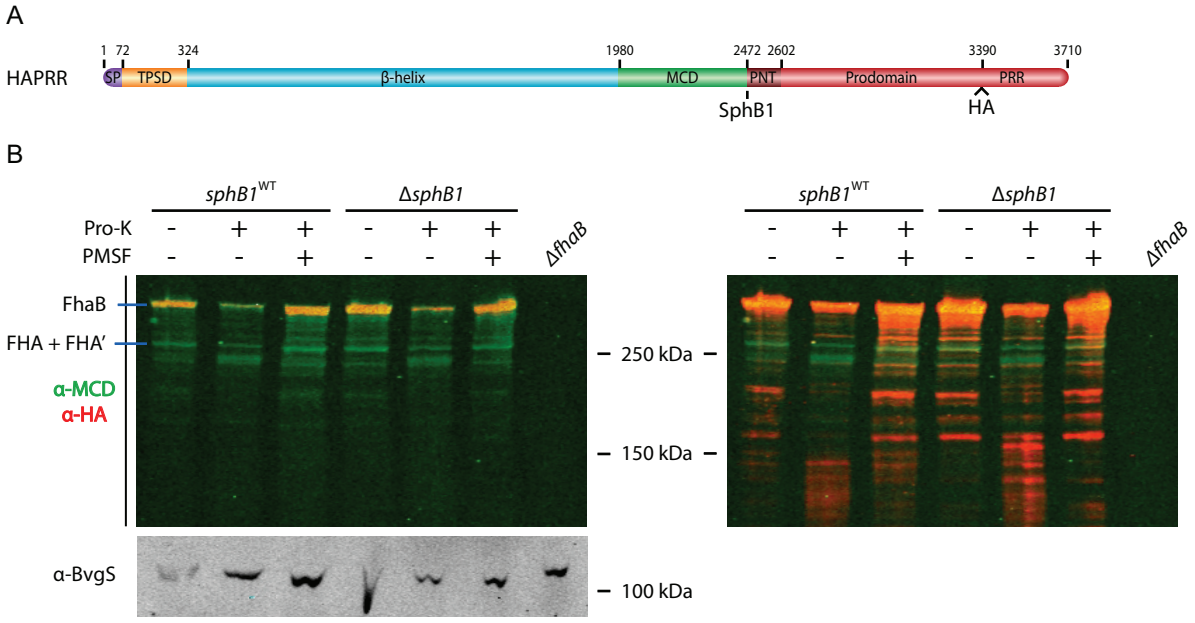

The C-terminus of the prodomain resides intracellularly during FHA maturation

A. Schematic of *B. bronchiseptica* HA-tagged FhaB protein used in proteinase-K digestion experiments. The site of the HA tag is noted. An HA tag was also introduced to a Δ*sphB1* background.
B. Left, anti-MCD (green) and anti-HA (red) immunoblot of proteinase-K treated whole-cells, lysed to evaluate cellular protein content. PMSF was added prior to proteinase-K incubation as indicated. The panel on the right is an analysis of the immunoblot on left, with the intensity of the 700 nm (anti-HA) channel increased for visualization of proteinase-K dependent intracellular prodomain. Bottom, anti-BvgS immunoblot of whole-cell lysates.

full-length, unprocessed FhaB (~375 kDa) was detected by both anti-MCD and anti-HA antibodies and mature FHA (FHA and FHA′, ~250 kDa) was detected by only the anti-MCD antibody. Some polypeptides of ~200 kDa were also detected by the anti-HA antibody (evident in the right panel), suggesting they result from proteolysis near the N-terminus of FhaB. Since FHA is anchored to the cell surface by its N-terminus, we hypothesize that these polypeptides result from proteolysis during sample preparation. Consistent with previous results indicating that the prodomain is degraded rapidly after FhaB processing (Delisse-Gathoye et al., 1990; Mazar and Cotter, 2006), no polypeptide of ~130 kDa was recognized by the anti-HA antibody in the untreated samples. Proteinase-K treatment caused a decrease in the amount of full-length FhaB (and mature FHA) and PMSF inhibited this proteolysis, indicating that this proteolysis was proteinase-K-dependent. Concomitant with the proteinase-K-dependent decrease in FhaB was the appearance of polypeptides of ~230 kDa that were recognized by only the anti-MCD antibody (green channel) and polypeptides of ~120-140 kDa that were recognized by only the anti-HA antibody (Figure 11B, red channel in the right panel). Proteinase-K activity was confined to the extracellular space, as indicated by the integrity of BvgS, a sensor kinase that spans the cytoplasmic membrane and contains a large periplasmic domain. The ~230 kDa polypeptide that predominates after proteinase-K treatment is most likely the N-terminus and β-helical shaft region of FHA, consistent with β-helical proteins' resistance to proteinase-K (Ieva and Bernstein, 2009; Julio et al., 2009). The appearance of cell-associated HA-containing polypeptides of ~120-140 kDa after

proteinase-K treatment, but not before proteinase-K treatment, suggests that they arose from polypeptides in which the C-terminus of the prodomain was intracellular while the central region of FhaB (most of the β-helical shaft, the MCD, and perhaps the N-terminus of the prodomain) was extracellular. In the Δ*sphB1* strain, more polypeptides in the range of ~120-160 kDa were recognized by the anti-HA antibody in the proteinase-K treated sample than in the proteinase-K treated sample of the strain that is wild-type for *sphB1* (Figure 11B, right). These data suggest that the C-terminus of the prodomain remains in an intracellular compartment during outer membrane translocation of the β-helix and MCD regions, but these data cannot distinguish between periplasmic versus cytoplasmic localization of the prodomain C-terminus.

The region surrounding FhaB maturation sites is required for the C-terminus of the prodomain to remain in an intracellular compartment and for mature FHA to be released from the cell surface

Although the data shown in Figure 11 suggest an intracellular location for the FhaB prodomain, the experiment is complicated by the fact that FhaB is processed by both SphB1 and one or more unidentified proteases, making it difficult to 'capture' the pre-cleavage FhaB secretion intermediate. In an attempt to eliminate both SphB1-dependent and SphB1-independent processing, we constructed a strain (HA-ΔCS) producing an FhaB protein with a 431 aa deletion encompassing the known SphB1-dependent cleavage sites and the region that becomes the C-terminus of

FHA′, which is produced by cleavage/degradation by the unidentified protease(s). The FhaB produced by this strain contains an HA epitope N-terminal to the PRR, the same as in the HAPRR strain (Figure 12A). Unprocessed FhaB in the HA-ΔCS strain was smaller than FhaB in wild-type bacteria (consistent with the size of the deletion) and was detected with both anti-MCD and anti-HA antibodies [(Figure 12B, band 5). Illustrations to the right of Figure 12B illustrate how we envision FhaB/FHA exist on the cell surface with and without proteinase-K treatment. Band numbers on the Western blot correspond to illustration numbers]. Unexpectedly, FhaB was still processed in this strain, resulting in the formation of polypeptides of ~250 and ~220 kDa [Figure 12B, bands 6 (green)] that were detected only by the anti-MCD antibody and therefore represent the N-terminal ~2300-2500 aa of FhaB. Processing to form these polypeptides did not occur in a strain that was isogenic except for deletion of *sphB1* (referred to as HA-ΔCS,Δ*sphB1*), indicating that the processing was SphB1-dependent (Figure 12B). (Note, however, that this strain contained an increased amount of FhaB in whole-cell lysate and many breakdown products were present that were recognized by the anti-HA antibody and therefore resulted from degradation from the N-terminus of FhaB, presumably during sample preparation.) Proteinase-K treatment of the HA-ΔCS strain resulted in cleavage of FhaB and FHA (Figure 12B, band 7), but no polypeptides recognized by the anti-HA antibody were generated that could be detected in whole-cell lysate. This result suggested that, in contrast to the case of wild-type bacteria, the C-terminus of the prodomain was not retained intracellularly in the HA-ΔCS strain. Comparison of proteins present in culture supernatants showed that wild-type and Δ*sphB1* bacteria released FHA and

Figure 12

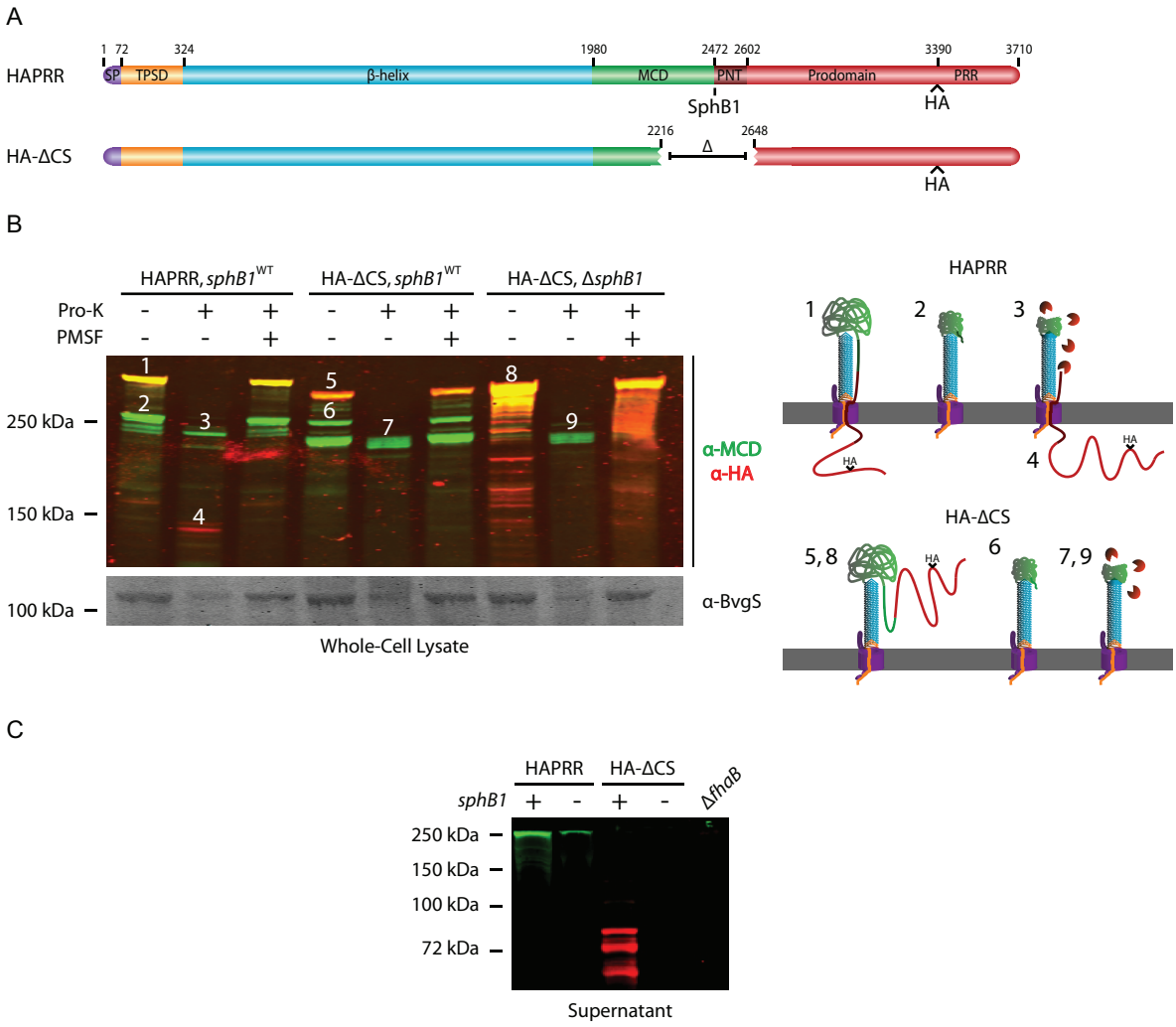
A
HAPRR
1 72 324 1980 2472 2602 3390 3710
SP TPSD β-helix MCD PNT Prodomain PRR
SphB1
HA
HA-ΔCS
2216 Δ 2648
HA
B
HAPRR, sphB1WT
HA-ΔCS, sphB1WT
HA-ΔCS, ΔsphB1
Pro-K
PMSF
250 kDa
150 kDa
100 kDa
α-MCD
α-HA
α-BvgS
Whole-Cell Lysate
HAPRR
HA-ΔCS
C
HAPRR
HA-ΔCS
sphB1
ΔfhaB
250 kDa
150 kDa
100 kDa
72 kDa
Supernatant

Figure 12

The region surrounding the native SphB1-dependent cleavage site regulates FHA release and keeps the C-terminus of the prodomain intracellular

A. Schematic of proteins used in proteinase-K digestion experiments. The ΔCS mutation was also made in a Δ*sphB1* background.
B. Top, anti-MCD (green) and anti-HA (red) immunoblot of whole-cell lysate of the cleavage-site deletion strain. Cells were incubated with proteinase-K as indicated. PMSF was added prior to proteinase-K incubation as indicated. Numbers above protein bands correspond to illustrations on the right side of the figure. Illustrations 1-4 represent products of the HAPRR strain, while illustrations 5-9 represent products of the HA-ΔCS strain. These illustrations show how we envision FhaB/FhaC exist at the outer membrane (OM, gray), with the area above the OM representing the extracellular space and the region below the OM representing the intracellular space. Proteinase-K is colored orange. Illustrations are not drawn to scale. Bottom, anti-BvgS immunoblot of whole-cell lysates.
C. Anti-MCD (green) and anti-HA (red) immunoblot of concentrated supernatants. Samples were run on an 8% polyacrylamide gel to resolve the released forms of FHA and prodomain.

FHA′, respectively, and did not release HA-containing polypeptides into the extracellular environment (Figure 12C). By contrast, the HA-ΔCS strain released a large amount of HA-containing polypeptides of about 50-80 kDa, but released no mature FHA into the culture supernatant. (Proteins were separated using an 8% polyacrylamide gel for the immunoblot shown in Figure 12C, which allows lower molecular weight proteins to be visualized, but limits resolution of higher molecular weight proteins.) The prodomain, therefore, appears to not be retained intracellularly in the HA-ΔCS strain and not only are prodomain polypeptides released into the culture supernatant, they are relatively stable. In the HA-ΔCS,Δ*sphB1* strain, FhaB remained predominantly unprocessed, as whole-cell lysate contained mostly full-length FhaB and several breakdown products, but no polypeptides corresponding to FHA. Proteinase-K treatment of the HA-ΔCS,Δ*sphB1* strain resulted in the formation of a predominant polypeptide of about 220 kDa that was recognized by the anti-MCD antibody but not the anti-HA antibody (Figure 12B, band 9), therefore corresponding to the β-helical shaft and part of the MCD. No HA-containing polypeptides were released into the culture supernatant of the HA-ΔCS,Δ*sphB1* strain, consistent with the conclusion that processing of FhaB does not occur in this strain and that the HA-containing polypeptides present in the supernatants of the HA-ΔCS strain were extracellularly located prodomain fragments released after SphB1-dependent processing. Together, these data indicate that sequences within the region deleted in the HA-ΔCS strain are required for retention of the C-terminal region of the prodomain in an intracellular compartment and are also required for release of mature FHA into the extracellular environment. Although some degradation of BvgS

by proteinase-K was evident in this experiment, indicating that some amount of proteinase-K entered the cells, the presence of large amounts of HA-stained polypeptides of ~75 kDa in supernatants of the HA-ΔCS strain, but no HA-containing polypeptides in supernatants of wild-type *B. bronchiseptica,* strongly suggests that the prodomain is retained in an intracellular compartment in wild-type bacteria but not in HA-ΔCS bacteria. Complete elimination of HA-containing polypeptides in the HA-ΔCS,Δ*sphB1* strain after proteinase-K treatment also supports this conclusion.

As an alternate approach, we performed dot blots of the HAPRR and HA-ΔCS strains (Figure 13). Whole cells in PBS were applied to a nitrocellulose membrane for detection of surface antigens and boiled lysates were applied to the membrane for detection of total cellular protein content. Whole cells of the HAPRR strains (*sphB1*^{WT} and Δ*sphB1* backgrounds) were stained by only the anti-MCD antibody (Figure 13B; note that the schematics below the dot blots indicate only the various polypeptide species, not their relative abundances). Boiling the samples however, allowed detection by both the anti-MCD and anti-HA anti-bodies, indicating that the C-terminus of the prodomain in the HAPRR strains was located intracellularly. In the HA-ΔCS strain (*sphB1*^{WT}), there was no surface detection of HA epitopes, consistent with the previous result indicating SphB1-dependent cleavage and release of a surface-localized prodomain in this strain. Boiling the sample resulted in weak detection of the HA tag, which we hypothesize represents FhaB molecules prior to translocation across the outer membrane. In the HA-ΔCS,Δ*sphB1* strain, detection of both surface proteins and cell lysate revealed MCD and HA epitopes, consistent

Figure 13

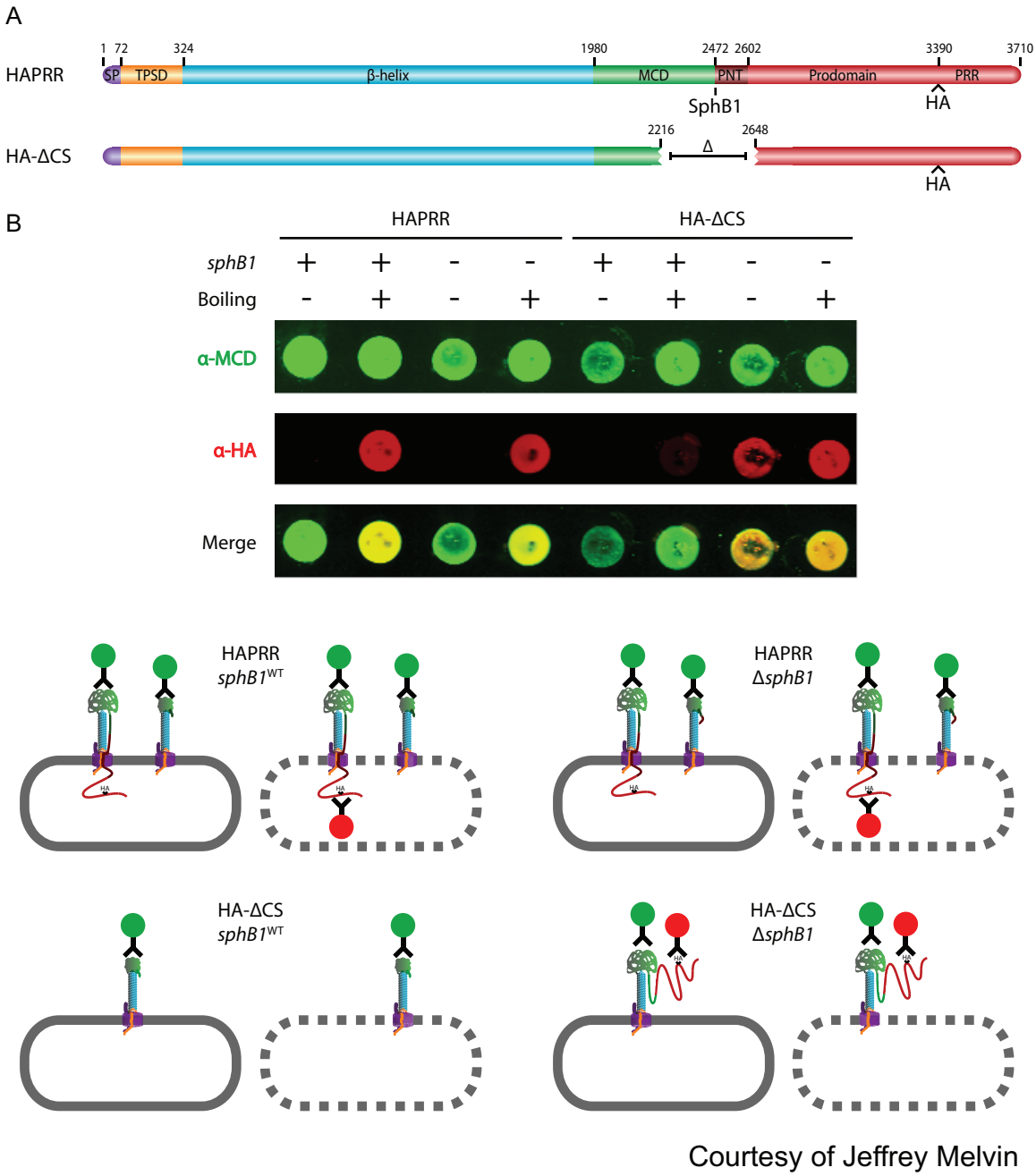
A
HAPRR
1 72 324 1980 2472 2602 3390 3710
SP TPSD β-helix MCD PNT Prodomain PRR
SphB1
HA
HA-ΔCS
2216 2648
Δ
HA
B
HAPRR
HA-ΔCS
sphB1 + + - - + + - -
Boiling - + - + - + - +
α-MCD
α-HA
Merge
HAPRR sphB1WT
HAPRR ΔsphB1
HA-ΔCS sphB1WT
HA-ΔCS ΔsphB1
Courtesy of Jeffrey Melvin

Figure 13

The prodomain C-terminus of full-length FhaB remains intracellular

A. Schematic of proteins used in dot blot experiments. The ΔCS mutation was also made in a Δ*sphB1* background.
B. At the top, anti-MCD (green) and anti-HA (red) immuno-dot-blot of HAPRR and HA-ΔCS strains. Normalized amounts of whole cells and boiled lysates were applied. Below, illustrations of immuno-stained samples. The rounded gray rectangle represents the *B. bronchiseptica* outer membrane, with a solid edge representing the outer membrane of an intact cell and a dashed edge representing an outer membrane disrupted by boiling. MCD staining is represented by green-circled antibodies and HA staining is represented by red-circled antibodies.

with idea that the prodomain crossed the outer membrane, but was not cleaved in the absence of SphB1. [Note: The Western blot in Figure 12B indicates that some full-length, surface-exposed FhaB is present in the HA-ΔCS,*sphB1*^{WT} strain (band 5). Although very faint staining of this strain by the anti-HA antibody was apparent in some dot blot experiments, it is not apparent in the one shown in Figure 13B. Lack of significant staining by dot blot compared with Western blot may be due to differences in sample preparation and differences in sensitivity of the two assays.] As a control, a *B. bronchiseptica* strain without an HA tag in FhaB (RBX11) was used in an identical experiment. Although both whole cells and boiled lysates were recognized by the anti-MCD antibody, neither were recognized by the anti-HA antibody (Figure 14B), demonstrating that there was no nonspecific fluorescence in our samples probed with the anti-HA antibody. Taken together, these data indicate that the C-terminus of the prodomain is retained in an intracellular compartment (either the periplasm or the cytoplasm) during translocation and maturation of FHA and that the prodomain is degraded rapidly after SphB1-dependent and/or SphB1-independent processing when retained intracellularly. Sequences within the region deleted in the HA-ΔCS strain are required for the C-terminus of the prodomain to remain intracellular and for mature FHA to be released from the cell surface.

The C-terminus of the MCD controls FHA release competency while the N-terminus of the prodomain controls intracellular prodomain retention

To investigate which sequences within the region deleted in the HA-ΔCS

Figure 14

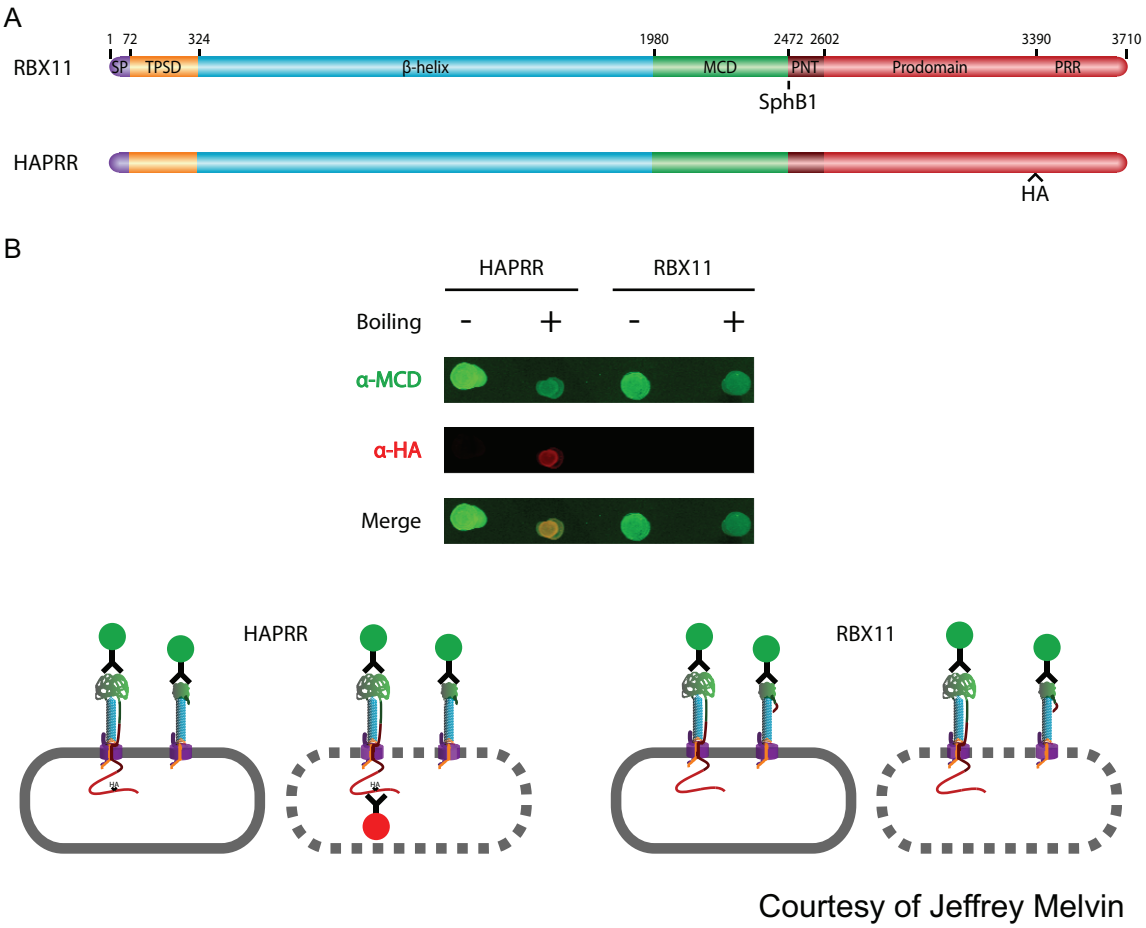

Courtesy of Jeffrey Melvin

Introduction of an HA tag to the FhaB prodomain suggests an intracellularly-localized prodomain

A. Schematic of FhaB proteins used in experiment.
B. At the top, anti-MCD (green) and anti-HA (red) immuno-dot-blot of HAPRR and RBX11 strains. Normalized amounts of whole cells and boiled lysates were applied. Below, illustrations of immuno-stained samples. Layout of these illustrations is as described in Figure 12B.

strain were responsible for retention of the prodomain in an intracellular compartment and for release of mature FHA, we constructed strains producing FhaB proteins with either a 255 aa deletion of the MCD C-terminus (the MCT, shaded dark green in Figure 15) or a 176 aa deletion of the prodomain N-terminus (the PNT, shaded dark red). These strains, which contain the sequence encoding an HA epitope just 5′ to the PRR-encoding region, were named HA-ΔMCT and HA-ΔPNT, respectively. The ΔPNT deletion encompasses the primary SphB1-dependent cleavage site (the sequence of which is PLFETRIKFID).

Immunoblot analysis (resolved by 5% polyacrylamide SDS-PAGE) showed that both unprocessed and processed FhaB/FHA polypeptides were detectable in whole-cell lysate of the HA-ΔMCT strain (Figure 15B, bands 8 and 9, respectively. Bands of the Western blot and illustration are labeled as in Figure 12B). In addition, a polypeptide of ~150 kDa that was recognized by both anti-MCD and anti-HA antibodies (Figure 15B, band 10), as well as a few slightly smaller polypeptides, was detected. Recognition of the ~150 kDa polypeptide by both antibodies indicates that it includes the prodomain and at least part of the MCD. These polypeptides were not detected in whole-cell lysate of the HA-ΔMCT strain that also contained the Δ*sphB1* deletion, demonstrating that they resulted from SphB1-dependent cleavage. The fact that analogous polypeptides are not present in the HAPRR strain suggests that SphB1-independent cleavage/degradation of the prodomain is inefficient in the HA-ΔMCT strain, since SphB1-independent cleavage would have separated the MCD part of the polypeptide from the C-terminus. The presence of these polypeptides in

Figure 15

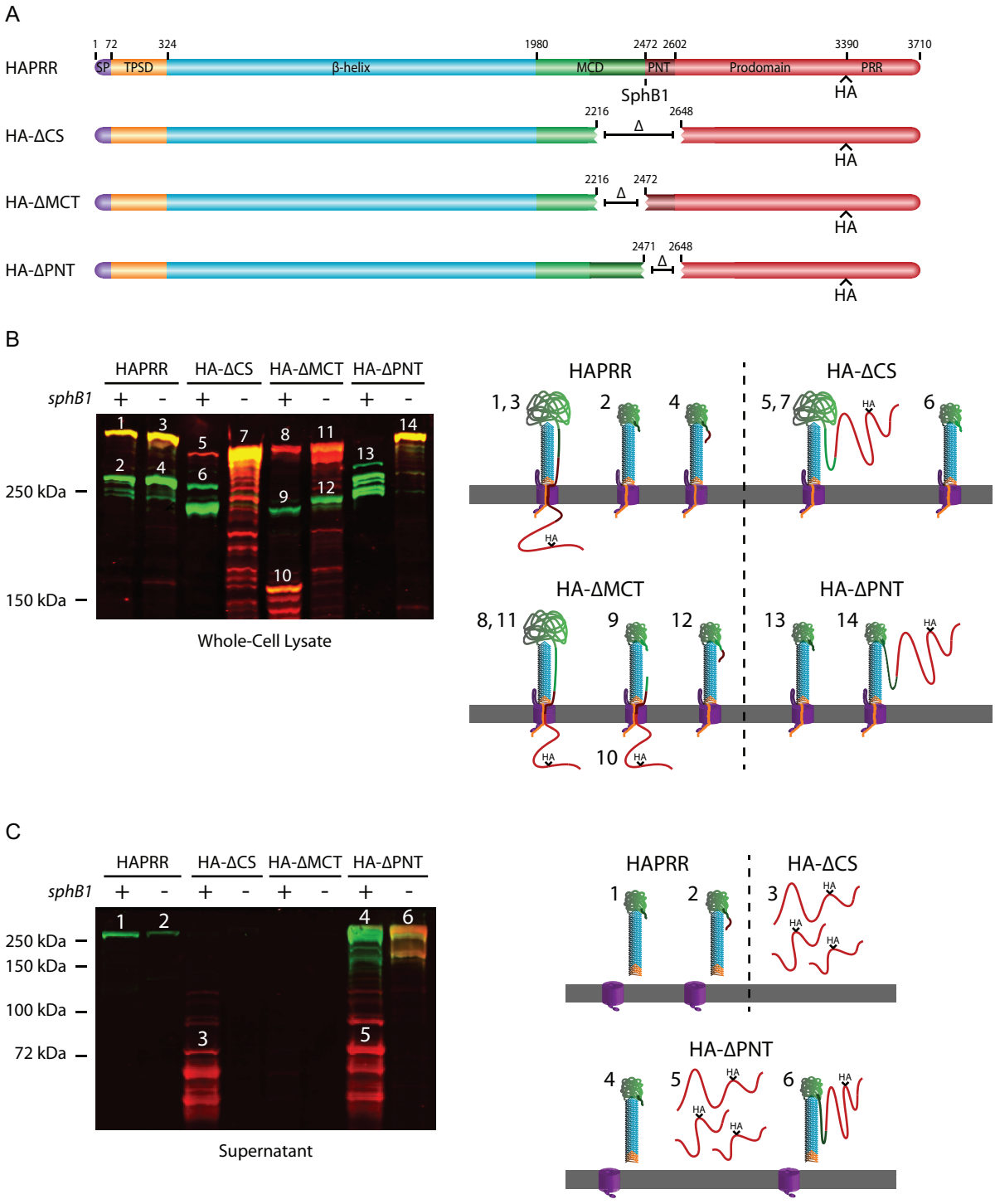
A
HAPRR
SP
TPSD
β-helix
MCD
PNT
Prodomain
PRR
SphB1
HA
HA-ΔCS
HA-ΔMCT
HA-ΔPNT
Δ
B
HAPRR
HA-ΔCS
HA-ΔMCT
HA-ΔPNT
sphB1
250 kDa
150 kDa
Whole-Cell Lysate
C
100 kDa
72 kDa
Supernatant

Figure 15

The MCT controls FHA release and the PNT keeps the prodomain C-terminus intracellular

A. Schematic of FhaB proteins used in experiment. The MCT is represented as dark green. Mutations were also made in a Δ*sphB1* background.
B. Anti-MCD (green) and anti-HA (red) immunoblot of whole-cell lysates. Numbers above protein bands correspond to illustrations on the right side of the figure. Illustrations 1-4 represent products of the HAPRR strain, 5-7 represent products of the HA-ΔCS strain, 8-12 represent products of the HA-ΔMCT strain, and 13 and 14 represent products of the HA-ΔPNT strain. Layout of these illustrations is as described in Figure 12B.
C. Anti-MCD (green) and anti-HA (red) immunoblot of concentrated supernatants. Numbers above protein bands correspond to illustrations on the right side of the figure. Illustrations 1 and 2 represent products of the HAPRR strain, 3 represents the product of the HA-ΔCS strain, and 4-6 represent products of the HA-ΔPNT strain. Layout of these illustrations is as described in Figure 12B. Deletion of the MCT prevents FHA release, while deletion of the PNT promotes release. Additionally, deletion of the PNT results in translocation of the prodomain into the extracellular space where it can be separated from FHA in an SphB1-dependent manner.

whole-cell lysate, but not in supernatants (Figure 15C; proteins in culture supernatants were resolved using an 8% polyacrylamide gel, allowing lower molecular weight proteins to be visualized at the expense of separating higher molecular weight proteins), also indicates that the C-terminus of the prodomain is present in an intracellular compartment in this strain as these polypeptides would have been released into the supernatant fraction if they had been located extracellularly. In whole-cell lysate of the HA-ΔMCT strain that also contains the Δ*sphB1* deletion, more unprocessed FhaB protein was detected, as well as a polypeptide of about 230 kDa, which is presumably a product of cleavage by the unidentified protease(s) (Figure 15B, bands 11 and 12, respectively). No polypeptides of any size were detected by either antibody in supernatant fractions of the HA-ΔMCT strain, regardless of whether *sphB1* was wild-type or deleted, indicating that the MCT is required for FHA release. The MCT, therefore, is required for release of FHA, but not for intracellular retention of the prodomain.

In the HA-ΔPNT strain, FhaB was extensively processed, resulting in the formation of several polypeptides of around 250 kDa (Figure 15B, bands 13). The processing was SphB1-dependent as only full-length FhaB, which was recognized by both the anti-MCD and anti-HA anti-bodies, was present in whole-cell lysate of the HA-ΔPNT strain that also contained the Δ*sphB1* deletion (Figure 15B, band 14). The HA-ΔPNT strain released a large amount of ~250 kDa polypeptides that were recognized by only the anti-MCD antibody and lower molecular weight (~50-100

kDa) polypeptides that were recognized only by the anti-HA antibody, into the culture supernatant (Figure 15C, bands 4 and 5, respectively). The HA-ΔPNT strain with the Δ*sphB1* deletion released a large amount of full-length protein that was recognized by both antibodies (Figure 15C, band 6). These results indicate that sequences within the PNT are required for retention of the C-terminus of the prodomain in an intracellular compartment and are not required for release of FhaB/FHA from the cell surface. In fact, the HA-ΔPNT strain releases more FhaB/FHA from the surface than the wild-type strain, suggesting that the PNT influences FHA release in a negative manner.

To further investigate the location of the prodomain in the HA-ΔMCT and HA-ΔPNT strains, we performed dot blots (Figure 16). In the HA-ΔMCT strain (*sphB1*^{WT}), only the MCD, and not the HA epitope, was detected on the surface of whole cells (Figure 16B; note that as with Figure 13B, the schematics below the dot blots indicate only the various polypeptide species, not their relative abundances). Lysing these cells resulted in detection of the HA tag, indicative of an intracellular prodomain C-terminus. Whole cells of the HA-ΔMCT,Δ*sphB1* strain were detected at a low level by the anti-HA antibody, suggesting that some prodomain C-terminus was surface-localized. This result suggests that lack of the MCT can overcome, to some extent, the ability of the PNT to block translocation of the prodomain through FhaC to the cell surface. If so, then in the HA-ΔMCT strain that is wild-type for *sphB1,* the small amount of prodomain that is translocated to the surface would be cleaved in an SphB1-dependent manner and released into the supernatant. Indeed,

Figure 16

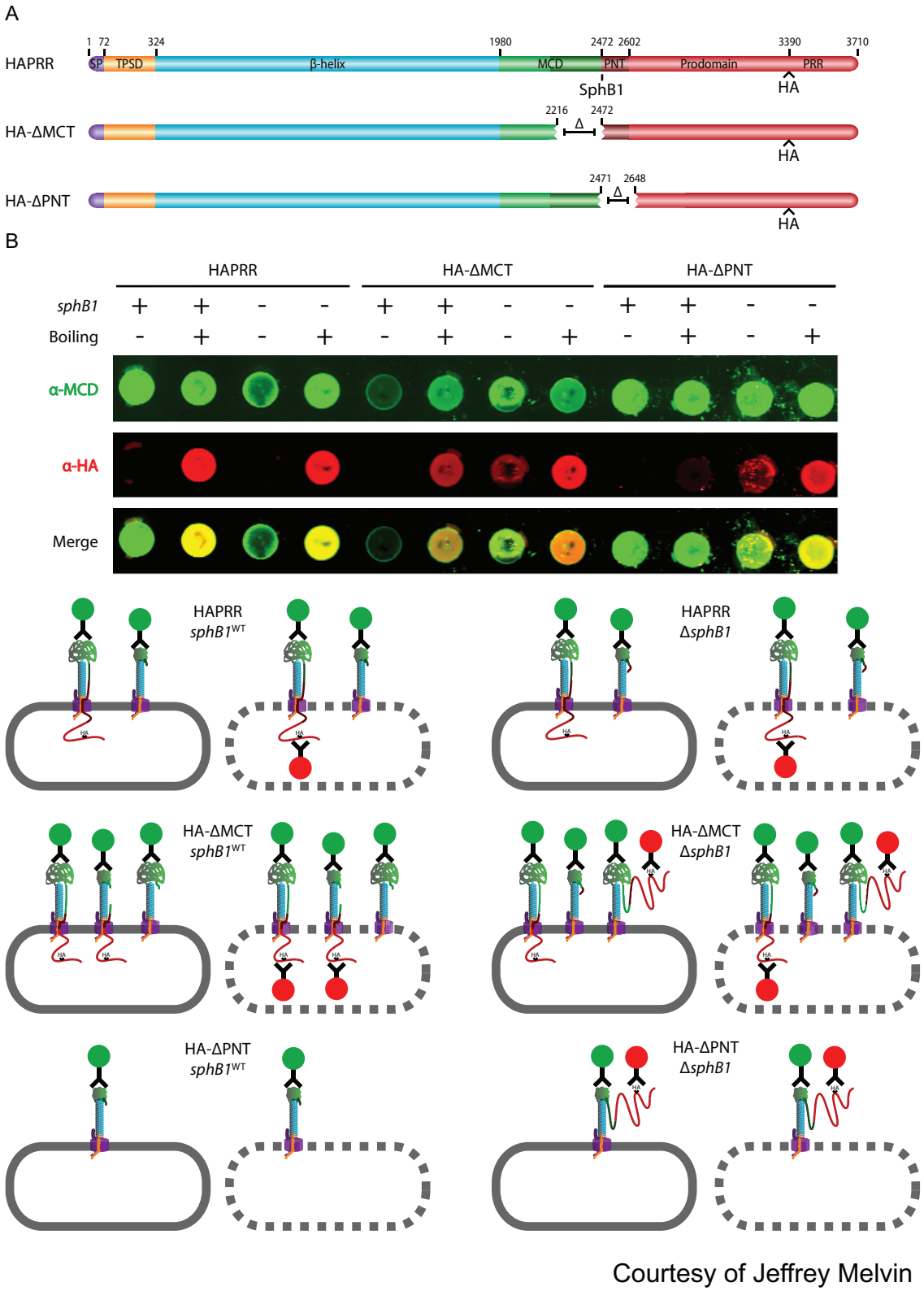

Courtesy of Jeffrey Melvin

Figure 16

The prodomain of the HA-ΔMCT strain is mostly intracellularly localized while that of the HA-ΔPNT strain is extracellularly localized

A. Schematic of proteins used in dot blot experiments. Mutations were also made in a Δ*sphB1* background.
B. At the top, anti-MCD (green) and anti-HA (red) immuno-dot-blot of HAPRR, HA-ΔMCT and HA-ΔPNT strains. Normalized amounts of whole cells and boiled lysates were applied. Below, illustrations of immuno-stained samples. Layout of these illustrations is as described in Figure 13B.

a closer analysis of concentrated supernatants revealed that the HA-ΔMCT strain released cleaved prodomain polypeptides, albeit much less efficiently than the HA-ΔCS and HA-ΔPNT strains (Figure 17B). Boiling the HA-ΔMCT,Δ*sphB1* strain increased detection by the anti-HA antibody, indicating that although some prodomain crossed the outer membrane, most of it was retained intracellularly.

In the HA-ΔPNT strain (*sphB1*^{WT}), no HA epitopes were detected on the surface of whole-cells (Figure 16B), consistent with the previous observation of extensive SphB1-dependent cleavage of surface-localized prodomain (which was also observed in the HA-ΔCS strain). Boiling these cells resulted in weak detection of the HA tag, which, as with the HA-ΔCS strain, likely represents FhaB prior to translocation across the outer membrane. In the HA-ΔPNT,Δ*sphB1* strain, both the anti-MCD and the anti-HA antibodies were able to detect surface protein, consistent with the prodomain crossing the outer membrane but not being cleaved in the absence of SphB1. Collectively, these data implicate the PNT as the subdomain responsible for intracellular localization of the prodomain C-terminus.

Figure 17

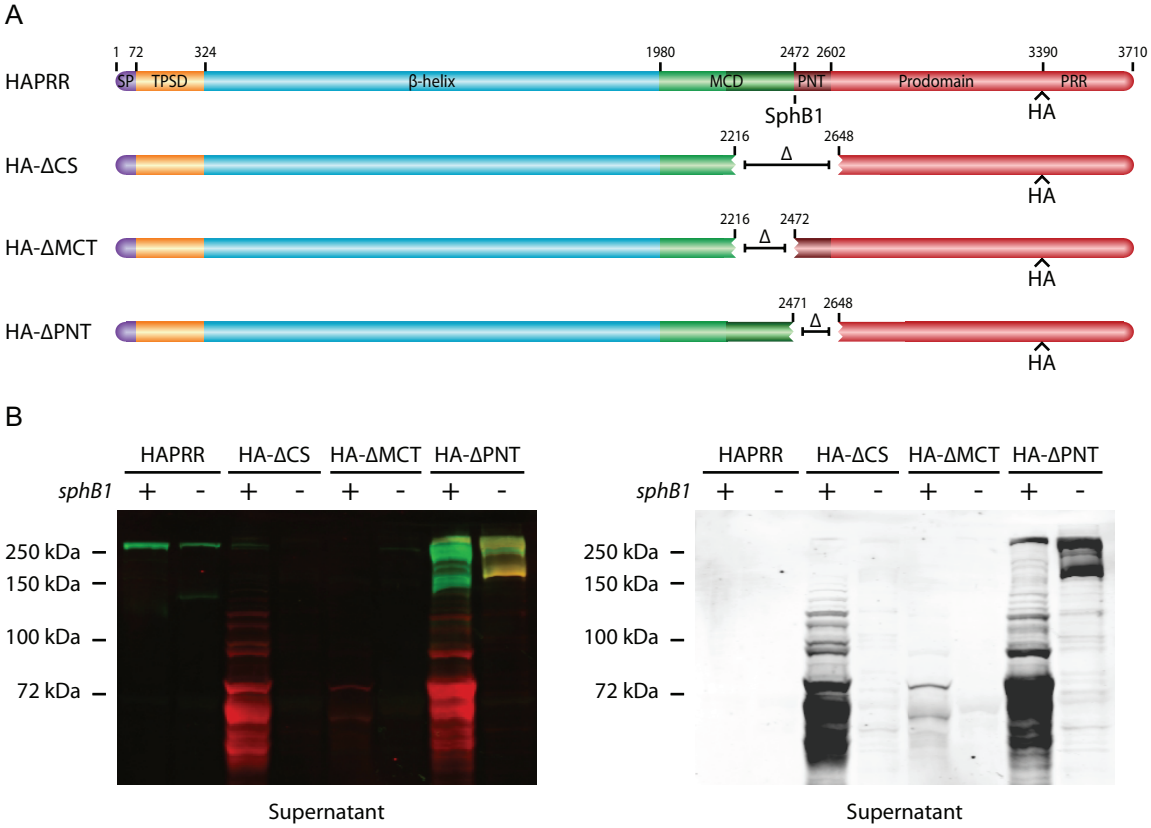

A small amount of prodomain is released from *B. bronchiseptica* with a deletion of the MCT

A. Schematic of FhaB proteins used in experiment. Domain layout is the same as that of Figure 14A. Mutations were also made in a Δ*sphB1* background.
B. Anti-MCD (green) and anti-HA (red) immunoblot of concentrated supernatants. On the left is a merge showing release of prodomain from HA-ΔCS, HA-ΔMCT, and HA-ΔPNT strain. On the right is an image of the same immunoblot, with the 700 nm (red) channel isolated and enhanced to facilitate the visualization of prodomain bands released into the supernatant of the ΔMCT strain.

Chapter IV – Identification of C-terminal determinants of FHA release

The MCD appears to contain determinants of FHA release

One of the unexpected results of deletion of the MCT was the prevention of FHA release from the surface of *B. bronchiseptica* (Figure 15C). This result prompted us to examine the extent of MCD-dependent FHA release. ΔMCD-PD (which contains a deletion of the region encoding the MCD and prodomain) and Δ28-PD (a strain that produces FhaB lacking the 28 aa absent from FhaS MCD and the entire prodomain) contain greater levels of protein corresponding to FHA in whole cell lysates than seen in RBX11 (Figure 18B). Concentrated supernatants showed that both ΔMCD-PD and Δ28-PD released much less FHA than RBX11. RBX20 (deleted for *fhaB* and *fhaS*) was used as a negative control for FHA detection. It is worth noting that while Δ28-PD released very little FHA, a strain producing a slightly larger FhaB protein (ΔPD) released wild-type levels of FHA (Chapter 5, Figure 20), suggesting that the 147 aa difference at these strains' C-termini could be a key determinant of release potential.

To expand our analysis, we constructed a strain with an in-frame deletion of the entire MCD (HA-ΔMCD) and a strain with a deletion of the MCD N-terminus (HA-ΔMNT). We also constructed a strain in which a stop codon was introduced before

Figure 18

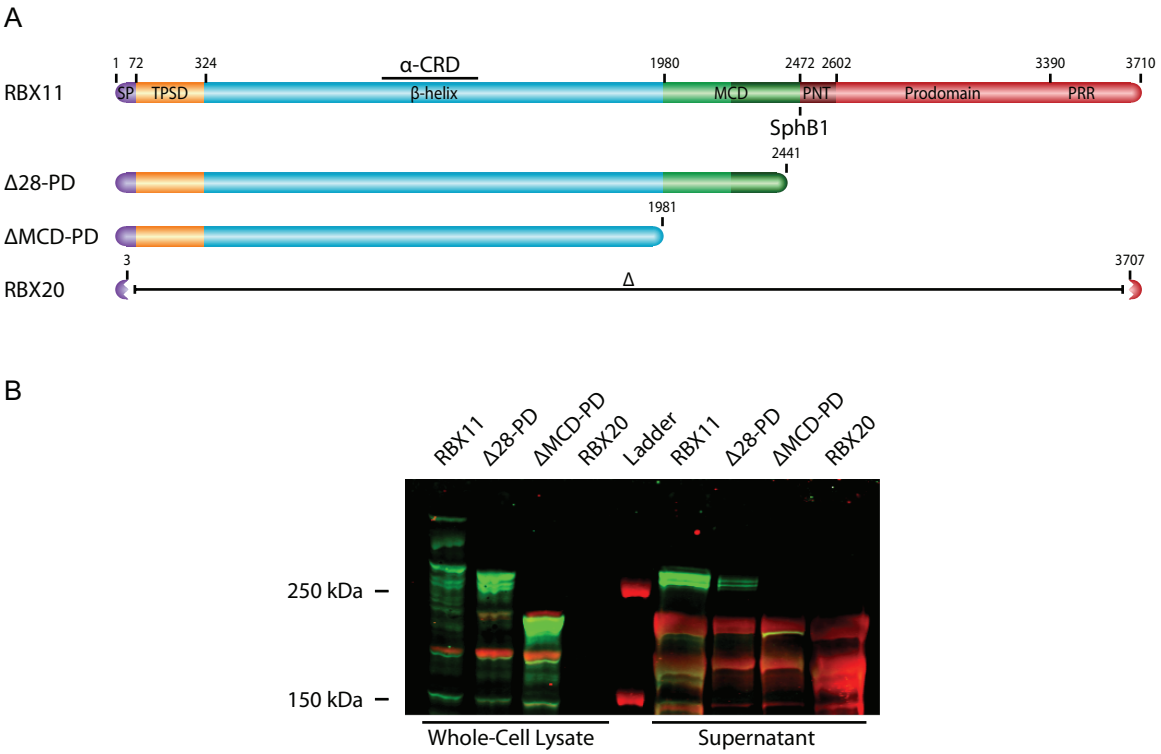

FhaB truncations within the MCD reduce FHA release efficiency

A. Schematic of FhaB proteins used in experiment.
B. Anti-CRD (green) and anti-CyaA (red) immunoblot of whole-cell lysates and concentrated supernatants. FhaB with truncations of the MCD result in increased levels of FHA in WCL and decreased levels of FHA in concentrated supernatants.

the MCT (ΔMCT-PD). While Western blot analysis of whole-cell lysate shows that these strains all contain cellular FhaB (Figure 19B), concentrated supernatants indicates that in all of these strains, mature FHA was poorly released from the cell surface (Figure 19C), reinforcing the idea that the MCD is an important determinant of FHA release competency.

While the above results indicate that the MCD plays an important role in the release of FHA from the cell surface, they also indicate that the FhaB prodomain is not a release determinant. This is best exemplified by MCD mutants made in wild-type and prodomain-deleted backgrounds. Comparison of i) ΔMCD-PD to HA-ΔMCD and ii) ΔMCT-PD to HA-ΔMCT demonstrated that the presence or absence of the prodomain alone does not affect FHA release. Though the results are preliminary, by identifying the FhaB MCD as a determinant of release competency, we further our understanding of the mechanism by which FHA is released from the cell surface. Previous reports arguing that the N-terminal 80 kDa of FhaB contain FHA-release information are only partially true, as it is now clear that sequences across the entire FHA protein may contribute to release competency.

Figure 19

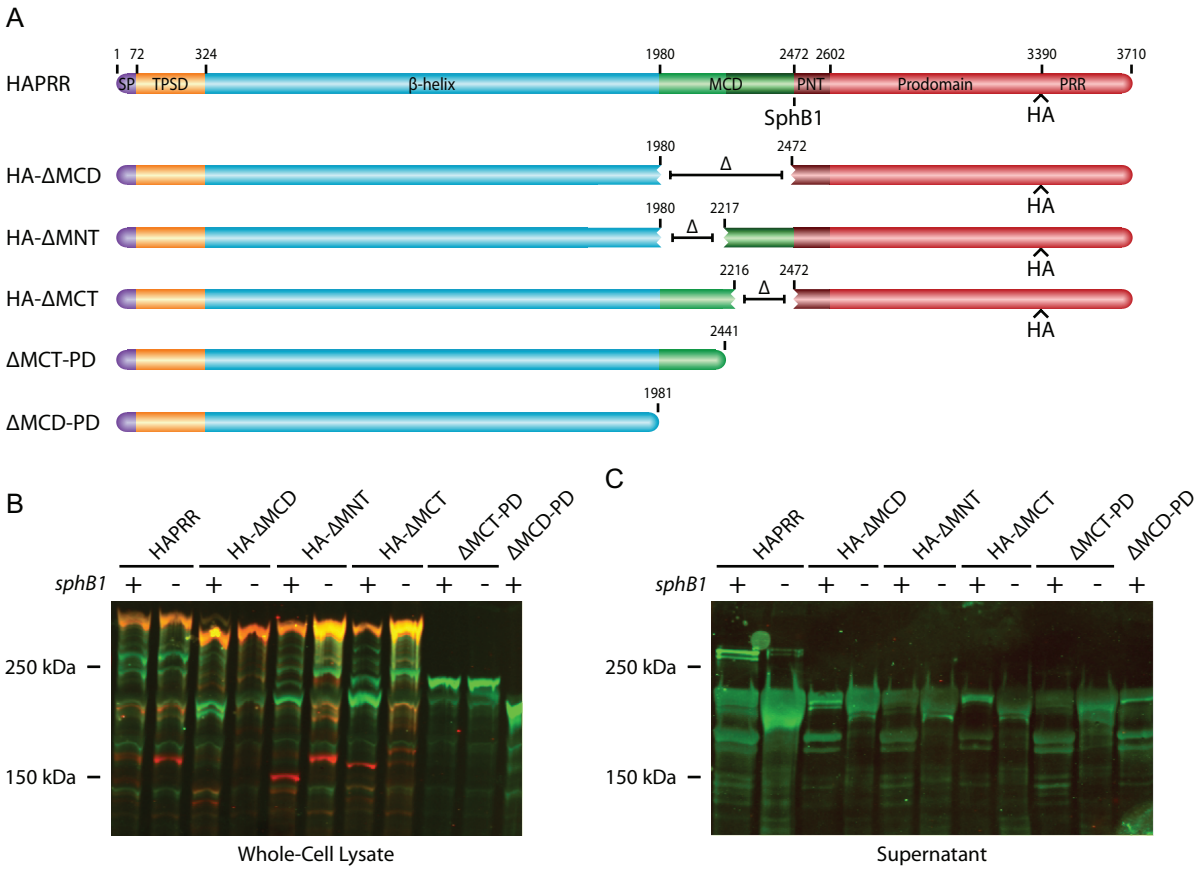

Deletion and truncations within the FhaB MCD reduce FHA release efficiency

A. Schematic of FhaB proteins used in experiment. Mutations were also made in a Δ*sphB1* background.
B. Anti-CRD (green) and anti-HA (red) immunoblot of whole-cell lysates.
C. Anti-CRD (green) immunoblot of concentrated supernatants. On the membrane onto which concentrated supernatants were transferred, CyaA was stained nonspecifically with anti-CRD antibody, resulting in false positives for FHA release.

Chapter V – Identification and characterization of additional subdomains of the FhaB prodomain

The prodomain comprises several distinct subdomains

Having demonstrated that the FhaB prodomain N-terminus (PNT) serves as an important subdomain for prodomain localization, we sought more specifically to identify subdomains that may have a role in FHA biogenesis and function. Residues 3390-3612 (numbering relative to FhaB of *B. bronchiseptica* RB50) contain a high number of prolines (Figure 5). The sequence of this proline-rich region (PRR) is highly conserved across all FhaB proteins of the *Bordetella* genus, but has no similarity to other bacterial proteins. Predictions using PHYRE2, however, indicate that the PRR may share structural similarity to TonB (Kelley and Sternberg, 2009). TonB is a highly conserved protein involved in iron acquisition in Gram-negative bacteria. A proline-rich portion of the TonB protein spans the periplasm in order to interact with and transduce conformation-shifting signals to outer membrane transport proteins (Postle and Larsen, 2007). A $(PK)_5$ motif of TonB has been implicated in outer membrane protein association *in vitro* (Brewer et al., 1990), though *in vivo* functions remain uncertain. In TonB, this $(PK)_5$ motif appears to be important for dimerization of TonB proteins when proximal to outer membrane iron

transporters. A $(PK)_5$ motif is also present within the PRRs of *B. pertussis* and *B. parapertussis*, while a $(PA)_6(PK)_4$ motif is present in the same position in FhaB of *B. bronchiseptica*. C-terminal to the PRR, the 98 aa at the extreme C-terminus (ECT) of the prodomain (Figure 5) are identical amongst the nine FhaB proteins of *B. bronchiseptica*, *B. pertussis*, and *B. parapertussis* strains for which genome information is available (sequences provided by the Wellcome Trust Sanger Institute). However, this region shows no similarity to other proteins. The central region of the prodomain, residues 2602-3389, also shares no significant similarity with other proteins.

The extreme C-terminus of the prodomain is a negative regulator of SphB1-independent FhaB processing and is required for virulence

To investigate the roles of the prodomain subdomains C-terminal to the PNT in FHA maturation and secretion, we constructed strains with stop codons at various locations in *fhaB* and compared FhaB maturation and FHA secretion in these strains to that of wild-type *B. bronchiseptica* (Figure 20A). Whole-cell lysates of strains producing FhaB proteins that lack the ECT (ΔECT), the PRR and ECT (ΔPRR-ECT), or most of the prodomain (ΔPD), contained no detectable full-length FhaB protein and the amount of mature FHA appeared to be increased relative to the amount present in wild-type bacteria (Figure 20B). The ECT therefore appears to function as a negative regulator of FhaB maturation; in its absence, FhaB is 'hyper-processed' such that none of the preprocessed FhaB protein is detectable. The fact that the

Figure 20

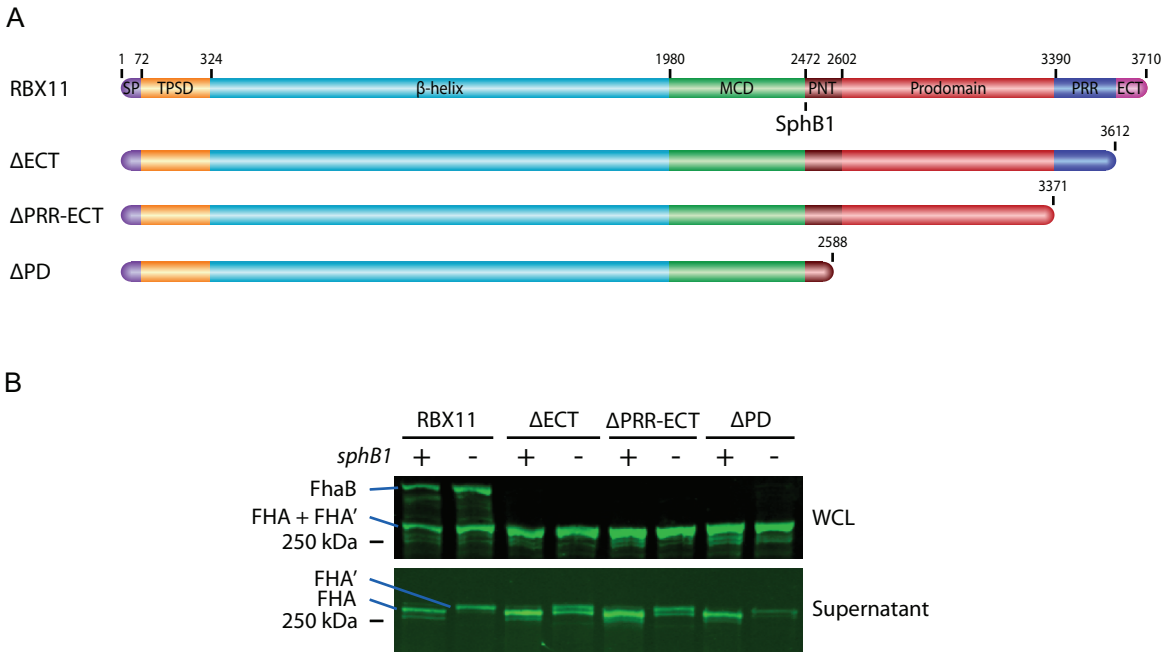

The ECT of the prodomain suppresses SphB1-independent processing of FhaB

A. Schematic of FhaB proteins used to demonstrate ECT suppression of SphB1-independent FhaB processing. Mutations were also made in a Δ*sphB1* background. B. Anti-MCD (green) immunoblot of strains used to demonstrate ECT-regulation of SphB1-independent of FhaB. In supernatant immunoblot, samples from wild-type *sphB1* background are diluted 1:2 in 1X sample buffer.

FhaB/FHA profiles in the ΔPRR-ECT and ΔPD strains were nearly identical to those of ΔECT strain suggests that either i) these regions of the prodomain do not contribute to FHA maturation in a manner that can be assessed using this assay, or ii) that deletion of the ECT is dominant to deletion of the other prodomain subdomains. The ECT-dependent hyper-processing of FhaB also occurred in Δ*sphB1* strains, indicating that the inhibitory activity of the ECT is directed at the unidentified protease and not SphB1. These data also suggest that the rate-limiting step in FhaB processing is cleavage by the unidentified protease.

The slightly different mobilities of FHA and FHA' are apparent in the immunoblot of proteins recovered from culture supernatants that is shown in Figure 20B. Slightly more FHA appeared to be released in ΔECT, ΔPRR-ECT and ΔPD, consistent with FhaB being hyper-processed in these strains, resulting in increased release of FHA. In Δ*sphB1* strains lacking the ECT, two mature polypeptides were detected – FHA′ and a slightly smaller protein. The latter is the size of the FHA isoform, but cannot be FHA since generation of FHA is SphB1-dependent. This suggests that in addition to affecting the rate of FhaB processing, the ECT may also affect the sites at which SphB1-independent cleavage occurs.

As mentioned in Chapter III (page 53), we originally constructed a strain producing FhaB with a hemagglutinin (HA) epitope seven residues N-terminal to the C-terminus of FhaB (CTHA) for prodomain localization studies (Figure 10). Immunoblot analysis indicated that FhaB was hyper-processed in this strain (Figure

10B), reminiscent of ECT truncations. These data suggest that the HA epitope of CTHA disrupted the function of the ECT and supports the conclusion that the ECT functions to inhibit FhaB processing.

We next examined *B. bronchiseptica* with truncations of the ECT *in vivo*. Mice were infected with ~5x10^4 CFU of either RBX11 (our wild-type *B. bronchiseptica* strain) or ΔECT. Lung burdens of both strains were the same 24 hpi (Figure 21B). At day 11, however, ΔECT had been completely cleared from the lungs while RBX11 persisted at a high level. Since the truncation in ΔECT was achieved by cointegration of a stop codon before the ECT, we wanted to be certain that the plasmid used for cointegration had not been lost from bacteria in the lungs. Plating of lung homogenates on LB-Gm plates revealed that no plasmid loss from cointegrates. Examination of histology showed RBX11-infected lungs with low to moderate inflammation at 24 hours and 11 days (Figure 22B). Interestingly, ΔECT induces an inflammatory response comparable to that of RBX11, despite complete clearance of bacteria 11 days post-infection.

The C-terminus of the MCD is required for relief of inhibition of the unidentified protease by the ECT

The presence of the ~150 kDa polypeptide recognized by both anti-MCD and anti-HA antibodies that was present in whole-cell lysate of the HA-ΔMCT strain (Figure 15B) suggests that the MCT may influence processing of FhaB by the

Figure 21

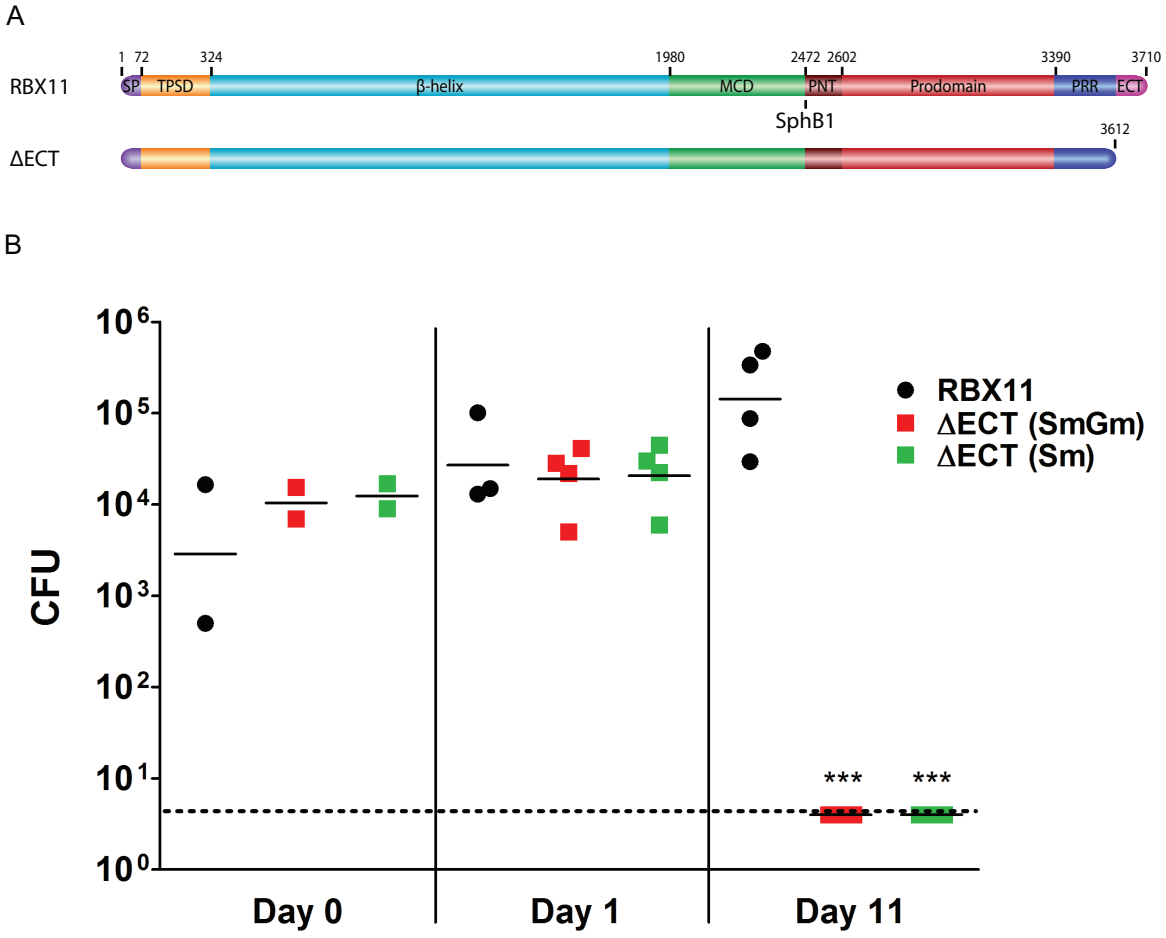

*** $p < 0.005$

Courtesy of Jeffrey Melvin and Kurtis Host

Truncation of the prodomain ECT causes a *Bordetella* persistence defect *in vivo*

A. Schematic of FhaB proteins in strains used to infect mice.
B. Bacterial burdens in mice. The right lungs of mice were harvested at the specified times, homogenized, and plated for burden counts. ΔECT homogenate was plated on BG-Sm and BG-SmGm plates to ensure that plasmid was not lost from the strain. Experiments were performed in duplicate.

Figure 22

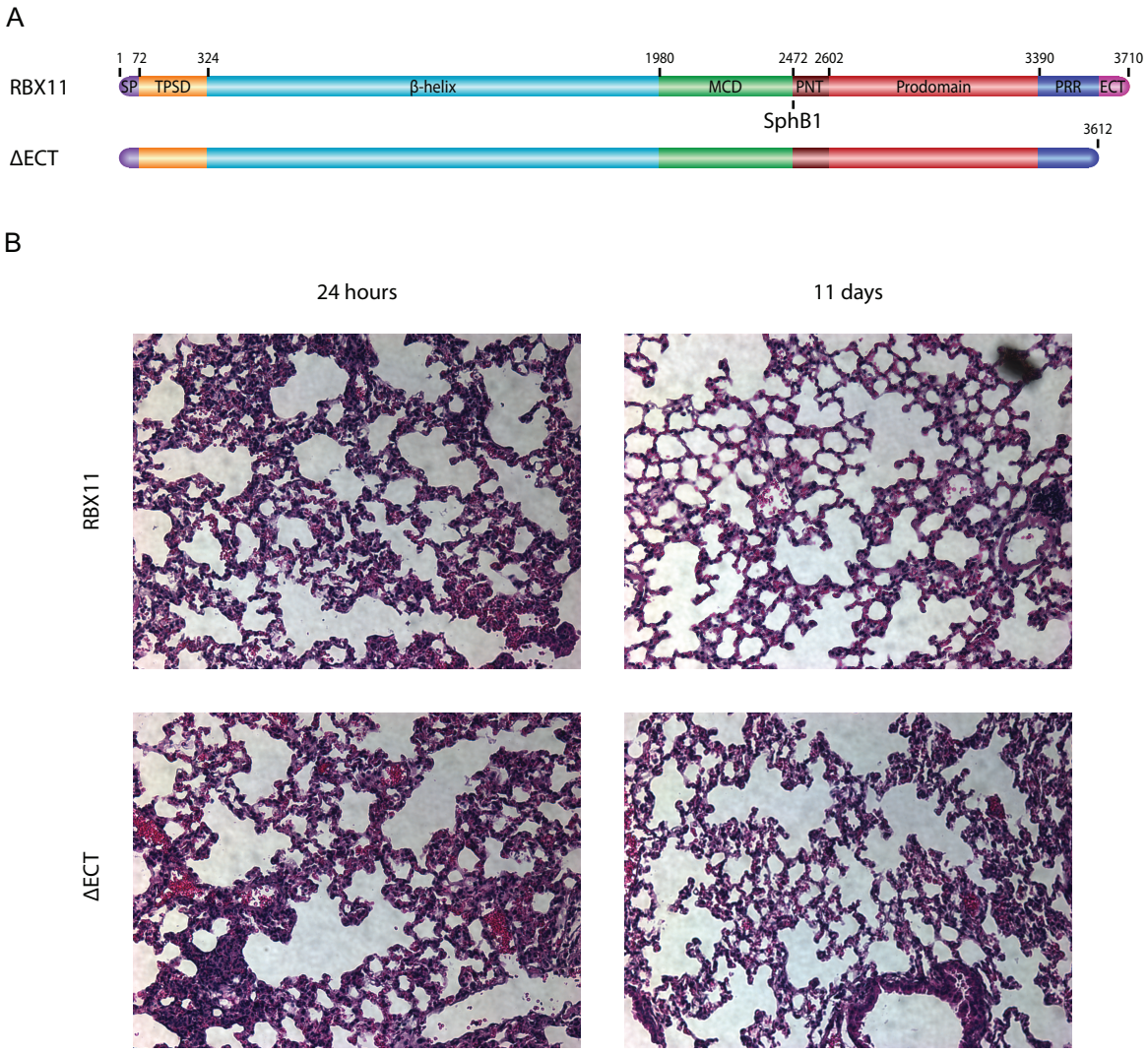

Courtesy of Jeffrey Melvin and Kurtis Host

The ΔECT strain causes a wild-type inflammatory response

A. Schematic of FhaB proteins in strains used to infect mice.
B. Histology of mice lungs. The left lungs of mice were sectioned for histopathology analysis. Despite burden discrepancies between wild-type *B. bronchiseptica* and ΔECT burdens, there is no apparent difference in host inflammatory response.

unidentified protease. We hypothesized that lack of the MCT could i) act to render the unidentified protease inactive, ii) cause the cleavage site to be inaccessible to the protease, or iii) cause the protease to be constitutively inhibited by the ECT. To investigate these possibilities, we constructed a strain producing FhaB with both the HA-ΔMCT deletion and the ECT truncation (HA-ΔMCTΔECT). The ~150 kDa polypeptide that was recognized by both antibodies in whole-cell lysate of the HA-ΔMCT strain was not detected in whole-cell lysate of the HA-ΔMCTΔECT strain in whole-cell lysate (Figure 23B), indicating that prodomain was being both cleaved from FhaB and efficiently degraded. Since this experiment implicates the ECT a determinant of prodomain degradation, we hypothesize that the unidentified protease (which appears to be regulated by the ECT) is more directly responsible for degradation. Consistent with previous data (Figure 15B), it appears that in the HA-ΔMCT strain, the ECT inhibited the activity of the unidentified protease. In fact, given the stability of the ~150 prodomain fragment, the ECT appears to be constitutively inhibitory of SphB1-independent proteolysis in the HA-ΔMCT strain. Such results are consistent with the hypothesis that the MCT is involved in delivering a signal to the ECT that causes the ECT to stop inhibiting the unidentified protease. Such a signal could be the folding of the MCD (and therefore folding of the MCT) into a functional conformation or the association of the MCD with its receptor on host cells, which may result in folding of the unidentified protease cleavage site into an accessible conformation.

Figure 23

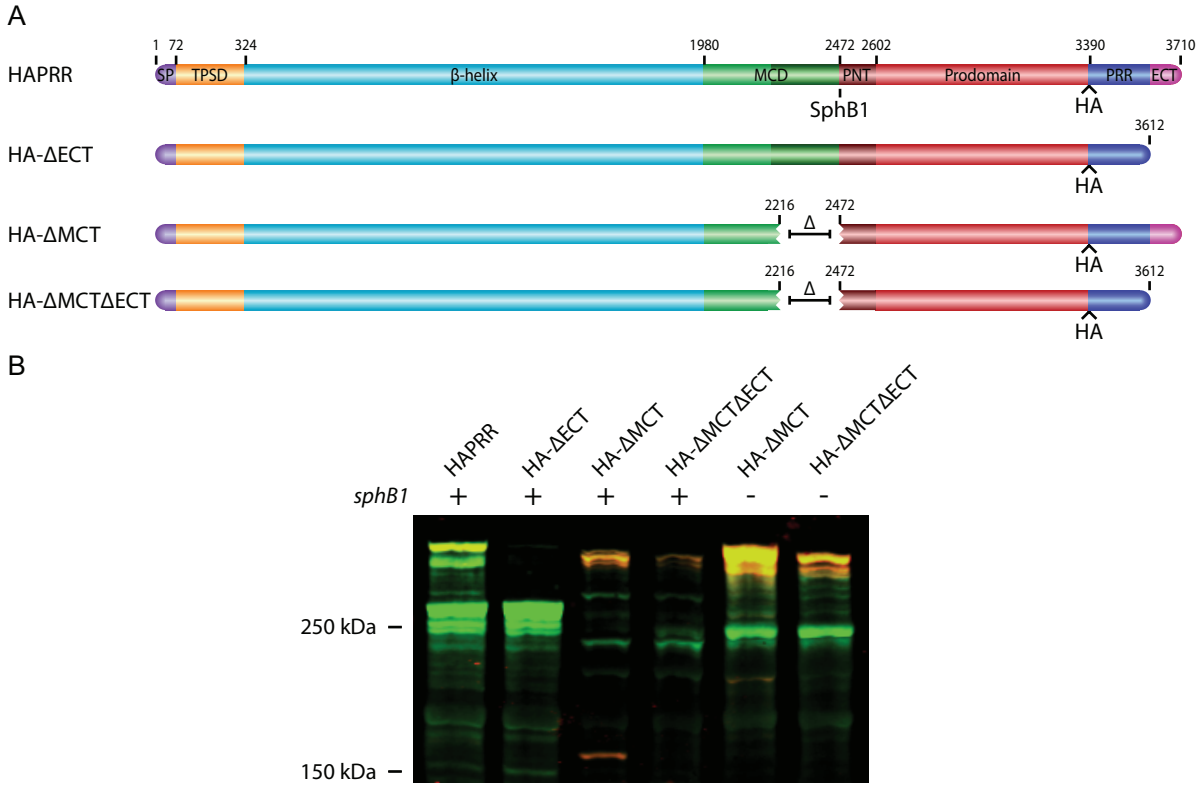

ECT-mediated suppression of FhaB maturation is dominant to MCT-maturation promotion of maturation

A. Schematic of FhaB proteins in strains used in experiment. Mutations in a Δ*sphB1* background are noted.
B. Anti-MCD (green) and anti-HA (red) immunoblot of whole cell lysates. Truncation of the ECT from FhaB of the ΔMCT strain restores degradation of the cleaved prodomain.

The proline-rich region of the FhaB prodomain does not affect FHA biogenesis but is required for virulence

While the hyper-processing phenotype of the ΔECT and ΔPRR-ECT strains implicated the ECT in FhaB stability and maturation dynamics, they did not reveal a role for the PRR. We, therefore, created a strain (ΔPRR) with an in-frame deletion of the prodomain's PRR in order to examine its role on the maturation of FHA. Whole-cell lysate analysis revealed that the PRR deletion strain produced similar levels of full-length FhaB and processed FHA as wild-type *B. bronchiseptica*, and that the FHA isoforms generated were of the same size as those made in our wild-type strain (Figure 24B). Release of FHA into the supernatant was also unaltered (Figure 24C). We also constructed a strain (ΔPK) in which the $(PA)_6(PK)_4$ motif of the PRR was deleted. Given the lack of biogenesis phenotype in the ΔPRR strain, it came as little surprise that the $(PA)_6(PK)_4$ deletion had no affect on the maturation profile of FHA (Figure 24B or 24C).

Since our *in vitro* experiments did not reveal a phenotype for the PRR, we examined the ΔPRR strain *in vivo*. Mice were infected with RBX11 (*B. bronchiseptica* deleted for *fhaS* to simply cloning) or ΔMCD-PD (a strain in which the region of *fhaB* encoding the MCD and prodomain has been deleted) as controls for typical and hyper-inflammatory host responses, respectively. RBX11 burdens peaked 3 days post-infection, but the strain persisted through day 11 (Figure 25). Over the course of infection, mice infected with ΔMCD-PD exhibited a 'bi-modal'

Figure 24

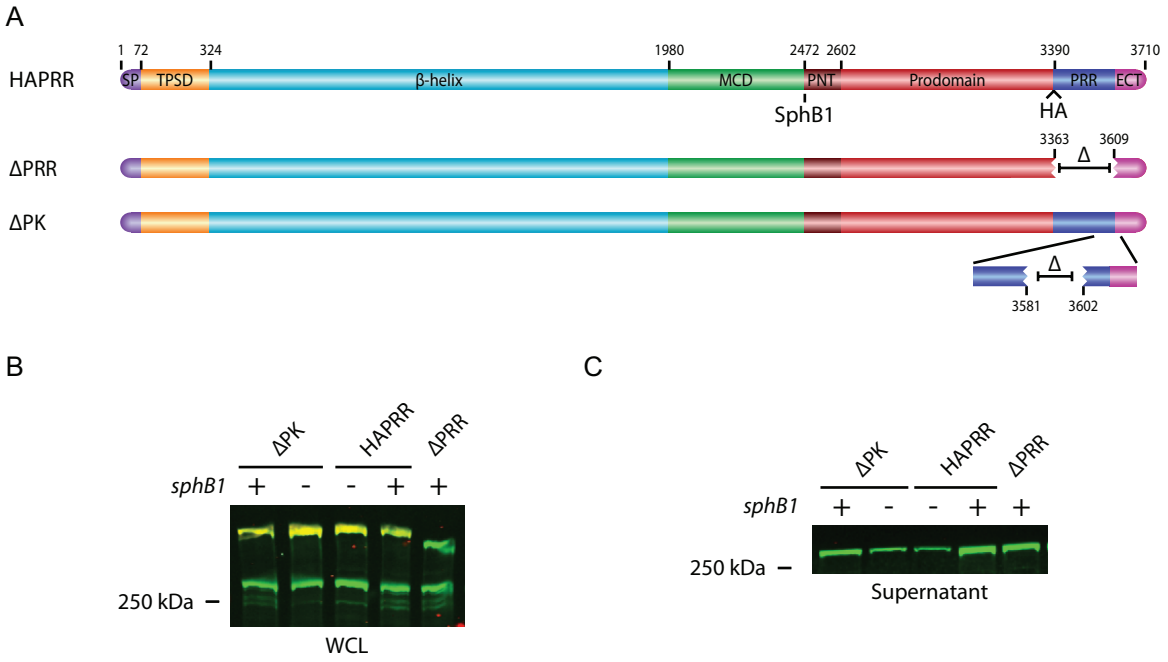

The proline-rich region of the FhaB prodomain does not affect the biogenesis of FHA

A. Schematics of FhaB proteins in strains used in experiment. Mutations in a Δ*sphB1* background are noted.
B. Anti-MCD (green) and anti-HA (red) immunoblot of whole-cell lysates. Deletions in the ΔPRR and ΔPK strains did not affect FhaB biogenesis.
C. Anti-MCD (green) immunoblot of concentrated supernatants. Deletions in the ΔPRR and ΔPK strains did not affect release of mature FHA.

Figure 25

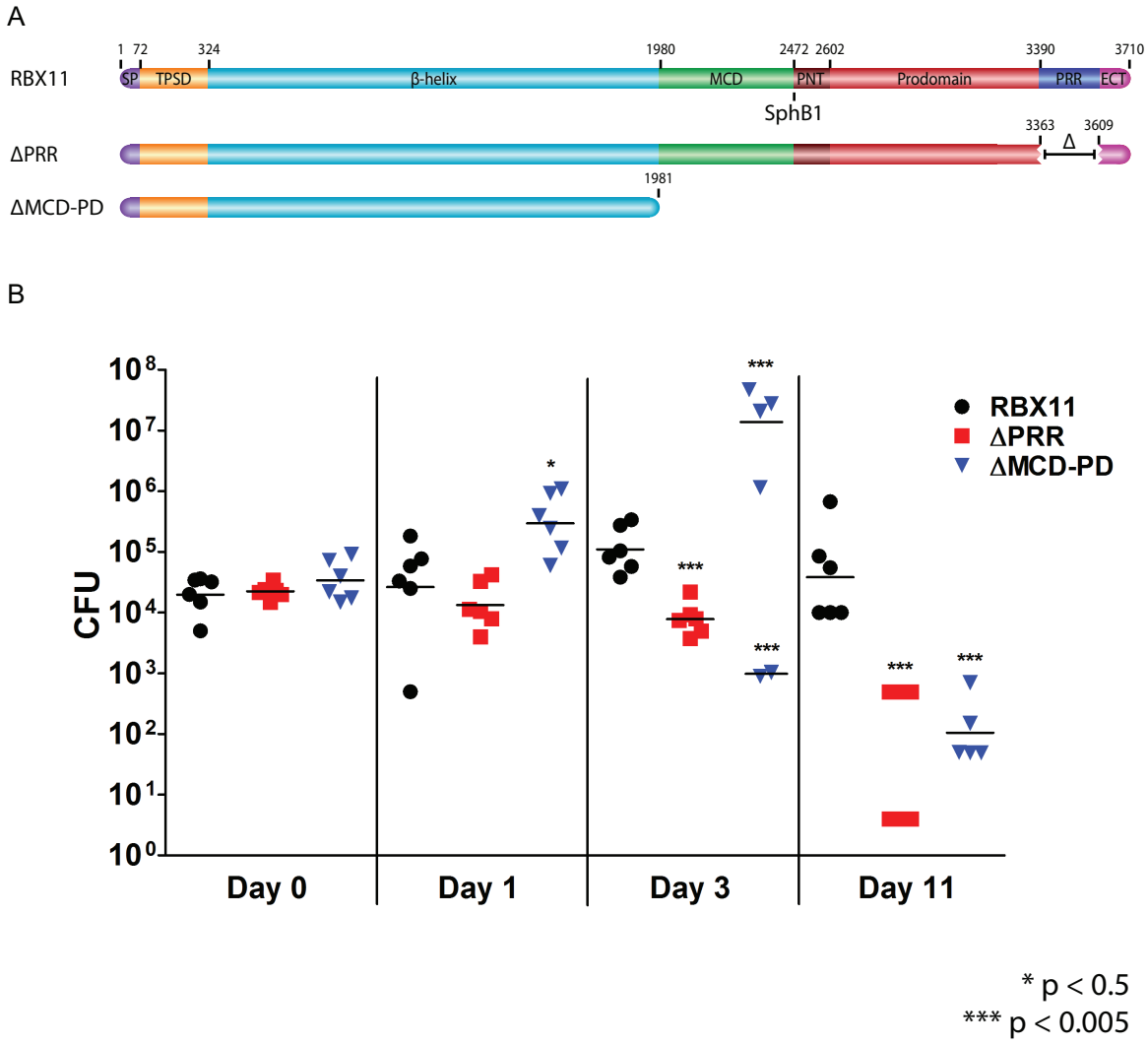

Deletion of the prodomain PRR causes a *Bordetella* persistence defect *in vivo*

A. Schematic of FhaB proteins in strains used to infect mice.
B. Bacterial burdens in mice. The right lungs of mice were harvested at the specified times, homogenized, and plated for burden counts. ΔMCD-PD was included as a control for persistence in response to the host bi-modal response. Experiments were performed twice.

response – a hyper-inflammatory response that will either clear bacteria or undermine the host's own defenses. By day 3, the consequence of such a response was efficient clearance of bacteria or dramatic proliferation of bacteria in immune-compromised hosts (Inatsuka et al., 2005; Henderson et al., 2012). The ΔPRR strain appeared defective for the initial colonization of mice at day 3. Burdens continued to decrease compared to RBX11, with bacteria cleared 11 days post-infection. Preliminary results suggest that deletion of the $(PA)_6(PK)_4$ motif had no affect on the ability of *B. bronchiseptica* to establish and maintain infection (Figure 26).

Histology revealed a host response to the ΔPRR strain dramatically different to that of RBX11 or ΔECT. While RBX11 caused low-to-moderate inflammation over the course of infection (day 11 lungs of RBX11-infected mice may serve as a reference for an uninflammed lung), ΔPRR caused a dramatic inflammatory response 1 and 3 days post-infection, as indicated by an influx of neutrophils and macrophages into the alveolar space (Figure 27B). By day 11, however, lung inflammation of mice infected with the ΔPRR strain was about as low as that of mice infected with RBX11. Despite the high degree of inflammation at days 1 and 3, mice infected by the ΔPRR strain were never moribund. Even ΔMCD-PD, noted in the past for its induction of a hyper-inflammatory response (Henderson et al., 2012), paled in comparison to ΔPRR in its ability to cause inflammation in mouse lungs. It is likely that the nature of hyper-inflammatory response caused by ΔPRR is different than that of ΔMCD-PD since no bi-modal response was observed in mice infected with ΔPRR despite greater inflammation in their lungs.

Figure 26

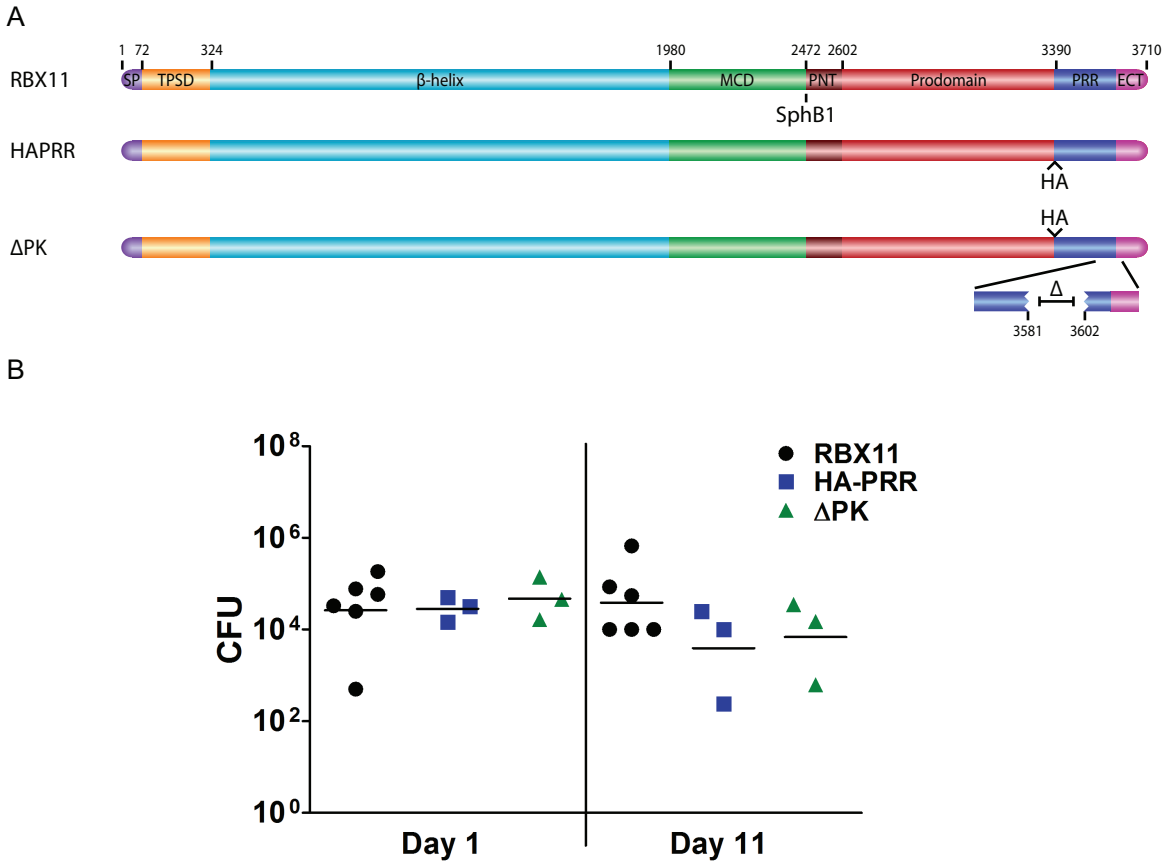

Deletion of the prodomain $(PA)_6(PK)_4$ motif causes no *Bordetella* persistence defect *in vivo*

A. Schematic of FhaB proteins in strains used to infect mice.
B. Bacterial burdens in mice. The right lungs of mice were harvested at the specified times, homogenized, and plated for burden counts. Since the ΔPK strain was made in an HAPRR background, RBX11 was included as a control against which HAPPR and ΔPK were compared. Experiments were performed once.

Figure 27

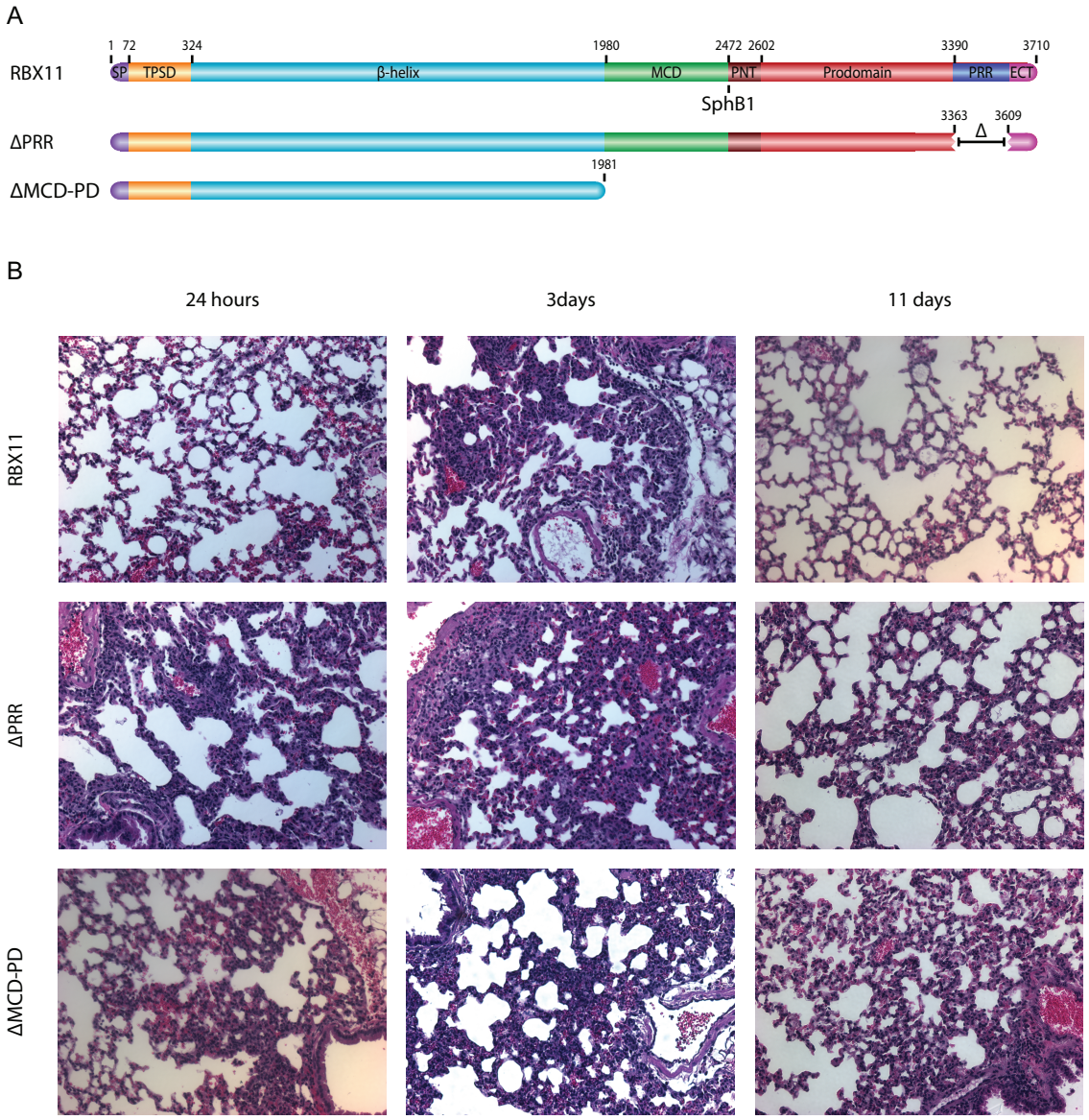

The ΔPRR strain causes an extreme hyper-inflammatory response

A. Schematic of FhaB proteins in strains used to infect mice.
B. Histology of mice lungs. The left lungs of mice were sectioned for histopathology analysis. Compared to the inflammatory response of wild-type *B. bronchiseptica* and ΔMCD-PD (which is characterized as being hyper-inflammatory), ΔPRR induces an extreme inflammatory response 24 and 72 hours post-infection, but returns to near-wild-type histopathology by day 11.

Plasmid-borne prodomain expression offer insights as to prodomain fate

As an alternative method to understanding the function of the prodomain, we examined whether the prodomain could function *in trans* to the N-terminal ~250 kDa of FhaB (corresponding to mature FHA). The approach was to design plasmid constructs in the broad-range vector pBBR1-MCS (medium copy in *B. bronchiseptica*). Sequences encoding the *fhaB* promoter and FhaB prodomain were cloned into the vector. The prodomain-encoding DNA was designed with and without sequences encoding (i) an FhaB signal peptide and (ii) a PRR/ECT, totaling four constructs (Figure 28A). Plasmids were introduced to *B. bronchiseptica* strains with varying *fhaB* mutations (Figure 28A), including RBX11 (wild-type FhaB), ΔPD (prodomain-truncated to test for *trans* complementation), PD^{Comp} (Δ28-PD with the prodomain complemented *in cis*), ΔMCD-PD (deleted of the MCD and prodomain), and RBX20 (Δ*fhaB*, a negative control for FhaB).

Western blots were performed whole-cell lysate of all the strain/plasmid combinations (Figures 28B). Staining against the N-terminus of the prodomain revealed that ~140 kDa prodomain could only be detected when the plasmid construct included the PRR and ECT of the prodomain (Figures 28B). It cannot be ruled out, however, that smaller peptide species existed that were not reactive to our antibody. This result parallels our previous result showing that the ECT is required for stability of the prodomain in the context of full-length FhaB, though the plasmid-based approach does not discern between the PRR or the ECT being responsible

for stability of the over-expressed prodomain. Furthermore, plasmid constructs were only introduced to *sphB1*^{WT} backgrounds, so we cannot conclude anything with regards to the proteases that are responsible for prodomain degradation in bacteria containing the PRR/ECT-deficient prodomain constructs.

The second result of the plasmid-based approach was that trans-conjugates suffered from toxicity when grown under BvgAS plus-phase modulating, with colonies growing very poorly compared to bacteria with no plasmid (Figures 29B and 29C). This toxicity was alleviated when strains were grown on plates containing 20 mM $MgSO_4$ (which modulates *Bordetella* to BvgAS minus-phase), indicating that toxicity was dependent on the expression of the plasmid-borne prodomain. Each of the four plasmid constructs caused toxicity to recipient bacteria, which is surprising given the apparent instability of prodomain polypeptides synthesized without a PRR/ECT – a result that suggests that even a transiently stable prodomain may be toxic. Of further curiosity was the fact that toxicity was less pronounced in trans-conjugates of the RBX20 (Δ*fhaB*) background (Figure 29C), suggesting that toxicity was partly dependent on FhaB. Indeed, based on toxicity to ΔMCD-PD trans-conjugates, it appears that the β-helix is the FhaB-dependent toxicity factor in our plasmid-based approach.

Figure 28

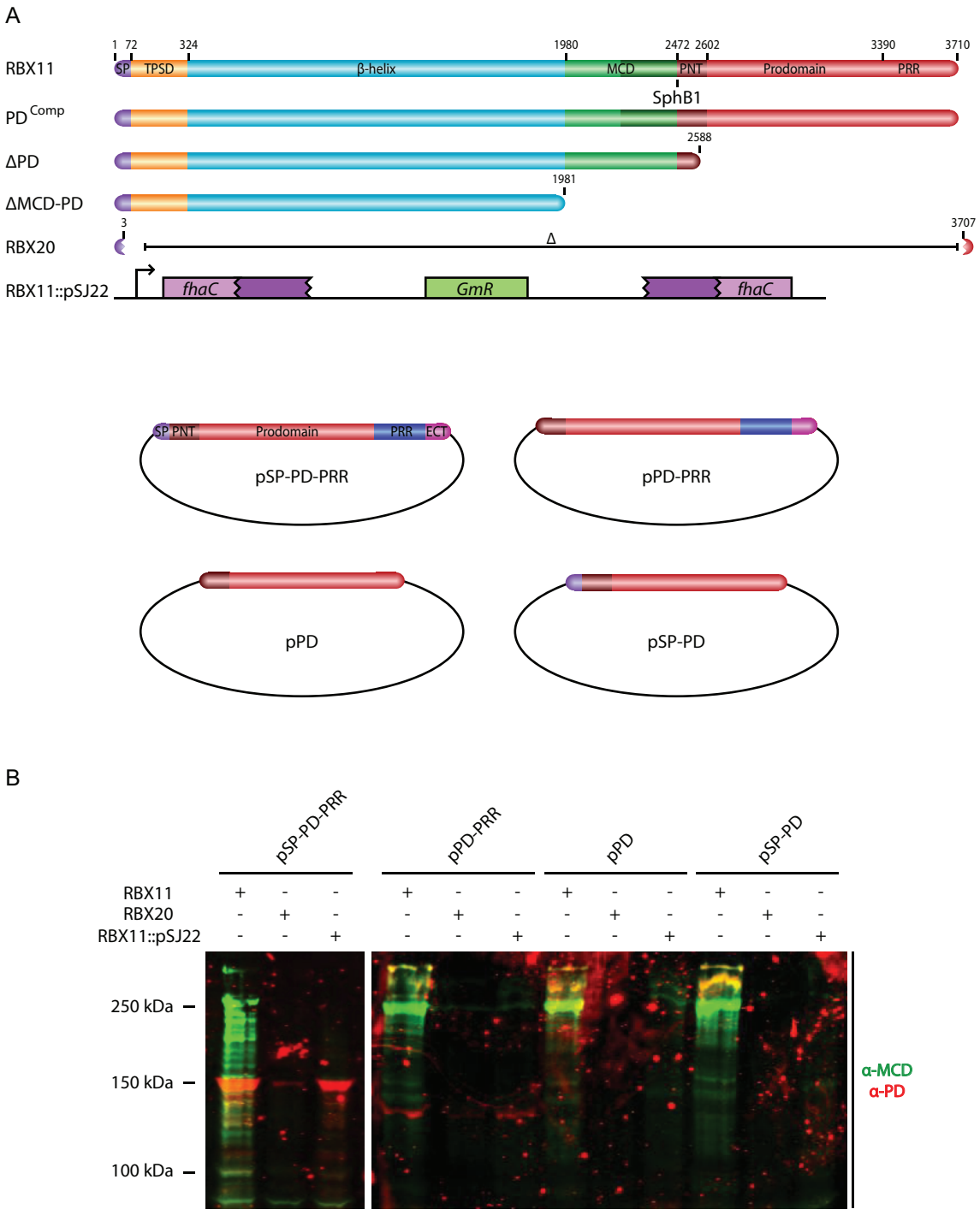
A
RBX11
SP
TPSD
β-helix
MCD
PNT
Prodomain
PRR
1
72
324
1980
2472
2602
3390
3710
SphB1
PD Comp
2588
ΔPD
1981
ΔMCD-PD
3
3707
RBX20
Δ
RBX11::pSJ22
fhaC
GmR
fhaC
SP
PNT
Prodomain
PRR
ECT
pSP-PD-PRR
pPD-PRR
pPD
pSP-PD
B
pSP-PD-PRR
pPD-PRR
pPD
pSP-PD
RBX11
RBX20
RBX11::pSJ22
250 kDa
150 kDa
100 kDa
α-MCD
α-PD

Figure 28, continued

C

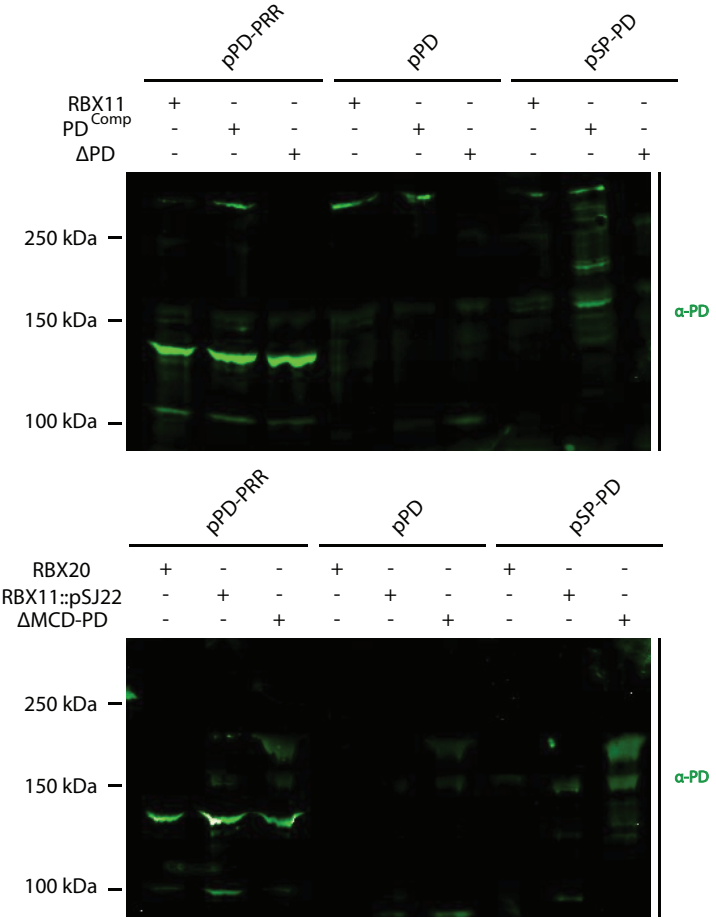

The PRR-ECT of the prodomain is necessary for prodomain standalone stability

A. Schematic of proteins, loci, and plasmids used in experiment. At the top are schematics of the proteins that were used and a schematic illustrating the disruption of *fhaC* in the RBX11::pSJ22 strain. At the bottom are plasmid constructs used in experiment containing variants of the FhaB prodomain.
B. Anti-MCD (green) and anti-PD (red) immunoblot of whole-cell lysates. Prodomain expressed from medium copy plasmids was only immuno-detected in trans-conjugates contained plasmid constructs that included the PRR-ECT.
C. Anti-PD (green) immunoblot of whole-cell lysates. Prodomain expressed from medium copy plasmids was only immuno-detected in trans-conjugates contained plasmid constructs that included the PRR-ECT.

Figure 29

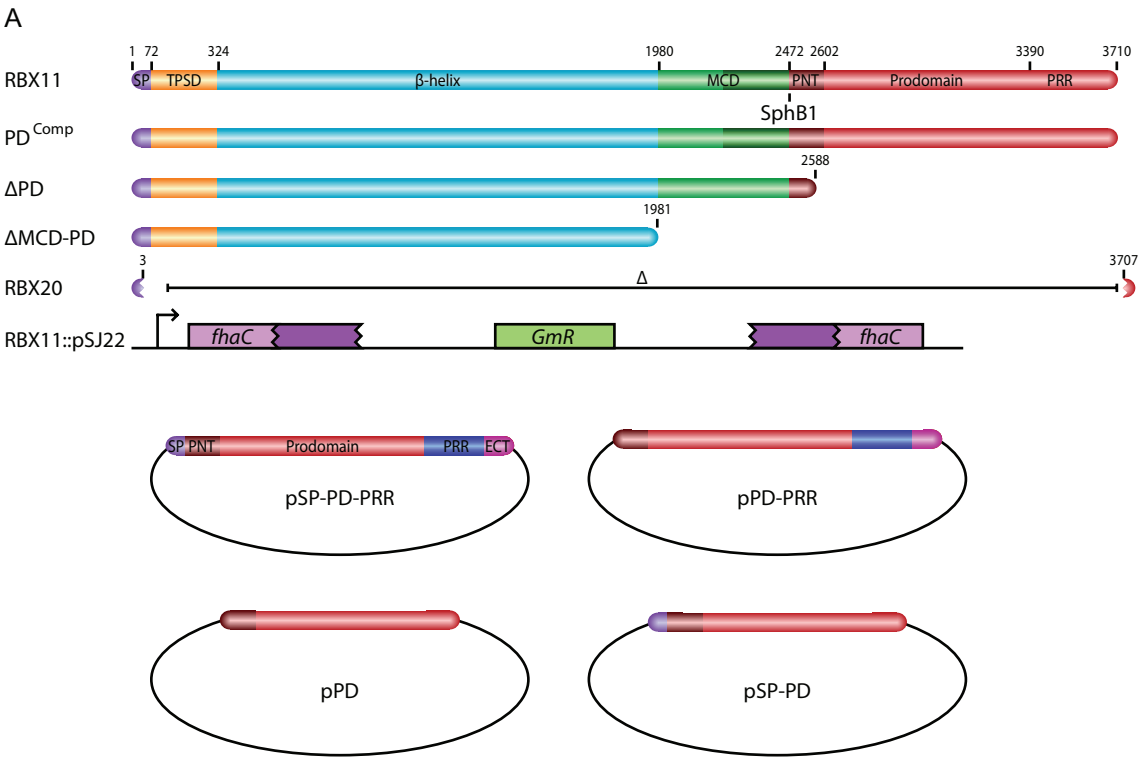
A
RBX11
PD Comp
ΔPD
ΔMCD-PD
RBX20
RBX11::pSJ22
SP
TPSD
β-helix
MCD
PNT
Prodomain
PRR
SphB1
Δ
fhaC
GmR
fhaC
SP PNT
Prodomain
PRR
ECT
pSP-PD-PRR
pPD-PRR
pPD
pSP-PD
B
Legend
No Vector, O mM MgSO4
RBX11
ΔMCD-PD
RBX20
PD Comp
RBX11 ::pSJ22
ΔPD

Figure 29, continued

C

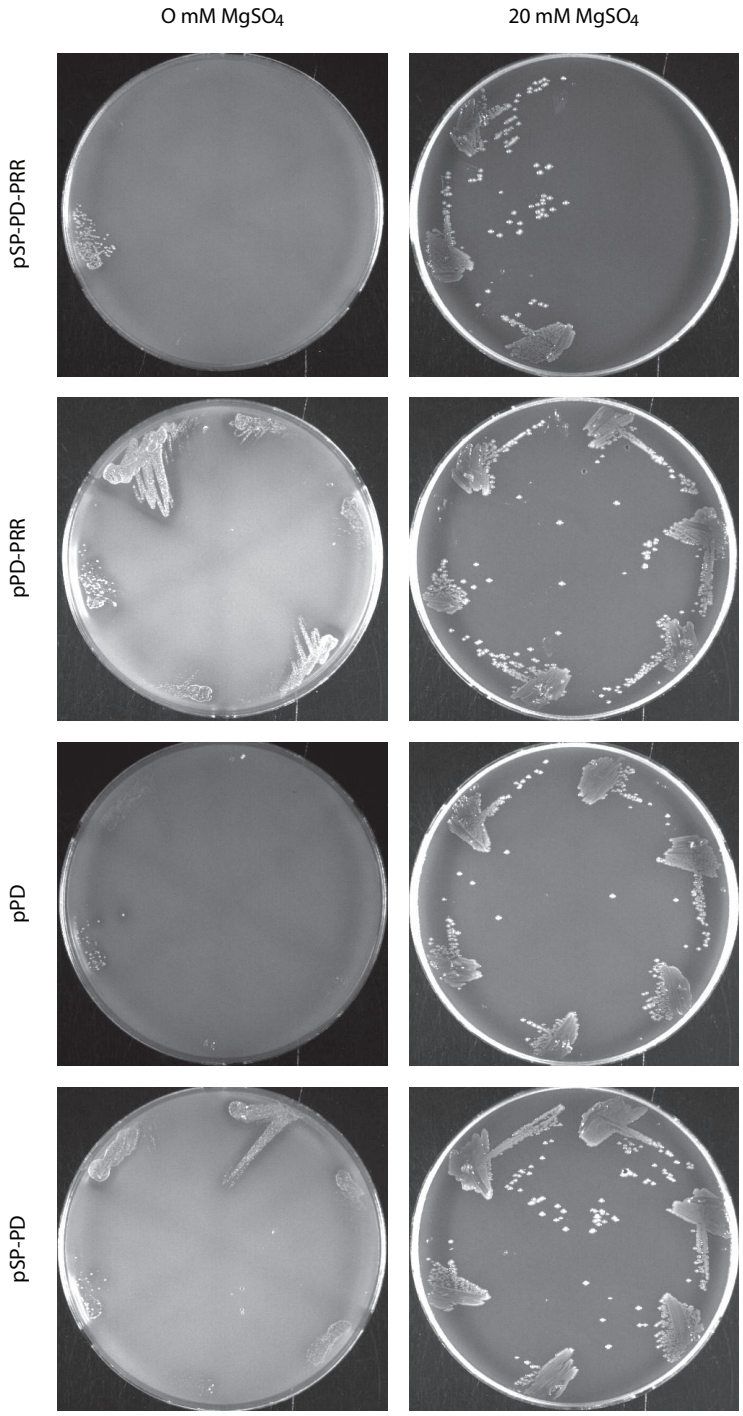

Figure 29

Over-expression of the prodomain alone causes toxicity to *B. bronchiseptica* in a manner co-dependent on the presence of the FhaB β-helical region

A. Schematic of proteins, loci, and plasmids used in experiment. At the top are schematics of the proteins that were used and a schematic illustrating the disruption of *fhaC* in the RBX11::pSJ22. At the bottom are plasmid constructs used in experiment containing variants of the FhaB prodomain.
B. Legend and healthy recipient *B. bronchiseptica*. On the left, a legend for recipient strains on the plates in Figure 29C. On the right, recipient strains with no prodomain plasmid construct develop healthy colonies on BG plates containing no $MgSO_4$.
C. Trans-conjugates containing prodomain plasmid constructs are unable to grow on Bvg plus-phase modulating plates, though trans-conjugated RBX20 grows moderately well. All trans-conjugates grow well on Bvg minus-phase modulating plates. Strains ΔMCD-PD, ΔPD and PD^{Comp} were not trans-conjugated with pSP-PD-PRR.

Chapter VI – Discussion and future directions

Summary and Concluding Thoughts

The experiments described in this work yielded four primary findings: (i) the FhaB prodomain remains in an intracellular compartment during FHA biogenesis, (ii) the prodomain affects the conformation of the FHA MCD, (iii) the PRR and ECT of the prodomain are important for FHA-mediated virulence, and (iv) the MCD of FhaB is determinant of FHA release potential. Based on these results, we propose a revised model for secretion by the FhaB-subfamily of TPS systems. The revisions relate primarily to events occurring after the β-helical shaft has been exported to the cell surface (Figure 30). The model states that as the MCT is secreted, FhaC changes from a release-incompetent state to a release-competent state (the shift in FhaC release competency is indicated in Figure 30 by a change in FhaC color from red to green). Subsequent FhaB transit through FhaC is halted by the PNT, which we postulate folds into a conformation that is incompatible with translocation. According to this model, the prodomain functions as a tether that constrains the conformations that the extracellularly located MCD may sample while folding into a functional structure. Alternatively, the prodomain may control the rate of translocation of the MCD, with rate-limited translocation being required for the MCD to fold properly. We hypothesize that upon achieving a functional conformation, the

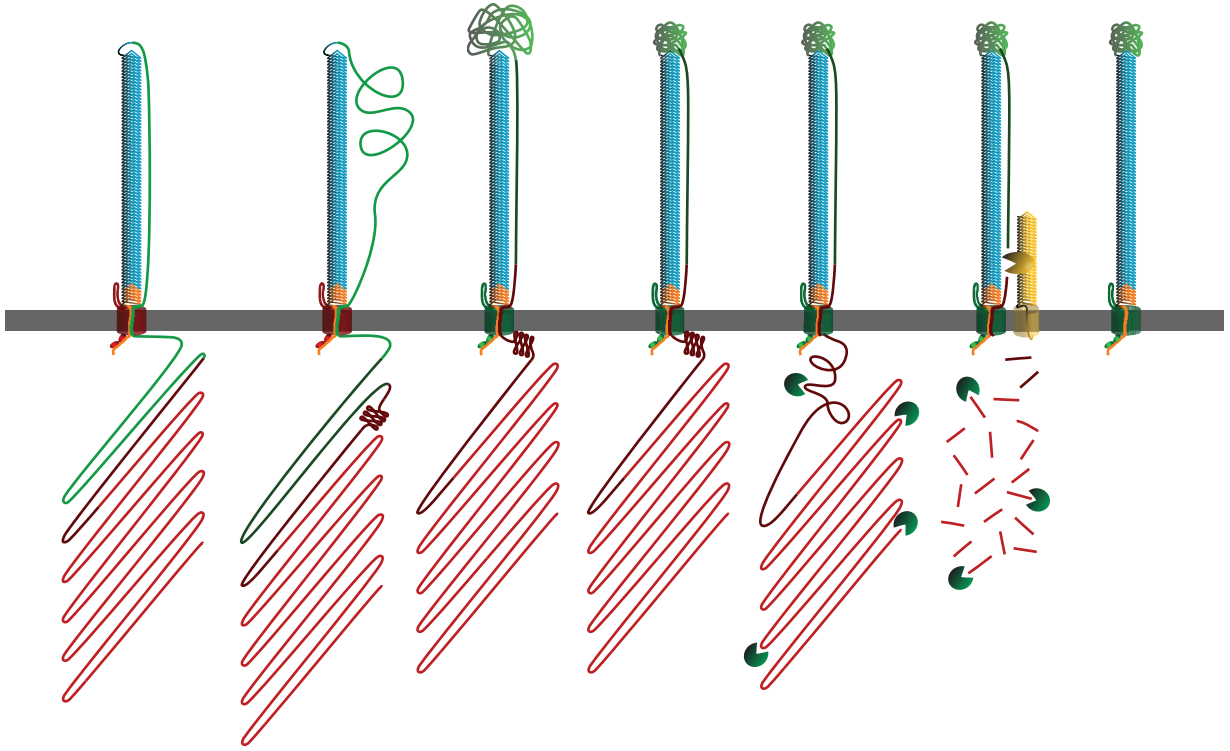

Revised model for FHA biogenesis

Our model continues from Figure 5A, with the β-helix surface-localized and the MCD and prodomain still inside the cell. During the secretion process, the PNT adopts a conformation that prevents prodomain transit through FhaC. Next, the MCT of FhaB translocates to the extracellular space, priming FhaC for release of FHA, as indicated by the shift in FhaC colour from red to green. The translocation-impaired PNT confers tension across the extracellular space to the MCD, restricting the conformations the MCD may sample while folding. FhaB undergoes maturation into FHA upon completion of MCD folding, with FHA maturation being accomplished by SphB1-independent cleavage, degradation of the prodomain and SphB1-dependent cleavage. At this point, FHA is fully mature and can remain either surface-associated or be released into the supernatant.

MCD signals maturation-cleavage readiness, resulting in FhaB cleavage by the unidentified protease(s). The prodomain is rapidly degraded and additional SphB1-dependent processing occurs. Fully matured FHA is then released into the extracellular environment by an, as yet, unknown mechanism.

We reported previously that the prodomain is required for FHA function *in vivo* and we also provided evidence that the MCD is an important functional domain, if not *the* functional domain, of FHA during infection (Mazar and Cotter, 2006; Julio et al., 2009). In this study we used semi-native PAGE, proteinase-K digestion and cysteine residue accessibility experiments to determine that the FhaB prodomain affects the conformation of the MCD. These results indicate that the prodomain functions as an intramolecular chaperone that controls the folding of the MCD. Proteinase-K digestion and dot blot experiments demonstrated that the prodomain remains intracellular while the MCD is extracellular, but they did not reveal whether the C-terminus of the prodomain remains in the cytoplasm or the periplasm. Regardless of its exact intracellular location, the FhaB intramolecular chaperone domain (the prodomain) and the functional domain it controls (the MCD) are separated by at least one membrane. Although intramolecular chaperones that affect the conformation of functional domains have been described, they typically colocalize with their functional domains, acting as molecular scaffolds that guide the folding of the active domain of the mature protein via direct protein-protein interactions. The best-characterized example of this family of intramolecular chaperones is subtilisin E of *B. subtilis* (Shinde and Thomas, 2011). The FhaB

prodomain appears to function in an entirely different manner since it does not colocalize with the conformationally mature MCD. The simplest model is that the prodomain, via its intracellular location, functions as a tether that constrains the folding space of the MCD such that its functional conformation is the preferred fold among those available for sampling. Although a more complex scenario, it is also possible that the FhaB prodomain, either directly or indirectly from inside the cell, influences the translocation rate of the MCD such that the MCD is translocated across the outer membrane in a manner compatible with its proper folding on the cell surface. To our knowledge, neither of these mechanisms for the control of protein folding has been described previously. However, a similar concept has been described in the case of the *E. coli* autotransporter EspP. In this case, it is hypothesized that, prior to cleavage by leader peptidase, a cytoplasmically located extended signal peptide alters the conformation of the periplasmically located β-domain and, consequently, its ability to integrate into the outer membrane (Szabady et al., 2005).

Our experiments identified the PNT as the subdomain responsible for intracellular retention of the prodomain. One mechanism by which the PNT may mediate intracellular prodomain retention is by folding into a conformation incompatible with translocation through FhaC (Figure 30). Alternatively, the PNT may interact with another molecule or molecular complex that prevents export through FhaC. Whatever the mechanism, because this subdomain is conserved

among TpsA proteins of the FHA subfamily, intracellular retention of C-terminal prodomains and the mechanism by which PNTs function may also be conserved.

As suggested by our model, we do not believe that the only role for the prodomain is to function as a tether (if the tether hypothesis is even correct). We showed previously that a *B. bronchiseptica* strain that produces an FhaB protein lacking only the C-terminal 339 aa (and hence containing an intact PNT) is defective for tracheal colonization in rats (Mazar and Cotter, 2006). These data provide evidence that sequences C-terminal to the PNT are required for prodomain function. We and others have also noted the presence of a proline-rich region near the C-terminus of the prodomain, but the role of this region is currently unknown. In this work, we examined the role of the proline-rich region (PRR) as well as the extreme C-terminus (ECT) subdomains. Given the unusual amino acid composition of the PRR, we were surprised to see no *in vitro* phenotype for the strain in terms of FHA biogenesis. Only when tested in mice did it become clear that the PRR has a dramatic role in virulence – histology showed that at a relatively low dose (~$5x10^4$ CFU), the ΔPRR strain induced a very strong inflammatory response in the lungs (remarkably, without affecting the outward health of infected mice), and bacteria were efficiently cleared from the lungs. Immediately C-terminal to the PRR is the ECT, and though the two subdomains are adjacent, they have rather different phenotypes. While the ΔPRR strain had no apparent FHA biogenesis phenotype, the ΔECT strain appeared to hyper-process full-length FhaB into mature FHA. Introduction of an HA epitope into the ECT, although unintended, also resulted in the

hyper-processing biogenesis. While the ΔPRR strain caused a severe inflammatory response in the lungs of mice, the ΔECT strain (though only examined at days 1 and 11 post-infection) appear to have elicited an inflammatory response matching that of wild-type *B. bronchiseptica*. The main commonality shared by the ΔPRR and ΔECT strains is that they are both fully cleared from the lungs of mice 11 days post-infection, indicating that both of these C-terminal subdomains are important for persistence.

As described, early experiments on prodomain function and fate yielded perplexing results. New insights and fresh eyes, fortunately, allow us to make some sense of our plasmid-based approach to prodomain studies. The experimental design was such that prodomain was over-expressed as a standalone unit. Under normal circumstances, *Bordetella* expresses, cleaves and degrades the prodomain at single copy – potentially in order to prevent prodomain-dependent toxicity. In contrast, our trans-conjugates may have synthesized plasmid-encoded prodomain to an extent that *B. bronchiseptica* was unable to degrade prodomain quickly enough to avoid toxicity. This hypothesis, however, does not reconcile with the fact that trans-conjugates expressing prodomain without the PRR/ECT also suffered from toxicity, despite the absence of prodomain detection on Western blots. Along a different line, our current understanding of intracellular prodomain localization gives us new perspective on the nature of the signal peptide included in some of our plasmid constructs. Two of the four plasmids contain no signal peptide, yet the cellular toxicity and prodomain Western blot profiles of trans-conjugates expressing signal

peptide-less prodomain are the same as those of trans-conjugates expressing signal-peptide-containing prodomain. Although these phenotypes may very well be artifacts of the over-expression system, they indicate that the signal peptide-mediated transit across Sec is not necessary for medium-copy prodomain function. Although preliminary, such data suggest that the prodomain may, in fact, function in the cytoplasm of *Bordetella* under wild-type circumstances.

Though it is too early to incorporate the PRR and ECT into our model of biogenesis and virulence, it is safe to say that subdomains C-terminal to the PNT (potentially including the PRR and ECT) play a role in FHA maturation. We hypothesize that proper folding of the MCD on the cell surface is somehow sensed by the prodomain to trigger continued FHA maturation (i.e. to stimulate cleavage and degradation of the prodomain and then release of mature FHA). This would occur regardless of whether the prodomain functions as a tether or a translocation rate limiter and we hypothesize that regions of the prodomain C-terminal to the PNT are important for these steps in FHA biogenesis. If the prodomain functions as a limiter of MCD translocation rate, then subdomains C-terminal to the PNT may also be involved in somehow controlling the rate of translocation through FhaC, possibly by transiently influencing the conformation of the MCD in the periplasm. Our future studies will be aimed at testing these hypotheses.

Our data on ECT-dependent maturation highlighted not only a potential intramolecular maturation regulator, but also in importance of SphB1-independent

proteolysis during FHA maturation. Although SphB1-independent proteolysis of FhaB to yield FHA* and FHA′ was apparent in previous studies (Coutte et al., 2001; Mazar and Cotter, 2006), this cleavage was considered 'aberrant' and occurring primarily in the absence of SphB1 (Coutte et al., 2001). In this work, we observed two circumstances in which prodomain polypeptides were generated that were not cleaved by the unidentified protease. In each case, the prodomain polypeptides were stable. The first instance was after proteinase-K digestion of the HAPRR strain (*sphB1*^{WT} and Δ*sphB1*). The second was in the ΔMCT strain, in which FhaB underwent SphB1-dependent cleavage, but not SphB1-independent proteolysis. The fact that stable prodomain polypeptides were present in both of these cases, despite the fact that they were localized intracellularly and hence presumably accessible to the unidentified protease(s), suggests that the unidentified protease(s) is responsible for degradation of the prodomain and that it does so only in response to the normal sequence of events that occurs during FhaB translocation and maturation. We speculate, therefore, that cleavage/degradation by the unidentified protease(s) is an important regulated event during FHA biogenesis, and having identified the ECT as a potential regulator of the protease(s), we hope to be able to identify it/them and determine its/their spectrum of activity.

While our results suggest a role for the unidentified protease(s), they fail to reveal an important role for SphB1 with regard to FHA biogenesis. SphB1-dependent cleavage of FhaB occurs at multiple locations and with varying efficiencies in wild-type *B. bronchiseptica* and *B. pertussis.* Target promiscuity is

especially evident in the HA-ΔCS strain, in which, despite a sizeable deletion surrounding the PLFETRIKFID region, SphB1-dependent cleavage of FhaB occurred at alternate sites. Furthermore, the FhaB prodomains in the HA-ΔCS and HA-ΔPNT strains reached the extracellular space, where they were cleaved in an SphB1-dependent manner, suggesting that SphB1-dependent cleavage occurs regardless of prodomain location. Although Δ*sphB1* mutants of *B. pertussis* and *B. bronchiseptica* are severely defective in mouse models of infection (Coutte et al., 2003) and our unpublished data), this virulence defect cannot be attributed solely to altered processing of FhaB because SphB1-dependent cleavage of other *Bordetella* proteins occurs (our unpublished data). It is also possible that SphB1 interacts with host cells in a manner independent of its affects on other bacterial proteins. Understanding the roles SphB1 plays in *Bordetella* biology, therefore, remains a challenging and currently unattained goal.

When grown in broth, *B. pertussis* and *B. bronchiseptica* release a substantial amount of FHA into the culture medium. As FHA contributes to adherence of the bacteria to eukaryotic cells *in vitro* more than any other *Bordetella* virulence factor (Relman et al., 1990; Cotter et al., 1998; Mattoo et al., 2000), the fact that FHA is so efficiently released from the cell surface has been perplexing. Recent data have indicated that FHA also functions to modulate the inflammatory response (Inatsuka et al., 2005; Julio et al., 2009; Henderson et al., 2012). Although *in vitro* studies suggest that the released form of FHA can affect host cell signaling (McGuirk and Mills, 2000; Abramson et al., 2008; Dieterich and Relman, 2011), whether the

released form of FHA plays an important role during infection is unknown. The major obstacle to addressing this question is our current inability to construct a strain that is defective only for FHA release. Previous studies with *B. pertussis* showed that although short FHA molecules corresponding to the N-terminal ~30 and ~80 kDa of the protein (the TPS domain and part of the β-helical shaft) were efficiently released into culture supernatants, longer molecules that included most of the β-helical shaft or all of the β-helical shaft plus the N-terminal half of the MCD were poorly released (Renauld-Mongenie et al., 1996). If the initially synthesized FhaB polypeptide contained most of the prodomain, however, mature FHA was efficiently released (Renauld-Mongenie et al., 1996). These data suggest that sequences within the C-terminal half of the β-helical shaft render the system incompetent for release and that sequences C-terminal to that region restore release competency. Our experiments now reveal a critical role for the MCD in allowing FHA release, suggesting that sequences within this region somehow cause the FhaB/FhaC complex to switch from a release-incompetent to release-competent state. How this switch might occur mechanistically is completely unknown, but the current body of knowledge allows us to propose a new model for molecular determinants of FHA release potential. Experiments done by us and others reaffirm at FHA44 (the TPS domain and ~75% of the R1 β-helical region) are efficiently released in both *E. coli* and *B. bronchiseptica* (Renauld-Mongenie et al., 1996) and our unpublished data). FHA release defects exhibited by strains such as ΔMCD-PD, ΔMCT-PD and Δ28-PD indicate that sequences in the C-terminal portion of the β-helix reduce the efficiency of FHA release (perhaps by reducing the rate of FhaB secretion). It is worth noting

that the predicted structures of the R1 and R2 β-helices are different (Kajava et al., 2001), and differential folding propensities between the two regions might affect the dynamics of FhaB secretion. Alternatively, 'covert' β-helical regions exist in the β-helical shaft that have non-repetitive sequence (Kajava et al., 2001), and it may be that these regions contains molecular directions that regulate secretion dynamics. The work presented here identifies sequences in MCD and PNT as additional determinants of FHA release efficiency, with the MCD promoting release and the PNT inhibiting it. Thus it appears that within the FhaB proprotein are quality control 'checkpoints' that that systematically ensure that the protein is folding into a proper conformation while being secreted (Figure 31). We hypothesize that only upon achieving a functional conformation does FhaB signal its own maturation/release readiness.

Although our results have provided insight into the mechanism of FHA secretion and maturation, they also raise the question of why FHA maturation and release is so complex, and they remind us that data obtained by studying bacteria in culture in the laboratory must be interpreted with caution. During infection, *Bordetella* spp. produce FHA while residing on the mucosal surface of the respiratory tract. We and others have assumed that the 'mature' ~250 kDa FHA protein is the functional form during infection. However, it is possible that precleaved FhaB (currently considered a secretion intermediate) performs an important biological role. Our data suggest that the prodomain confers tension across the outer membrane, restraining mobility of the MCD, and we propose that once the MCD has folded, conformational

Figure 31

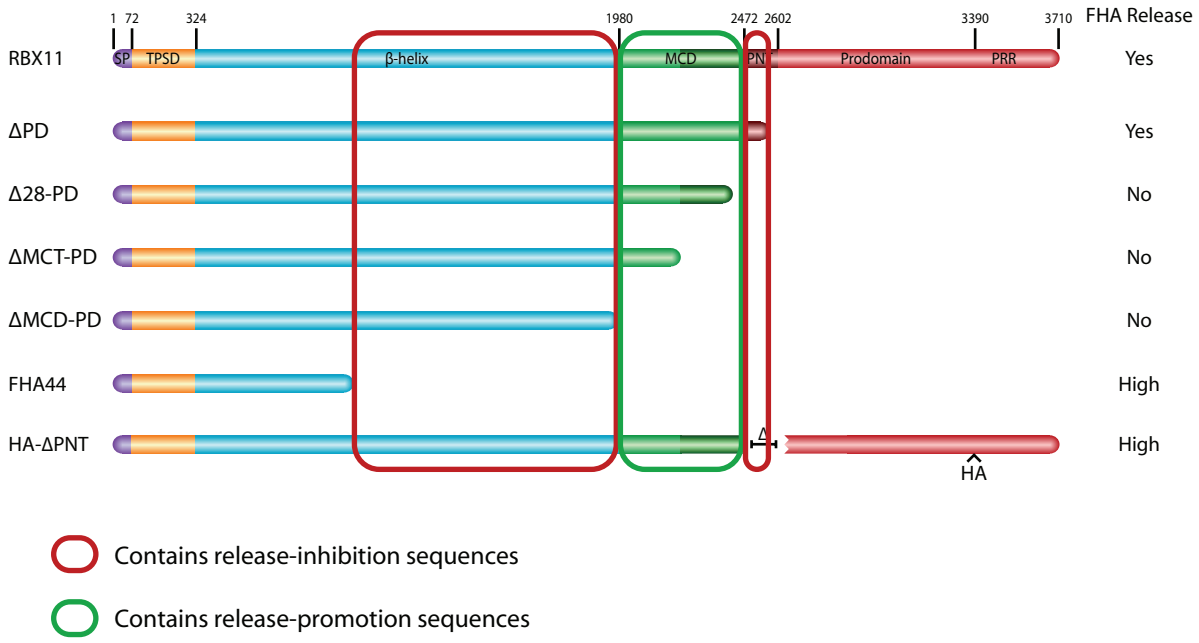

The ‘checkpoint’ model of FhaB secretion efficiency and FHA release rate

Wild-type and mutant FhaB proteins are listed, as are their respective release profiles. Based on release patterns, we propose that the FhaB proprotein contains a hierarchical system of molecular determinants of secretion efficiency, with release-inhibition sequences (circled red) suppressing secretion rate and release-promotion sequences (circled green) increasing secretion rate. Absence of inhibition sequences results in increased FHA release. Absence of promotion sequences results in decreased FHA release. We hypothesize that by affecting the rate of secretion, these sequences influence the rate at which FHA can achieve a functional conformation, and therefore the rate at which FHA can achieve a release-competent state.

information may also be sent back across the membrane to trigger cleavage and degradation of the prodomain by the unidentified protease(s). The potential for the MCD to communicate signals across the outer membrane to the prodomain raises the intriguing possibility that those signals could be generated in response to events that occur during infection, such as binding to specific host cell receptors. Moreover, the possibility exists that those signals could affect processes in the bacterial cell in addition to those related to FHA maturation, such as, perhaps, signal transduction and gene expression changes.

The PRR is a particularly attractive candidate for such signaling functions. Thus far, our *in vitro* experiments suggest that the PRR is not an FHA biogenesis factor, yet deletion of the PRR from *B. bronchiseptica* has a dramatic phenotype *in vivo*. Since, to the best of our knowledge, the prodomain is degraded after cleavage from FhaB, it stands to reason that the PRR performs its *in vivo* function exclusively in the context of full-length FhaB. Proteins containing regions of high proline concentration are not uncommon. The functions of these proteins and the functional/mechanistic contribution of their respective PRRs vary widely, however (Williamson, 1994). Our attention has especially been drawn to TonB, a protein ubiquitous to Gram-negative bacteria that is involved in acquisition of iron from the extracellular environment. TonB spans the periplasm via a central proline-rich region (Hannavy et al., 1990; Postle and Larsen, 2007). Doing so allows TonB to conduct energy generated in the cytoplasmic membrane by the electrochemical gradient to the outer membrane. It is thought that the ‘charging’ of TonB at the inner membrane

stores potential energy that is used to induce conformational changes of TonB's outer membrane binding partners, siderophore transporters, such that iron can be translocated from the extracellular space to the periplasm. The proline-rich region of TonB is believed to provide trans-periplasmic structure to TonB, and is part of the C-terminal portion of TonB that binds siderophore transporters. TonB also contains a $(PK)_5$ motif, like that found in the PRR of *B. pertussis* and *B. parapertussis* FhaB, although this motif has not been characterized to have a standalone function.

Future Directions

The body of work discussed in this dissertation reveals that the prodomain is a complex polypeptide composed of numerous subdomains have distinct roles in FHA biogenesis and *Bordetella* infection. Having demonstrated that the PNT is required to keep the remainder of the prodomain intracellular, our attention now shifts to understanding the function of the intracellular PRR and ECT. The PRR is of particular interest since we observe such a dramatic PRR-dependent phenotype *in vivo* in terms of bacterial burden and lung inflammation, despite no readily apparent affect on FHA biogenesis *in vitro*. It is worth noting that the following experiments, while focused on characterizing the PRR, would be equally relevant to studies of the PNT, ECT and any subdomains that are later identified.

The foremost priority for PRR studies is better characterize the host response to PRR-deficient *Bordetella*. In addition to examining lung histopathology and

bacterial burdens, studies of bacterial dissemination, host cytokine production, immune cell recruitment, and host weight loss will provide valuable insight as to how the PRR of FhaB affects host interactions with *Bordetella*. These *in vivo* experiments would be nicely complemented by *in vitro* studies assessing the role of the *Bordetella* PRR in adherence to host cells, cytokine response to infection, and internalization by phagocytes.

Understanding molecular and mechanistic bases for PRR-dependent phenotypes will be necessary to explain any host-side phenotypes that we observe. It is of particular interest to determine if the PRR, specifically, affects the conformation of the MCD, as we previously demonstrated the dependency of MCD conformation on the presence of the entire prodomain. While we are now able to claim that the prodomain (and therefore the PRR) remain intracellular during FHA biogenesis, we have not identified the subcellular compartment in which it resides. We hope that selective permeabilization studies will distinguish between cytoplasmic and periplasmic localization of the PRR, thereby offering insight as to its precise mechanism of virulence. Furthermore, since PRRs are often involved in protein-protein interactions, it would be revealing to perform co-immunoprecipitation experiments to identify any binding partners for the PRR. PRRs have also been implicated as DNA binding domains, serving as transcription regulators (Williamson, 1994). Although perhaps a stretch, the intracellular PRR may influence intracellular signaling events in response to host ieractions, ultimately regulating the expression of *Bordetella* virulence genes. Incubation of cell lines with wild-type and ΔPRR *B.*

bronchiseptica, followed by RT-qPCR of bacterial RNA would reveal any PRR-dependent changes in virulence regulation.

The work presented in Chapter IV highlights TpsA release as one of the current frontiers in TPS pathway research. The 'checkpoint' model of FHA secretion and release discussed above provides a starting point for systematic analysis of FhaB, with the goal of identifying and characterizing sequences that promote or hinder trafficking of FhaB to the extracellular space. Additionally, studies on FhaC may provide valuable insight into FHA release mechanics. Though preliminarily characterized in *E. coli* (Clantin et al., 2007), examinations of H1 and L6 of FhaC in *Bordetella* are warranted. Furthermore, structural predictions of *B. bronchiseptica* FhaC suggest that extracellular loop 5 is comparably long and flexible to L6, and thus studies of loop 5 might offer insights as to FhaC secretion and release mechanics. Finally, efforts are underway to engineer FhaB such that it cannot be released. One approach to accomplishing this goal is the addition of structural motifs to the N-terminus of the FhaB proprotein that preclude its transit through FhaC. Alternatively, we aim to create a fusion between the C-terminus of FhaC and the TPS domain of FhaB such that the N-terminus of mature FHA is linked to FhaC by a peptide bond. Should we be successful in constructing a strain of *Bordetella* that secretes but does not release functional FHA, we will have an invaluable tool for determining the function of FHA *in vivo*.

Appendix A – Experimental Methods

Bioinformatics

Proteins containing regions of similarity to the FhaB PNT were identified with a PSI-BLAST search. ClustalW alignment was used to identify similar and identical residues among the resulting TpsA proteins. WebLogo 3 was used for presentation of the ClustalW alignment (Crooks et al., 2004).

Adherence assay

Adherence to rat lung epithelial cells (L2) was performed as described (Cotter et al., 1998).

Semi-native polyacrylamide gel analysis of FHA MCD

Overnight cultures (25 mL) of BPSMAQ and BPSMAQT-N were grown to OD_{600} of 3-5. Cultures were spun down at 11,000 r.p.m. for 10 min at 4°C. Supernatants were collected and sterilized using a 0.22 µm PVDF Millex-GV syringe-driven filter unit (Millipore). Two milliliters of ProBond slurry were added to filter-sterilized supernatants and the mixes were incubated end-over-end for 1 h at room temperature. The slurry-supernatant mixes were spun at 3,500 r.p.m. for 5 min and supernatant set aside. The pelleted resin was washed twice in Native Binding Buffer

and twice in Native Washing Buffer. The pelleted resin was then washed twice in 250 mL of Native Elution Buffer (500 mM imidazole), with each wash and the resin being saved for analysis. Samples can be stored overnight at 4°C. Samples were resolved on 6% SDS-PAGE gel (10 mL loaded). The gel was stained by Coomassie blue to assess elution yields. The elution with the highest FHA yield was dialyzed in 1 L sterile PBS pH 7.4 overnight at 4°C to remove excess imidazole. TEV buffer (20X), 1 mL (10 units) AcTEV protease and 1 mM DTT (final) were added to dialyzed samples. Samples were incubated at 30°C for 6 h. Two hundred and fifty microliters of ProBond resin was added to the samples and samples were incubated end-over-end overnight at 4°C to remove N-terminal portion of TEV protease-cleaved FHA from the supernatant, leaving behind cleaved MCD in the flow-through. Fifteen microliters of the flow-through sample was added to 15 mL of 2X Native Sample Buffer. Samples were incubated at room temperature or 95°C for 5 min. Samples were resolved on 0.6% and 2.0% SDS-PAGE gels.

Proteinase-K digest of purified MCD

For digest of native MCD, 100 ng of protein was digested with various concentrations of proteinase-K (from 0 to 100 µg/mL) for 15 min at RT. Sample buffer (2X) was then added to each digest. After boiling, samples were separated using SDS- PAGE, transferred to nitrocellulose, and probed with the anti-MCD antibody. For digest of denatured/renatured MCD, 1 mg of protein was incubated in 50 mL 6 M guanidinium-HCl for 30 min at 50°C, then raised to 1 mL with PBS and

concentrated using 10 kDa MW cut-off centrifugation filters. The sample was then resuspended in PBS and incubated for 30 min at 37°C, vortexing consistently. Samples were then split, loading 1/10 of each sample into individual tubes and digested with various concentrations of proteinase-K (from 0 to 100 µg/mL) for 15 min at RT. Sample buffer (2X) was then added to each digest. After boiling, samples were separated using SDS-PAGE, transferred to nitrocellulose, and probed with the anti- MCD antibody. Densitometry analyses were performed using ImageJ (Schneider et al., 2012).

Accessibility of cysteine substitutions in the MCD

Overnight cultures of RBX11, ΔPD, their respective cysteine substitutions and RBX20 were grown overnight. Cultures were spun down at 14,000 r.p.m. for 3 min. Supernatants were collected and sterilized with a 0.22 µm filter. Filter-sterilized supernatants were then concentrated using a Microcon Ultracel YM-100, spun at 14,000 for 15 min until all supernatant had been concentrated. Columns were washed in 500 mL sterile PBS, pH 7.4. One hundred microliters of PBS was added to the columns; the columns were then inverted in the Eppendorf tube and spun to elute concentrated and washed supernatant protein. Samples were brought to 10 mM DTT and incubated at room temperature for 30 min. Two microliters of 10 mM DyLight 680 Maleimide (1 mg in 100 mL DMF) was added to each sample to bring them to 0.2 mM DyLight. Samples were incubated for 2 h at room temperature.

Sample buffer (2X) was added to samples, which were resolved by SDS-PAGE gel, transferred to nitrocellulose membrane and analyzed by Western blot.

Immunoblotting

Whole-cell lysates and concentrated supernatants were prepared from *Bordetella* cultures as described (Mazar and Cotter, 2006). Samples were resolved by 5.0% and 8.0% polyacrylamide gels (2.0% SDS) as indicated in results section. For anti-MCD immunodetection, IRDye 800CW Goat anti-Rabbit IgG (H + L) was used (Li-cor, diluted 1:25,000). For anti-CRD immunodetection, IRDye 800CW Goat anti-Chicken IgG (H + L) was used (Li-cor, diluted 1:15,000). For anti-PD immunodetection, IRDye 800CW Goat anti-Chicken IgG (H + L) and IRDye 700LT Goat anti-Chicken IgG (H+L) (Li-Cor, diluted 1:25,000) were used. For anti-HA immunodetection, IRDye 680LT Goat anti-Mouse IgG (H + L) was used (Li-Cor, diluted 1:15,000). For anti-BvgS immunodetection, IRDye 800CW Goat anti-Mouse IgG (H + L) was used (Li-Cor, diluted 1:25,000). Membranes were imaged on a Li-Cor Odyssey infrared imaging system.

Proteinase-K digestion of FhaB

Bordetella bronchiseptica cultures were grown to an OD600 of 1.5-3.0. Three samples per strain of 2 OD units were spun at 5,000 r.p.m. for 10 min at 4°C to pellet bacteria. Supernatants were aspirated and pellets were suspended to 200 mL cold

HEPES buffer, pH 7.4. Samples were spun at 5,000 r.p.m. for 5 min at 4°C and supernatants were aspirated. Two hundred microliters of mock reaction buffer (HEPES, pH7.4), 1.0 µg/mL proteinase-K (Sigma-Aldrich) in HEPES, or 1.0 µg/mL proteinase-K with 1 mM PMSF (MP Biomedicals) in HEPES were added to each of the three samples per strain. Reactions proceeded for 30 min at 16°C. Two microliters of PMSF (1 mM final) were added to proteinase-K digested samples to neutralize digestion. All samples were spun at maximum speed for 1 min at room temperature and supernatants were aspirated. Whole-cell lysates were prepared, resolved and immunoblotted as described.

Dot blot analysis

Bordetella bronchiseptica cultures were grown to an OD600 of 2.0-4.0. Volumes equivalent to 2 OD units were spun at max speed for 1 min to pellet bacteria. Supernatants were aspirated and pellets were washed in PBS. Samples were spun again at max speed for 1 min and the wash was aspirated. Samples were suspended in 1 mL of PBS and split into 500 mL aliquots. Bacteria in one tube were boiled for 5 min to lyse cells. Intact and lysed cells in were spotted (50 mL) onto a nitrocellulose membrane using a Whatman® Minifold® I 96-well slot-blot array system. The membrane was blocked in 5% milk-PBS for 1 h. Immunodetection by anti-MCD and anti-HA primary antibodies and goat anti-rabbit and goat anti-mouse secondary antibodies proceeded as described (here and (Mazar and Cotter, 2006).

Growth of prodomain trans-conjugates

In order to avoid cytotoxicty, bacterial cultures were grown overnight in Stainer-Scholte media with a final $MgSO_4$ concentration of 20 mM. After growth, cells were pelleted to remove media, washed three times, then suspended in fresh Stainer-Scholte with no $MgSO_4$ in order to induce expression of the plasmid-borne prodomain.

Mouse experiments

Isofluorane-anesthetized 6-8 week old female BALB/c mice were inoculated intranasally with $5x10^4$ colony forming units of *B. bronchiseptica* in 50 µL volume phosphate-buffered saline. At specified times post-inoculation, all three lobes of right lungs were removed from mice for bacterial burden determination and the large lobe of the left lungs were removed for histopathology analysis. Protocol IACUC ID: 10-134.0-B.

Appendix B – Strain and plasmid list

Strain list

Strain name	Description	Reference
RBX11	RB50 containing a deletion of codons 4-3203 of *fhaS*	(Julio and Cotter, 2005)
RBX11,Δ*sphB1*	RB50 containing a deletion of codons 4-3203 of *fhaS* and a deletion of codons 5-1035 of *sphB1*	This work
RBX20	RB50 containing a deletion of codons 4-3705 of *fhaB* and a deletion of codons 4-3203 of *fhaS*	(Julio and Cotter, 2005)
CTHA	RBX11 containing nine codons encoding the HA epitope (YPYDVPDYA) following codon 3703 in *fhaB*	This work
HAPRR	RBX11 containing nine codons encoding the HA epitope (YPYDVPDYA) following codon 3375 in *fhaB*	This work
HAPRR,Δ*sphB1*	RBX11 containing nine codons encoding the HA epitope (YPYDVPDYA) following codon 3375 in *fhaB* and a deletion of codons 5-1035 of *sphB1*	This work
BPSMAQ	Bp strain containing His7 following Q72 and AcTEV following Y1871 in FhaB	This work
BPSMAQT-N	Bp strain with His7 at Q72, AcTEV at Y1871, truncated at aa 2330, complemented to aa 2410	This work
ΔMCD-PD	RBX11 with a stop codon after bp 5943	
JS26	ΔMCD-PD::pJB51 substituting A1983C, containing codons 1815-3710 followed immediately by a stop codon	This work
JS55	ΔMCD-PD::pJB127 substituting A1983C, containing codons 1815-2588 followed immediately by a stop codon	This work
JS27	ΔMCD-PD::pJB52 substituting V2032C, containing codons 1815-3710 followed immediately by a stop codon	This work

JS56	ΔMCD-PD::pJB128 substituting V2032C, containing codons 1815-2588 followed immediately by a stop codon	This work
JS28	ΔMCD-PD::pJB53 substituting V2081C, containing codons 1815-3710 followed immediately by a stop codon	This work
JS57	ΔMCD-PD::pJB129 substituting V2081C, containing codons 1815-2588 followed immediately by a stop codon	This work
JS48	ΔMCD-PD::pJB87 substituting G2132C, containing codons 1815-3710 followed immediately by a stop codon	This work
JS58	ΔMCD-PD::pJB130 substituting G2132C, containing codons 1815-2588 followed immediately by a stop codon	This work
JS52	ΔMCD-PD::pJB93 substituting A2182C, containing codons 1815-3710 followed immediately by a stop codon	This work
JS59	ΔMCD-PD::pJB131 substituting A2182C, containing codons 1815-2588 followed immediately by a stop codon	This work
JS49	ΔMCD-PD::pJB88 substituting A2233C, containing codons 1815-3710 followed immediately by a stop codon	This work
JS60	ΔMCD-PD::pJB132 substituting A2233C, containing codons 1815-2588 followed immediately by a stop codon	This work
JS51	ΔMCD-PD::pJB89 substituting L2284C, containing codons 1815-3710 followed immediately by a stop codon	This work
JS61	ΔMCD-PD::pJB133 substituting L2284C, containing codons 1815-2588 followed immediately by a stop codon	This work
JS50	ΔMCD-PD::pJB90 substituting I2333C, containing codons 1815-	This work

	3710 followed immediately by a stop codon	
JS62	ΔMCD-PD::pJB134 substituting I2333C, containing codons 1815-2588 followed immediately by a stop codon	This work
JS53	ΔMCD-PD::pJB94 substituting A2382C, containing codons 1815-3710 followed immediately by a stop codon	This work
JS63	ΔMCD-PD::pJB135 substituting A2382C, containing codons 1815-2588 followed immediately by a stop codon	This work
JS54	ΔMCD-PD::pJB95 substituting A2432C, containing codons 1815-3710 followed immediately by a stop codon	This work
JS64	ΔMCD-PD::pJB136 substituting A2432C, containing codons 1815-2588 followed immediately by a stop codon	This work
HA-ΔCS	HAPRR containing a deletion of codons 2217-2647	This work
HA-ΔCS,Δ*sphB1*	HAPRR,Δ*sphB1*containing a deletion of codons 2217-2647	This work
HA-ΔMCT	HAPRR containing deletion of codons 2217-2471	This work
HA-ΔMCT,Δ*sphB1*	HAPRR,Δ*sphB1* containing deletion of codons 2217-2471	This work
HA-ΔPNT	HAPRR containing deletion of codons 2472-2647	This work
HA-ΔPNT,Δ*sphB1*	HAPRR,Δ*sphB1* containing deletion of codons 2472-2647	This work
Δ28-PD	RBX11 containing a stop codon in *fhaB* at position 2441	(Mazar and Cotter, 2006)
HA-ΔMCD	HAPRR containing deletion of codons 1981-2471	This work
HA-ΔMCD,Δ*sphB1*	HAPRR,Δ*sphB1* containing deletion of codons 1981-2471	This work
HA-ΔMNT	HAPRR containing deletion of codons 1981-2216	This work
HA-ΔMNT,Δ*sphB1*	HAPRR,Δ*sphB1* containing deletion of codons 1981-2216	This work
ΔMCT-PD	RBX11::pEG7-TX containing codons 2217-2441 followed immediately by a	This work

	stop codon	
ΔMCT-PD,Δ*sphB1*	RBX11,Δ*sphB1*::pEG7-TX containing codons 2217-2441 followed immediately by a stop codon	This work
ΔECT	RBX11::pEG7-TX containing codons 3417-3612 followed immediately by a stop codon	This work
ΔECT,Δ*sphB1*	RBX11,Δ*sphB1*::pEG7-TX containing codons 3417-3612 followed immediately by a stop codon	This work
ΔPRR-ECT	Δ28-PD::pEG7-T-E containing codons 2228-3371 followed immediately by a stop codon	(Mazar and Cotter, 2006)
ΔPRR-ECT,Δ*sphB1*	RBX11,Δ*sphB1*::pEG7-T-E containing codons 2228-3371 followed immediately by a stop codon	This work
ΔPD	Δ28-PD::pEG7-T-N containing codons 2228-2588 followed immediately by a stop codon	(Mazar and Cotter, 2007)
ΔPD,Δ*sphB1*	RBX11,Δ*sphB1*::pEG7-T-N containing codons 2228-2588 followed immediately by a stop codon	This work
HA-ΔECT	HAPRR::pEG7-TX containing codons 3417-3612 followed immediately by a stop codon	This work
HA-ΔMCTΔECT	HA-ΔMCT::pEG7-TX containing codons 3417-3612 followed immediately by a stop codon	This work
HA-ΔMCTΔECT, Δ*sphB1*	HA-ΔMCT,Δ*sphB1*::pEG7-TX containing codons 3417-3612 followed immediately by a stop codon	This work
ΔPRR	HAPRR containing deletion of codons 3364-3608	This work
ΔPK	HAPRR containing a deletion of codons 3582-3601	This work
ΔPK,Δ*sphB1*	HAPRR,Δ*sphB1* containing deletion of codons 3582-3601	This work
PD^{Comp}	Δ28-PD::pEG7-T-C containing codons 2228-3710 followed immediately by a stop codon (equivalent to wild-type *fhaB*)	(Mazar and Cotter, 2006)
RBX11::pSJ22	Δ*fhaS* containing a plasmid insertion (null mutation) in *fhaC*	(Julio and Cotter, 2005)

RBX11/pSP-PD-PRR	RBX11 containing the medium copy plasmid pSP-PD-PRR	This work
RBX20/pSP-PD-PRR	RBX20 containing the medium copy plasmid pSP-PD-PRR	This work
RBX11::pSJ22/pSP-PD-PRR	RBX11::pSJ22 containing the medium copy plasmid pSP-PD-PRR	This work
RBX11/pPD-PRR	RBX11 containing the medium copy plasmid pPD-PRR	This work
PD^{Comp}/pPD-PRR	PD^{Comp} containing the medium copy plasmid pPD-PRR	This work
ΔPD/pPD-PRR	RBX11 containing the medium copy plasmid pPD-PRR	This work
ΔMCD-PD /pPD-PRR	ΔMCD-PD containing the medium copy plasmid pPD-PRR	This work
RBX20/pPD-PRR	RBX20 containing the medium copy plasmid pPD-PRR	This work
RBX11::pSJ22/pPD-PRR	RBX11::pSJ22 containing the medium copy plasmid pPD-PRR	This work
RBX11/pPD	RBX11 containing the medium copy plasmid pPD	This work
PD^{Comp}/pPD	PD^{Comp} containing the medium copy plasmid pPD	This work
ΔPD/pPD	RBX11 containing the medium copy plasmid pPD	This work
ΔMCD-PD /pPD	ΔMCD-PD containing the medium copy plasmid pPD	This work
RBX20/pPD	RBX20 containing the medium copy plasmid pPD	This work
RBX11::pSJ22/pPD	RBX11::pSJ22 containing the medium copy plasmid pPD	This work
RBX11/ pSP-PD	RBX11 containing the medium copy plasmid pSP-PD	This work
PD^{Comp}/pSP-PD	PD^{Comp} containing the medium copy plasmid pSP-PD	This work
ΔPD/pSP-PD	RBX11 containing the medium copy plasmid pSP-PD	This work
ΔMCD-PD /pSP-PD	ΔMCD-PD containing the medium copy plasmid pSP-PD	This work
RBX20/pSP-PD	RBX20 containing the medium copy plasmid pSP-PD	This work
RBX11::pSJ22/pSP-PD	RBX11::pSJ22 containing the medium copy plasmid pSP-PD	This work
DH5α	*E. coli* molecular cloning strain	BRL; Gaithersburg, MD

SM10λpir	Conjugation strain	(Miller and Mekalanos, 1988)
RHO3	Conjugation strain	(López et al., 2009)

Plasmid list

Plasmid name	Description	Reference
pEG7	Suicide plasmid used to construct *B. pertussis* and *B. bronchiseptica* strains containing co-integrates	(Akerley et al., 1995)
pEG7S	*sacB*-containing allelic exchange plasmid used to construct *B. bronchiseptica* strains	(Martínez de Tejada et al., 1996)
pSORTP1	Allelic Exchange vector for *B. pertussis*	(Mazar and Cotter, 2006)
pBBR1-MCS	*Bordetella* self-replicating plasmid	(Kovach et al., 1994)
pSS4245	pBR322-based allelic exchange plasmid for use in *Bordetella* species. Contains I-SceI cleavage site and encodes restriction endonuclease, I-SceI, under the control of the pertussis toxin (ptx) promoter	(Inatsuka et al., 2010)
pEG7S-Δ*sphB1*	pEG7S derivative used to introduce the Δ*sphB1* deletion mutation into *B. bronchiseptica* strains	(Mazar and Cotter, 2006)
pEG7-CTHA	pEG7 derivative containing nucleotides corresponding to codons 3429-3710 followed immediately by a stop codon and then 500 bp corresponding to the region immediately 3′ of *fhaB* with nucleotides encoding the HA epitope following codon 3703	This work
pSS4245-HAPRR	pSS4245 derivative containing nucleotides corresponding to codons 3208-3567 with nucleotides encoding the HA	This work

	epitope following codon 3375	
pSORTP1-Bp MCI/Y1871/AcTEV	Bp mating vector for Y1871AcTEV mutagenesis in FhaB	This work
pSORTP1-SS Template/Q72His7	Bp mating vector for Q72His7 mutagenesis in FhaB	This work
pJB48	pEG7 derivative containing nucleotides corresponding to codons 1814-3710 of *fhaB* followed immediately by a stop codon	This work
pJB101	pEG7 derivative containing nucleotides corresponding to codons 1814-2588 of *fhaB* followed immediately by a stop codon	This work
pJB28	pCR2.1 derivative containing nucleotides 5441-7410 of *fhaB*. Used for QuickChange substitutions. QuickChange derivatives were subcloned into pJB48 and pJB101.	This work
pJB51	pJB48 in which codon 1983 has been changed to encode Cys instead of Ala	This work
pJB127	pJB101 in which codon 1983 has been changed to encode Cys instead of Ala	This work
pJB52	pJB48 in which codon 2032 has been changed to encode Cys instead of Val	This work
pJB128	pJB101 in which codon 2032 has been changed to encode Cys instead of Val	This work
pJB53	pJB48 in which codon 2081 has been changed to encode Cys instead of Val	This work
pJB129	pJB101 in which codon 2081 has been changed to encode Cys instead of Val	This work
pJB87	pJB48 in which codon 2132 has been changed to encode Cys instead of Gly	This work
pJB130	pJB101 in which codon 2132 has been changed to encode Cys instead of Gly	This work

pJB93	pJB48 in which codon 2182 has been changed to encode Cys instead of Ala	This work
pJB131	pJB101 in which codon 2182 has been changed to encode Cys instead of Ala	This work
pJB88	pJB48 in which codon 2233 has been changed to encode Cys instead of Ala	This work
pJB132	pJB101 in which codon 2233 has been changed to encode Cys instead of Ala	This work
pJB89	pJB48 in which codon 2284 has been changed to encode Cys instead of Leu	This work
pJB133	pJB101 in which codon 2284 has been changed to encode Cys instead of Leu	This work
pJB90	pJB48 in which codon 2333 has been changed to encode Cys instead of Ile	This work
pJB134	pJB101 in which codon 2333 has been changed to encode Cys instead of Ile	This work
pJB94	pJB48 in which codon 2382 has been changed to encode Cys instead of Ala	This work
pJB135	pJB101 in which codon 2382 has been changed to encode Cys instead of Ala	This work
pJB95	pJB48 in which codon 2432 has been changed to encode Cys instead of Ala	This work
pJB136	pJB101 in which codon 2432 has been changed to encode Cys instead of Ala	This work
pSS4245-ΔCS	pSS4245 derivative containing nucleotides corresponding to codons 2048-2216 and 2648-2808 of *fhaB*	This work
pSS4245-ΔMCT	pSS4245 derivative containing nucleotides corresponding to codons 2048-2216 and 2472-3640 of *fhaB*	This work
pSS4245-ΔPNT	pSS4245 derivative containing nucleotides corresponding to	This work

	codons 2295-2471 and 2648-2808 of *fhaB*	
pSS4245-ΔMCD	pSS4245 derivative containing nucleotides corresponding to codons 1800-1980 and 2472-3640 of *fhaB*	This work
pSS4245-ΔMNT	pSS4245 derivative containing nucleotides corresponding to codons 1800-1980 and 2217-2400 of *fhaB*	This work
pEG7-ΔMCT-PD	pEG7 derivative containing nucleotides corresponding to codons 2256-2441 of *fhaB* followed immediately by a stop codon	This work
pEG7-TX	pEG7 derivative containing nucleotides corresponding to codons 3418-3612 of *fhaB* followed immediately by a stop codon	This work
pEG7-T-E	pEG7 derivative containing nucleotides corresponding to codons 2228-3371 of *fhaB* followed immediately by a stop codon	(Mazar and Cotter, 2006)
pSS4245-ΔPRR	pSS4245 derivative containing nucleotides corresponding to codons 3178-3363 and 500 nucleotides beginning at codon 3609 of *fhaB*	This work
pSS4245-ΔPK	pSS4245 derivative containing nucleotides corresponding to codons 3400-3581 and 500 nucleotides beginning at codon 3602 of *fhaB*	This work
pSJ22	pEG7 derivative containing an internal fragment of *fhaC* for disruption	(Julio and Cotter, 2005)
pSP-PD-PRR	pBBR1-MCS derivative containing nucleotides encoding the *fhaB* promoter, signal peptide, prodomain, and PRR/ECT	This work
pPD-PRR	pBBR1-MCS derivative containing nucleotides encoding the *fhaB* promoter,	This work

	prodomain, and PRR/ECT	
pPD	pBBR1-MCS derivative containing nucleotides encoding the *fhaB* promoter and prodomain	This work
pSP-PD	pBBR1-MCS derivative containing nucleotides encoding the *fhaB* promoter, signal peptide and prodomain	This work

Appendix C – Strain and plasmid construction

Strain construction

RBX11Δ,*sphB1* was constructed by performing allelic exchange on RBX11 using plasmid pEG7S-Δ*sphB1* as described (Martínez de Tejada et al., 1996). The strain was confirmed to be constructed as intended by PCR and nucleotide sequence analysis.

HAPRR and HAPRR,Δ*sphB1* were constructed by performing allelic exchange on RBX11 and RBX11,Δ*sphB1*, respectively, using plasmid pSS4245-HAPRR as described (Inatsuka et al., 2010). The strains were confirmed to be constructed as intended by PCR and nucleotide sequence analysis.

HA-ΔCS and HA-ΔCSΔ,*sphB1* were constructed by performing allelic exchange on HAPRR and HAPRR,Δ*sphB1*, respectively, using plasmid pSS4245-ΔCS. The strains were confirmed to be constructed as intended by PCR and nucleotide sequence analysis.

HA-ΔMCT and HA-ΔMCT,Δ*sphB1* were constructed by performing allelic exchange on HAPRR and HAPRR,Δ*sphB1*, respectively, using plasmid pSS4245-ΔMCT. The strains were confirmed to be constructed as intended by PCR and nucleotide sequence analysis.

HA-ΔPNT and HA-ΔPNT,Δ*sphB1* were constructed by performing allelic exchange on HAPRR and HAPRR,Δ*sphB1*, respectively, using plasmid pSS4245-ΔPNT. The strains were confirmed to be constructed as intended by PCR and nucleotide sequence analysis.

HA-ΔMCD and HA-ΔMCD,Δ*sphB1* were constructed by performing allelic exchange on HAPRR and HAPRR,Δ*sphB1*, respectively, using plasmid pSS4245-ΔMCD. The strains were confirmed to be constructed as intended by PCR and nucleotide sequence analysis.

HA-ΔMNT and HA-ΔMNT,Δ*sphB1* were constructed by performing allelic exchange on HAPRR and HAPRR,Δ*sphB1*, respectively, using plasmid pSS4245-ΔMNT. The strains were confirmed to be constructed as intended by PCR and nucleotide sequence analysis.

ΔPRR was constructed by performing allelic exchange on HAPRR using plasmid pSS4245-ΔPRR. The strain was confirmed to be constructed as intended by PCR and nucleotide sequence analysis.

ΔPK and ΔPK,Δ*sphB1* were constructed by performing allelic exchange on HAPRR and HAPRR,Δ*sphB1*, respectively, using plasmid pSS4245-ΔPK. The strains were confirmed to be constructed as intended by PCR and nucleotide sequence analysis.

BPSMAQ was constructed by performing allelic exchange on BPSM using plasmids pSORTP1-Bp MCI/Y1871/AcTEV and pSORTP1-SS Template/Q72His7. The strains were confirmed to be constructed as intended by PCR and nucleotide sequence analysis

BPSMAQT-N was constructed by introducing pEG7-FI1a/C&R-N into BPSMAQ by conjugation and selecting co-integrates on BG-Sm-Gm agar as described (Akerley et al., 1995) Integration of plasmids at the correct site in the chromosome was confirmed by PCR.

CTHA was constructed by introducing pEG7-CTHA into RBX11 by conjugation and selecting co-integrates on BG-Sm-Gm agar. Integration of the plasmids at the correct site in the chromosome was confirmed by PCR.

ΔMCT-PD and ΔMCT-PD,Δ*sphB1* were constructed by introducing pEG7-ΔMCT-PD into RBX11 and RBX11,Δ*sphB1*, respectively, by conjugation and selecting co-integrates on BG-Sm-Gm agar. Integration of the plasmids at the correct site in the chromosome was confirmed by PCR.

ΔECT, ΔECT,Δ*sphB1*, HA-ΔECT, HA-ΔMCTΔECT, and HA-ΔMCTΔECT,Δ*sphB1* were constructed by introducing pEG7-TX into RBX11, RBX11,Δ*sphB1*, HAPRR, HA-ΔMCT, and HA-ΔMCT,Δ*sphB1*, respectively, by conjugation and selecting co-

integrates on BG-Sm-Gm agar. Integration of the plasmids at the correct site in the chromosome was confirmed by PCR.

ΔPRR-ECT,Δ*sphB1* and ΔPD,Δ*sphB1* were constructed by introducing pEG7-T-E and pEG7-T-N, respectively, into RBX11,Δ*sphB1* by conjugation and selecting co-integrates on BG-Sm-Gm agar. Integration of the plasmids at the correct site in the chromosome was confirmed by PCR.

JS26, JS55, JS27, JS56, JS28, JS57, JS48, JS58, JS52, JS59, JS49, JS60, JS51, JS61, JS50, JS62, JS53, JS63, JS54, and JS64 were constructed by introducing - pJB51, pJB127, pJB52, pJB128, pJB53, pJB129, pJB87, pJB130, pJB93, pJB131, pJB88, pJB132, pJB89, pJB133, pJB90, pJB134, pJB94, pJB135, pJB95, and pJB136, respectively, into ΔMCD-PD by conjugation and selecting co-integrates on BG-Sm-Gm agar. Integration of the plasmids at the correct site in the chromosome was confirmed by PCR.

RBX11/pSP-PD-PRR, RBX20/pSP-PD-PRR and RBX11::pSJ22/pSP-PD-PRR were constructed by introducing pSP-PD-PRR into RBX11, RBX20 and RBX11::pSJ22, respectively, by conjugation and selecting trans-conjugates on BG-Sm-Cm agar. Plasmid acquisition was confirmed by PCR.

RBX11/pPD-PRR, PD^{Comp}/pPD-PRR, ΔPD /pPD-PRR, ΔMCD-PD/pPD-PRR, RBX20/pPD-PRR, and RBX11::pSJ22/pPD-PRR were constructed by introducing pPD-PRR into RBX11, PD^{Comp}, ΔPD, ΔMCD-PD, RBX20, and RBX11::pSJ22, respectively, by conjugation and selecting trans-conjugates on BG-Sm-Cm agar. Plasmid acquisition was confirmed by PCR.

RBX11/pPD, PD^{Comp}/pPD, ΔPD /pPD, ΔMCD-PD/pPD, RBX20/pPD, and RBX11::pSJ22/pPD were constructed by introducing pPD into RBX11, PD^{Comp}, ΔPD, ΔMCD-PD, RBX20, and RBX11::pSJ22, respectively, by conjugation and selecting trans-conjugates on BG-Sm-Cm agar. Plasmid acquisition was confirmed by PCR.

RBX11/pSP-PD, PD^{Comp} /pSP-PD, ΔPD /pSP-PD, ΔMCD-PD/pSP-PD, RBX20/pSP-PD, and RBX11::pSJ22/pSP-PD were constructed by introducing pSP-PD into RBX11, PD^{Comp}, ΔPD, ΔMCD-PD, RBX20, and RBX11::pSJ22, respectively, by conjugation and selecting trans-conjugates on BG-Sm-Cm agar. Plasmid acquisition was confirmed by PCR.

Plasmid construction

pJB28 is a pCR2.1 derivative that contains a PCR-amplified 2.0 kb fragment of RBX11 *fhaB* (corresponding to codons 1814 through 2470).

The following plasmids are pEG7 derivatives used to construct co-integrate strains. Sequences cloned into this plasmid between the gentamicin resistance gene and ampicilin resistance gene are described.

pJB48 contains PCR-amplified 2.0 kb, and 3.8 kb fragments of RBX11 *fhaB* (corresponding to codons 1814 through 2470 and codons 2471-3710 followed by a STOP codon) from RBX11 ligated together.

pJB101 contains PCR-amplified 2.0 kb, and 350 bp fragments of RBX11 *fhaB* (corresponding to codons 1814 through 2470 and codons 2471-2588 followed by a STOP codon) from RBX11 ligated together.

pJB51, pJB52, pJB53, pJB87, pJB93, pJB88, pJB89, pJB90, pJB94 and pJB95 contain PCR-amplified 2.0 kb, and 3.8 kb fragments of RBX11 *fhaB* (corresponding to codons 1814 through 2470 and codons 2471-3710 followed by a STOP codon) from RBX11 ligated together with a QuickChange mutagenesis of the residues specified in plasmid list.

pJB127, pJB128, pJB129, pJB130, pJB131, pJB132, pJB133, pJB134, pJB135 and pJB136 contain PCR-amplified 2.0 kb, and 350 bp fragments of RBX11 *fhaB* (corresponding to codons 1814 through 2470 and codons 2471-2588 followed by a stop codon) from RBX11 ligated together with a QuickChange mutagenesis of the residues specified in plasmid list.

pEG7-CTHA contains PCR-amplified 0.6 kb (corresponding to codons 3429 through 3703) and 0.5 kb fragments of RBX11 *fhaB* (corresponding to codon 3703 extending to 457 bp 3′ of STOP codon) ligated together with nucleotides encoding an HA epitope following codon 3703.

pEG7-TX contains PCR-amplified 0.6 kb (corresponding to codons 3418 through 3612) followed immediately by a STOP codon.

The following plasmids are pSS4245 derivatives used for allelic exchange in *B. bronchiseptica*. Sequences cloned into this plasmid between the I-SceI cleavage site and the tetracycline resistance gene are described.

pSS4245-HAPRR contains PCR-amplified 0.5 kb (corresponding to codons 3208 through 3375) and 0.6 kb fragments of RBX11 *fhaB* (corresponding to codons 3375 through 3567) ligated together with nucleotides encoding an HA epitope following codon 3375.

pSS4245-ΔCS contains PCR-amplified 0.5 kb (corresponding to codons 2048 through 2216) and 0.5 kb fragments of RBX11 *fhaB* (corresponding to codons 2648 through 2808) ligated together.

pSS4245-ΔMCT contains PCR-amplified 0.5 kb (corresponding to codons 2048 through 2216) and 0.5 kb fragments of RBX11 *fhaB* (corresponding to codons 2472 through 2640) ligated together.

pSS4245-ΔPNT contains PCR-amplified 0.5 kb (corresponding to codons 2295 through 2471) and 0.5 kb fragments of RBX11 *fhaB* (corresponding to codons 2648 through 2808) ligated together.

pSS4245-ΔMCD contains PCR-amplified 0.5 kb (corresponding to codons 1800 through 1980) and 0.5 kb fragments of RBX11 *fhaB* (corresponding to codons 2472 through 3640) ligated together.

pSS4245-ΔMNT contains PCR-amplified 0.5 kb (corresponding to codons 1800 through 1980) and 0.5 kb fragments of RBX11 *fhaB* (corresponding to codons 2217 through 2400) ligated together.

pSS4245-ΔPRR contains PCR-amplified 0.5 kb (corresponding to codons 3178 through 3363) and 0.5 kb fragments of RBX11 *fhaB* (beginning at codon 3609 and extending past the *fhaB* stop codon) ligated together.

pSS4245-ΔPK contains PCR-amplified 0.5 kb (corresponding to codons 3400 through 3581) and 0.5 kb fragments of RBX11 *fhaB* (beginning at codon 3602 and extending past the *fhaB* stop codon) ligated together.

The following plasmids are pBBR1-MCS derivatives used for trans-conjugation in *B. bronchiseptica*. Sequences cloned into this plasmid into the *lacZ* gene are described.

pSP-PD-PRR contains a 600 bp fragment (corresponding to the *fhaB* promoter and signal peptide) and a 3.6 kb fragment (corresponding to the *fhaB* prodomain) ligated together.

pPD-PRR contains a 400 bp fragment (corresponding to the *fhaB* promoter) and a 3.6 kb fragment (corresponding to the *fhaB* prodomain) ligated together.

pPD contains a 400 bp fragment (corresponding to the *fhaB* promoter) and a 2.6 kb fragment (corresponding to the beginning of the *fhaB* prodomain) ligated together.

pSP-PD contains a 600 bp fragment (corresponding to the *fhaB* promoter and signal peptide) and a 2.6 kb fragment (corresponding to the beginning of the *fhaB* prodomain) ligated together.

The following plasmids are pSORTP1 derivatives used for allelic exchange in *B. pertussis*. Sequences cloned into this plasmid between the gentamicin resistance gene and ampicilin resistance gene are described.

pSORTP1-Bp MCI/Y1871/AcTEV contains PCR-amplified 600 bp fragments flanking the codon for Y1871 of RBX11 *fhaB* with nucleotides encoding an AcTEV cleavage site inserted following Y1871.

pSORTP1-SS Template/Q72His7 contains PCR-amplified 600 bp fragments flanking the codon for Q72 of RBX11 *fhaB* with nucleotides encoding a His7 epitope inserted following Q72.

References

Abramson, T., Kedem, H., and Relman, D.A. (2008). Modulation of the NF-kappaB pathway by Bordetella pertussis filamentous hemagglutinin. PLoS ONE *3*, e3825.

Adams, T.M., Wentzel, A., and Kolmar, H. (2005). Intimin-mediated export of passenger proteins requires maintenance of a translocation-competent conformation. J. Bacteriol. *187*, 522–533.

Akerley, B.J., Cotter, P.A., and Miller, J.F. (1995). Ectopic expression of the flagellar regulon alters development of the Bordetella-host interaction. Cell *80*, 611–620.

Albers, S.-V., Szabó, Z., and Driessen, A.J.M. (2006). Protein secretion in the Archaea: multiple paths towards a unique cell surface. Nat. Rev. Microbiol. *4*, 537–547.

Anderson, M.S., Garcia, E.C., and Cotter, P.A. (2012). The Burkholderia bcpAIOB Genes Define Unique Classes of Two-Partner Secretion and Contact Dependent Growth Inhibition Systems. PLoS Genet. *8*, e1002877.

Antoine, R., and Locht, C. (1992). Isolation and molecular characterization of a novel broad-host-range plasmid from Bordetella bronchiseptica with sequence similarities to plasmids from gram-positive organisms. Mol. Microbiol. *6*, 1785–1799.

Aoki, S.K., Diner, E.J., de Roodenbeke, C.T., Burgess, B.R., Poole, S.J., Braaten, B.A., Jones, A.M., Webb, J.S., Hayes, C.S., Cotter, P.A., et al. (2010). A widespread family of polymorphic contact-dependent toxin delivery systems in bacteria. Nature *468*, 439–442.

Aoki, S.K., Pamma, R., Hernday, A.D., Bickham, J.E., Braaten, B.A., and Low, D.A. (2005). Contact-dependent inhibition of growth in Escherichia coli. Science *309*, 1245–1248.

Aricò, B., Nuti, S., Scarlato, V., and Rappuoli, R. (1993). Adhesion of Bordetella pertussis to eukaryotic cells requires a time-dependent export and maturation of filamentous hemagglutinin. Proc. Natl. Acad. Sci. U.S.a. *90*, 9204–9208.

Batchelor, M., Prasannan, S., Daniell, S., Reece, S., Connerton, I., Bloomberg, G., Dougan, G., Frankel, G., and Matthews, S. (2000). Structural basis for recognition of the translocated intimin receptor (Tir) by intimin from enteropathogenic Escherichia coli. Embo J. *19*, 2452–2464.

Baud, C., Gutsche, I., Willery, E., de Paepe, D., Drobecq, H., Gilleron, M., Locht, C., Jamin, M., and Jacob-Dubuisson, F. (2011). Membrane-associated DegP in Bordetella chaperones a repeat-rich secretory protein. Mol. Microbiol. *80*, 1625–1636.

Baud, C., Hodak, H., Willery, E., Drobecq, H., Locht, C., Jamin, M., and Jacob-Dubuisson, F. (2009). Role of DegP for two-partner secretion in Bordetella. Mol. Microbiol. *74*, 315–329.

Bodelón, G., Marín, E., and Fernández, L.A. (2009). Role of periplasmic chaperones and BamA (YaeT/Omp85) in folding and secretion of intimin from enteropathogenic Escherichia coli strains. J. Bacteriol. *191*, 5169–5179.

Boucher, P.E., Murakami, K., Ishihama, A., and Stibitz, S. (1997). Nature of DNA binding and RNA polymerase interaction of the Bordetella pertussis BvgA transcriptional activator at the fha promoter. J. Bacteriol. *179*, 1755–1763.

Boucher, P.E., Yang, M.S., and Stibitz, S. (2001). Mutational analysis of the high-affinity BvgA binding site in the fha promoter of Bordetella pertussis. Mol. Microbiol. *40*, 991–999.

Braakman, I., and Bulleid, N.J. (2011). Protein folding and modification in the mammalian endoplasmic reticulum. Annu. Rev. Biochem. *80*, 71–99.

Brewer, S., Tolley, M., Trayer, I.P., Barr, G.C., Dorman, C.J., Hannavy, K., Higgins, C.F., Evans, J.S., Levine, B.A., and Wormald, M.R. (1990). Structure and function of X-Pro dipeptide repeats in the TonB proteins of Salmonella typhimurium and Escherichia coli. J. Mol. Biol. *216*, 883–895.

Brillard, J., Duchaud, E., Boemare, N., Kunst, F., and Givaudan, A. (2002). The PhlA hemolysin from the entomopathogenic bacterium Photorhabdus luminescens belongs to the two-partner secretion family of hemolysins. J. Bacteriol. *184*, 3871–3878.

Buscher, A.Z., Grass, S., Heuser, J., Roth, R., and St Geme, J.W. (2006). Surface anchoring of a bacterial adhesin secreted by the two-partner secretion pathway. Mol. Microbiol. *61*, 470–483.

Chevalier, N., Moser, M., Koch, H.G., Schimz, K.L., Willery, E., Locht, C., Jacob-Dubuisson, F., and Muller, M. (2004). Membrane targeting of a bacterial virulence factor harbouring an extended signal peptide. J Mol Microbiol Biotechnol *8*, 7–18.

Choi, P.S., Dawson, A.J., and Bernstein, H.D. (2007). Characterization of a novel two-partner secretion system in Escherichia coli O157:H7. J. Bacteriol. *189*, 3452–3461.

Clantin, B., Delattre, A.S., Rucktooa, P., Saint, N., Meli, A.C., Locht, C., Jacob-Dubuisson, F., and Villeret, V. (2007). Structure of the membrane protein FhaC: a member of the Omp85-TpsB transporter superfamily. Science *317*, 957–961.

Clantin, B., Hodak, H., Willery, E., Locht, C., Jacob-Dubuisson, F., and Villeret, V. (2004). The crystal structure of filamentous hemagglutinin secretion domain and its implications for the two-partner secretion pathway. Proc. Natl. Acad. Sci. U.S.a. *101*,

6194–6199.

Cotter, P.A., and Miller, J.F. (1994). BvgAS-mediated signal transduction: analysis of phase-locked regulatory mutants of Bordetella bronchiseptica in a rabbit model. Infect. Immun. *62*, 3381–3390.

Cotter, P.A., Yuk, M.H., Mattoo, S., Akerley, B.J., Boschwitz, J., Relman, D.A., and Miller, J.F. (1998). Filamentous hemagglutinin of Bordetella bronchiseptica is required for efficient establishment of tracheal colonization. Infect. Immun. *66*, 5921–5929.

Cotter, S.E., Surana, N.K., and St Geme, J.W. (2005). Trimeric autotransporters: a distinct subfamily of autotransporter proteins. Trends Microbiol. *13*, 199–205.

Coutte, L., Alonso, S., Reveneau, N., Willery, E., Quatannens, B., Locht, C., and Jacob-Dubuisson, F. (2003). Role of adhesin release for mucosal colonization by a bacterial pathogen. J. Exp. Med. *197*, 735–742.

Coutte, L., Antoine, R., Drobecq, H., Locht, C., and Jacob-Dubuisson, F. (2001). Subtilisin-like autotransporter serves as maturation protease in a bacterial secretion pathway. Embo J. *20*, 5040–5048.

Crooks, G.E., Hon, G., Chandonia, J.-M., and Brenner, S.E. (2004). WebLogo: a sequence logo generator. Genome Res. *14*, 1188–1190.

Dautin, N., and Bernstein, H.D. (2007). Protein secretion in gram-negative bacteria via the autotransporter pathway. Annu. Rev. Microbiol. *61*, 89–112.

Dawid, S., Grass, S., and St Geme, J.W. (2001). Mapping of binding domains of nontypeable Haemophilus influenzae HMW1 and HMW2 adhesins. Infect. Immun. *69*, 307–314.

Delattre, A.-S., Clantin, B., Saint, N., Locht, C., Villeret, V., and Jacob-Dubuisson, F. (2010). Functional importance of a conserved sequence motif in FhaC, a prototypic member of the TpsB/Omp85 superfamily. Febs J. *277*, 4755–4765.

Delattre, A.-S., Saint, N., Clantin, B., Willery, E., Lippens, G., Locht, C., Villeret, V., and Jacob-Dubuisson, F. (2011). Substrate recognition by the POTRA domains of TpsB transporter FhaC. Mol. Microbiol. *81*, 99–112.

Delisse-Gathoye, A.M., Locht, C., Jacob, F., Raaschou-Nielsen, M., Heron, I., Ruelle, J.L., de Wilde, M., and Cabezon, T. (1990). Cloning, partial sequence, expression, and antigenic analysis of the filamentous hemagglutinin gene of Bordetella pertussis. Infect. Immun. *58*, 2895–2905.

Desvaux, M., Scott-Tucker, A., Turner, S.M., Cooper, L.M., Huber, D., Nataro, J.P., and Henderson, I.R. (2007). A conserved extended signal peptide region directs posttranslational protein translocation via a novel mechanism. Microbiology

(Reading, Engl.) *153*, 59–70.

Dieterich, C., and Relman, D.A. (2011). Modulation of the host interferon response and ISGylation pathway by B. pertussis filamentous hemagglutinin. PLoS ONE *6*, e27535.

Emsley, P., Charles, I.G., Fairweather, N.F., and Isaacs, N.W. (1996). Structure of Bordetella pertussis virulence factor P.69 pertactin. Nature *381*, 90–92.

Genevrois, S., Steeghs, L., Roholl, P., Letesson, J.-J., and van der Ley, P. (2003). The Omp85 protein of Neisseria meningitidis is required for lipid export to the outer membrane. Embo J. *22*, 1780–1789.

Gentle, I., Gabriel, K., Beech, P., Waller, R., and Lithgow, T. (2004). The Omp85 family of proteins is essential for outer membrane biogenesis in mitochondria and bacteria. J. Cell Biol. *164*, 19–24.

Gentle, I.E., Burri, L., and Lithgow, T. (2005). Molecular architecture and function of the Omp85 family of proteins. Mol. Microbiol. *58*, 1216–1225.

Grass, S., and St Geme, J.W. (2000). Maturation and secretion of the non-typable Haemophilus influenzae HMW1 adhesin: roles of the N-terminal and C-terminal domains. Mol. Microbiol. *36*, 55–67.

Guedin, S., Willery, E., Locht, C., and Jacob-Dubuisson, F. (1998). Evidence that a globular conformation is not compatible with FhaC-mediated secretion of the Bordetella pertussis filamentous haemagglutinin. Mol. Microbiol. *29*, 763–774.

Guedin, S., Willery, E., Tommassen, J., Fort, E., Drobecq, H., Locht, C., and Jacob-Dubuisson, F. (2000). Novel topological features of FhaC, the outer membrane transporter involved in the secretion of the Bordetella pertussis filamentous hemagglutinin. J. Biol. Chem. *275*, 30202–30210.

Hamburger, Z.A., Brown, M.S., Isberg, R.R., and Bjorkman, P.J. (1999). Crystal structure of invasin: a bacterial integrin-binding protein. Science *286*, 291–295.

Hannavy, K., Barr, G.C., Dorman, C.J., Adamson, J., Mazengera, L.R., Gallagher, M.P., Evans, J.S., Levine, B.A., Trayer, I.P., and Higgins, C.F. (1990). TonB protein of Salmonella typhimurium. A model for signal transduction between membranes. J. Mol. Biol. *216*, 897–910.

Hayes, C.S., Aoki, S.K., and Low, D.A. (2010). Bacterial contact-dependent delivery systems. Annu. Rev. Genet. *44*, 71–90.

Henderson, I.R., Navarro-Garcia, F., Desvaux, M., Fernandez, R.C., and Ala'Aldeen, D. (2004). Type V protein secretion pathway: the autotransporter story. Microbiol Mol Biol Rev *68*, 692–744.

Henderson, M.W., Inatsuka, C.S., Sheets, A.J., Williams, C.L., Benaron, D.J., Donato, G.M., Gray, M.C., Hewlett, E.L., and Cotter, P.A. (2012). Contribution of Bordetella filamentous hemagglutinin and adenylate cyclase toxin to suppression and evasion of interleukin-17-mediated inflammation. Infect. Immun. *80*, 2061–2075.

Hertle, R. (2005). The family of Serratia type pore forming toxins. Curr. Protein Pept. Sci. *6*, 313–325.

Hertle, R., Hilger, M., Weingardt-Kocher, S., and Walev, I. (1999). Cytotoxic action of Serratia marcescens hemolysin on human epithelial cells. Infect. Immun. *67*, 817–825.

Hiss, J.A., and Schneider, G. (2009). Domain organization of long autotransporter signal sequences. Bioinform Biol Insights *3*, 189–204.

Hodak, H., Clantin, B., Willery, E., Villeret, V., Locht, C., and Jacob-Dubuisson, F. (2006). Secretion signal of the filamentous haemagglutinin, a model two-partner secretion substrate. Mol. Microbiol. *61*, 368–382.

Hodak, H., Wohlkonig, A., Smet-Nocca, C., Drobecq, H., Wieruszeski, J.M., Senechal, M., Landrieu, I., Locht, C., Jamin, M., and Jacob-Dubuisson, F. (2008). The peptidyl-prolyl isomerase and chaperone Par27 of Bordetella pertussis as the prototype for a new group of parvulins. J. Mol. Biol. *376*, 414–426.

Ieva, R., and Bernstein, H.D. (2009). Interaction of an autotransporter passenger domain with BamA during its translocation across the bacterial outer membrane. Proc. Natl. Acad. Sci. U.S.a. *106*, 19120–19125.

Ieva, R., Skillman, K.M., and Bernstein, H.D. (2008). Incorporation of a polypeptide segment into the beta-domain pore during the assembly of a bacterial autotransporter. Mol. Microbiol. *67*, 188–201.

Inatsuka, C.S., Julio, S.M., and Cotter, P.A. (2005). Bordetella filamentous hemagglutinin plays a critical role in immunomodulation, suggesting a mechanism for host specificity. Proc. Natl. Acad. Sci. U.S.a. *102*, 18578–18583.

Inatsuka, C.S., Xu, Q., Vujkovic-Cvijin, I., Wong, S., Stibitz, S., Miller, J.F., and Cotter, P.A. (2010). Pertactin is required for Bordetella species to resist neutrophil-mediated clearance. Infect. Immun. *78*, 2901–2909.

Isberg, R.R., and Barnes, P. (2001). Subversion of integrins by enteropathogenic Yersinia. J. Cell. Sci. *114*, 21–28.

Ishibashi, Y., Claus, S., and Relman, D.A. (1994). Bordetella pertussis filamentous hemagglutinin interacts with a leukocyte signal transduction complex and stimulates bacterial adherence to monocyte CR3 (CD11b/CD18). J. Exp. Med. *180*, 1225–1233.

Ishibashi, Y., Relman, D.A., and Nishikawa, A. (2001). Invasion of human respiratory epithelial cells by Bordetella pertussis: possible role for a filamentous hemagglutinin Arg-Gly-Asp sequence and alpha5beta1 integrin. Microb. Pathog. *30*, 279–288.

Jacob-Dubuisson, F., Buisine, C., Willery, E., Renauld-Mongenie, G., and Locht, C. (1997). Lack of functional complementation between Bordetella pertussis filamentous hemagglutinin and Proteus mirabilis HpmA hemolysin secretion machineries. J. Bacteriol. *179*, 775–783.

Jacob-Dubuisson, F., Fernandez, R., and Coutte, L. (2004). Protein secretion through autotransporter and two-partner pathways. Biochim Biophys Acta *1694*, 235–257.

Jacob-Dubuisson, F., Kehoe, B., Willery, E., Reveneau, N., Locht, C., and Relman, D.A. (2000). Molecular characterization of Bordetella bronchiseptica filamentous haemagglutinin and its secretion machinery. Microbiology (Reading, Engl.) *146 (Pt 5)*, 1211–1221.

Jacob-Dubuisson, F., Locht, C., and Antoine, R. (2001). Two-partner secretion in Gram-negative bacteria: a thrifty, specific pathway for large virulence proteins. Mol. Microbiol. *40*, 306–313.

Jacob-Dubuisson, F., Villeret, V., Clantin, B., Delattre, A.S., and Saint, N. (2009). First structural insights into the TpsB/Omp85 superfamily. Biol Chem *390*, 675–684.

Jones, A.M., Boucher, P.E., Williams, C.L., Stibitz, S., and Cotter, P.A. (2005). Role of BvgA phosphorylation and DNA binding affinity in control of Bvg-mediated phenotypic phase transition in Bordetella pertussis. Mol. Microbiol. *58*, 700–713.

Julio, S.M., and Cotter, P.A. (2005). Characterization of the filamentous hemagglutinin-like protein FhaS in Bordetella bronchiseptica. Infect. Immun. *73*, 4960–4971.

Julio, S.M., Inatsuka, C.S., Mazar, J., Dieterich, C., Relman, D.A., and Cotter, P.A. (2009). Natural-host animal models indicate functional interchangeability between the filamentous haemagglutinins of Bordetella pertussis and Bordetella bronchiseptica and reveal a role for the mature C-terminal domain, but not the RGD motif, during infection. Mol. Microbiol. *71*, 1574–1590.

Junker, M., Besingi, R.N., and Clark, P.L. (2009). Vectorial transport and folding of an autotransporter virulence protein during outer membrane secretion. Mol. Microbiol. *71*, 1323–1332.

Junker, M., Schuster, C.C., McDonnell, A.V., Sorg, K.A., Finn, M.C., Berger, B., and Clark, P.L. (2006). Pertactin beta-helix folding mechanism suggests common themes for the secretion and folding of autotransporter proteins. Proc. Natl. Acad. Sci. U.S.a. *103*, 4918–4923.

Kajava, A.V., and Steven, A.C. (2006). The turn of the screw: variations of the abundant beta-solenoid motif in passenger domains of Type V secretory proteins. J. Struct. Biol. *155*, 306–315.

Kajava, A.V., Cheng, N., Cleaver, R., Kessel, M., Simon, M.N., Willery, E., Jacob-Dubuisson, F., Locht, C., and Steven, A.C. (2001). Beta-helix model for the filamentous haemagglutinin adhesin of Bordetella pertussis and related bacterial secretory proteins. Mol. Microbiol. *42*, 279–292.

Kelley, L.A., and Sternberg, M.J.E. (2009). Protein structure prediction on the Web: a case study using the Phyre server. Nat Protoc *4*, 363–371.

Kelly, G., Prasannan, S., Daniell, S., Fleming, K., Frankel, G., Dougan, G., Connerton, I., and Matthews, S. (1999). Structure of the cell-adhesion fragment of intimin from enteropathogenic Escherichia coli. Nat. Struct. Biol. *6*, 313–318.

Khan, S., Mian, H.S., Sandercock, L.E., Chirgadze, N.Y., and Pai, E.F. (2011). Crystal structure of the passenger domain of the Escherichia coli autotransporter EspP. J. Mol. Biol. *413*, 985–1000.

Kim, S., Malinverni, J.C., Sliz, P., Silhavy, T.J., Harrison, S.C., and Kahne, D. (2007). Structure and function of an essential component of the outer membrane protein assembly machine. Science *317*, 961–964.

Klemm, P., Vejborg, R.M., and Sherlock, O. (2006). Self-associating autotransporters, SAATs: functional and structural similarities. Int. J. Med. Microbiol. *296*, 187–195.

Kovach, M.E., Phillips, R.W., Elzer, P.H., Roop, R.M., and Peterson, K.M. (1994). pBBR1MCS: a broad-host-range cloning vector. BioTechniques *16*, 800–802.

Könninger, U.W., Hobbie, S., Benz, R., and Braun, V. (1999). The haemolysin-secreting ShlB protein of the outer membrane of Serratia marcescens: determination of surface-exposed residues and formation of ion-permeable pores by ShlB mutants in artificial lipid bilayer membranes. Mol. Microbiol. *32*, 1212–1225.

Lambert-Buisine, C., Willery, E., Locht, C., and Jacob-Dubuisson, F. (1998). N-terminal characterization of the Bordetella pertussis filamentous haemagglutinin. Mol. Microbiol. *28*, 1283–1293.

Lehr, U., Schütz, M., Oberhettinger, P., Ruiz-Perez, F., Donald, J.W., Palmer, T., Linke, D., Henderson, I.R., and Autenrieth, I.B. (2010). C-terminal amino acid residues of the trimeric autotransporter adhesin YadA of Yersinia enterocolitica are decisive for its recognition and assembly by BamA. Mol. Microbiol. *78*, 932–946.

Leo, J.C., Grin, I., and Linke, D. (2012). Type V secretion: mechanism(s) of autotransport through the bacterial outer membrane. Philos. Trans. R. Soc. Lond., B, Biol. Sci. *367*, 1088–1101.

Leong, J.M., Fournier, R.S., and Isberg, R.R. (1990). Identification of the integrin binding domain of the Yersinia pseudotuberculosis invasin protein. Embo J. *9*, 1979–1989.

Leyton, D.L., Rossiter, A.E., and Henderson, I.R. (2012). From self sufficiency to dependence: mechanisms and factors important for autotransporter biogenesis. Nat. Rev. Microbiol. *10*, 213–225.

Locht, C., Bertin, P., Menozzi, F.D., and Renauld, G. (1993). The filamentous haemagglutinin, a multifaceted adhesion produced by virulent Bordetella spp. Mol. Microbiol. *9*, 653–660.

Locht, C., Geoffroy, M.C., and Renauld, G. (1992). Common accessory genes for the Bordetella pertussis filamentous hemagglutinin and fimbriae share sequence similarities with the papC and papD gene families. Embo J. *11*, 3175–3183.

López, C.M., Rholl, D.A., Trunck, L.A., and Schweizer, H.P. (2009). Versatile dual-technology system for markerless allele replacement in Burkholderia pseudomallei. Appl. Environ. Microbiol. *75*, 6496–6503.

Makhov, A.M., Hannah, J.H., Brennan, M.J., Trus, B.L., Kocsis, E., Conway, J.F., Wingfield, P.T., Simon, M.N., and Steven, A.C. (1994). Filamentous hemagglutinin of Bordetella pertussis. A bacterial adhesin formed as a 50-nm monomeric rigid rod based on a 19-residue repeat motif rich in beta strands and turns. J. Mol. Biol. *241*, 110–124.

Martínez de Tejada, G., Miller, J.F., and Cotter, P.A. (1996). Comparative analysis of the virulence control systems of Bordetella pertussis and Bordetella bronchiseptica. Mol. Microbiol. *22*, 895–908.

Mattoo, S., Miller, J.F., and Cotter, P.A. (2000). Role of Bordetella bronchiseptica fimbriae in tracheal colonization and development of a humoral immune response. Infect. Immun. *68*, 2024–2033.

Mazar, J., and Cotter, P.A. (2006). Topology and maturation of filamentous haemagglutinin suggest a new model for two-partner secretion. Mol. Microbiol. *62*, 641–654.

Mazar, J., and Cotter, P.A. (2007). New insight into the molecular mechanisms of two-partner secretion. Trends Microbiol. *15*, 508–515.

McGuirk, P., and Mills, K.H. (2000). Direct anti-inflammatory effect of a bacterial virulence factor: IL-10-dependent suppression of IL-12 production by filamentous hemagglutinin from Bordetella pertussis. Eur. J. Immunol. *30*, 415–422.

Méli, A.C., Hodak, H., Clantin, B., Locht, C., Molle, G., Jacob-Dubuisson, F., and Saint, N. (2006). Channel properties of TpsB transporter FhaC point to two functional domains with a C-terminal protein-conducting pore. J. Biol. Chem. *281*,

158–166.

Méli, A.C., Kondratova, M., Molle, V., Coquet, L., Kajava, A.V., and Saint, N. (2009). EtpB is a pore-forming outer membrane protein showing TpsB protein features involved in the two-partner secretion system. J. Membr. Biol. *230*, 143–154.

Miller, J.F., Roy, C.R., and Falkow, S. (1989). Analysis of Bordetella pertussis virulence gene regulation by use of transcriptional fusions in Escherichia coli. J. Bacteriol. *171*, 6345–6348.

Miller, V.L., and Mekalanos, J.J. (1988). A novel suicide vector and its use in construction of insertion mutations: osmoregulation of outer membrane proteins and virulence determinants in Vibrio cholerae requires toxR. J. Bacteriol. *170*, 2575–2583.

Moslavac, S., Mirus, O., Bredemeier, R., Soll, J., Haeseler, von, A., and Schleiff, E. (2005). Conserved pore-forming regions in polypeptide-transporting proteins. Febs J. *272*, 1367–1378.

Newman, C.L., and Stathopoulos, C. (2004). Autotransporter and two-partner secretion: delivery of large-size virulence factors by gram-negative bacterial pathogens. Crit Rev Microbiol *30*, 275–286.

Niemann, H.H., Schubert, W.D., and Heinz, D.W. (2004). Adhesins and invasins of pathogenic bacteria: a structural view. Microbes Infect. *6*, 101–112.

Nougayrède, J.-P., Fernandes, P.J., and Donnenberg, M.S. (2003). Adhesion of enteropathogenic Escherichia coli to host cells. Cell. Microbiol. *5*, 359–372.

Oliver, D.C., Huang, G., Nodel, E., Pleasance, S., and Fernandez, R.C. (2003). A conserved region within the Bordetella pertussis autotransporter BrkA is necessary for folding of its passenger domain. Mol. Microbiol. *47*, 1367–1383.

Peterson, J.H., Tian, P., Ieva, R., Dautin, N., and Bernstein, H.D. (2010). Secretion of a bacterial virulence factor is driven by the folding of a C-terminal segment. Proc. Natl. Acad. Sci. U.S.a. *107*, 17739–17744.

Poole, K., Schiebel, E., and Braun, V. (1988). Molecular characterization of the hemolysin determinant of Serratia marcescens. J. Bacteriol. *170*, 3177–3188.

Postle, K., and Larsen, R.A. (2007). TonB-dependent energy transduction between outer and cytoplasmic membranes. Biometals *20*, 453–465.

Prasad, S.M., Yin, Y., Rodzinski, E., Tuomanen, E.I., and Masure, H.R. (1993). Identification of a carbohydrate recognition domain in filamentous hemagglutinin from Bordetella pertussis. Infect. Immun. *61*, 2780–2785.

Relman, D., Tuomanen, E., Falkow, S., Golenbock, D.T., Saukkonen, K., and

Wright, S.D. (1990). Recognition of a bacterial adhesion by an integrin: macrophage CR3 (alpha M beta 2, CD11b/CD18) binds filamentous hemagglutinin of Bordetella pertussis. Cell *61*, 1375–1382.

Relman, D.A., Domenighini, M., Tuomanen, E., Rappuoli, R., and Falkow, S. (1989). Filamentous hemagglutinin of Bordetella pertussis: nucleotide sequence and crucial role in adherence. Proc. Natl. Acad. Sci. U.S.a. *86*, 2637–2641.

Renauld-Mongenie, G., Cornette, J., Mielcarek, N., Menozzi, F.D., and Locht, C. (1996). Distinct roles of the N-terminal and C-terminal precursor domains in the biogenesis of the Bordetella pertussis filamentous hemagglutinin. J. Bacteriol. *178*, 1053–1060.

Renn, J.P., Junker, M., Besingi, R.N., Braselmann, E., and Clark, P.L. (2012). ATP-independent control of autotransporter virulence protein transport via the folding properties of the secreted protein. Chem. Biol. *19*, 287–296.

Sanchez-Pulido, L., Devos, D., Genevrois, S., Vicente, M., and Valencia, A. (2003). POTRA: a conserved domain in the FtsQ family and a class of beta-barrel outer membrane proteins. Trends Biochem Sci *28*, 523–526.

Sato, Y., and Sato, H. (1999). Development of acellular pertussis vaccines. Biologicals *27*, 61–69.

Saukkonen, K., Cabellos, C., Burroughs, M., Prasad, S., and Tuomanen, E. (1991). Integrin-mediated localization of Bordetella pertussis within macrophages: role in pulmonary colonization. J. Exp. Med. *173*, 1143–1149.

Schneider, C.A., Rasband, W.S., and Eliceiri, K.W. (2012). NIH Image to ImageJ: 25 years of image analysis. Nat. Methods *9*, 671–675.

Schönherr, R., Tsolis, R., Focareta, T., and Braun, V. (1993). Amino acid replacements in the Serratia marcescens haemolysin ShlA define sites involved in activation and secretion. Mol. Microbiol. *9*, 1229–1237.

Scott, J.R., and Barnett, T.C. (2006). Surface proteins of gram-positive bacteria and how they get there. Annu. Rev. Microbiol. *60*, 397–423.

Shinde, U., and Thomas, G. (2011). Insights from bacterial subtilases into the mechanisms of intramolecular chaperone-mediated activation of furin. Methods Mol. Biol. *768*, 59–106.

Sijbrandi, R., Urbanus, M.L., Hagen-Jongman, ten, C.M., Bernstein, H.D., Oudega, B., Otto, B.R., and Luirink, J. (2003). Signal recognition particle (SRP)-mediated targeting and Sec-dependent translocation of an extracellular Escherichia coli protein. J. Biol. Chem. *278*, 4654–4659.

Skillman, K.M., Barnard, T.J., Peterson, J.H., Ghirlando, R., and Bernstein, H.D.

(2005). Efficient secretion of a folded protein domain by a monomeric bacterial autotransporter. Mol. Microbiol. *58*, 945–958.

St Geme, J.W. (1994). The HMW1 adhesin of nontypeable Haemophilus influenzae recognizes sialylated glycoprotein receptors on cultured human epithelial cells. Infect. Immun. *62*, 3881–3889.

St Geme, J.W., and Grass, S. (1998). Secretion of the Haemophilus influenzae HMW1 and HMW2 adhesins involves a periplasmic intermediate and requires the HMWB and HMWC proteins. Mol. Microbiol. *27*, 617–630.

St Geme, J.W., Falkow, S., and Barenkamp, S.J. (1993). High-molecular-weight proteins of nontypable Haemophilus influenzae mediate attachment to human epithelial cells. Proc. Natl. Acad. Sci. U.S.a. *90*, 2875–2879.

St Geme, J.W.3., and Yeo, H.J. (2009). A prototype two-partner secretion pathway: the Haemophilus influenzae HMW1 and HMW2 adhesin systems. Trends Microbiol. *17*, 355–360.

Stockbauer, K.E., Fuchslocher, B., Miller, J.F., and Cotter, P.A. (2001). Identification and characterization of BipA, a Bordetella Bvg-intermediate phase protein. Mol. Microbiol. *39*, 65–78.

Surana, N.K., Buscher, A.Z., Hardy, G.G., Grass, S., Kehl-Fie, T., and St Geme, J.W. (2006). Translocator proteins in the two-partner secretion family have multiple domains. J. Biol. Chem. *281*, 18051–18058.

Szabady, R.L., Peterson, J.H., Skillman, K.M., and Bernstein, H.D. (2005). An unusual signal peptide facilitates late steps in the biogenesis of a bacterial autotransporter. Proc. Natl. Acad. Sci. U.S.a. *102*, 221–226.

Tsai, J.C., Yen, M.-R., Castillo, R., Leyton, D.L., Henderson, I.R., and Saier, M.H. (2010). The bacterial intimins and invasins: a large and novel family of secreted proteins. PLoS ONE *5*, e14403.

Tuomanen, E., Towbin, H., Rosenfelder, G., Braun, D., Larson, G., Hansson, G.C., and Hill, R. (1988). Receptor analogs and monoclonal antibodies that inhibit adherence of Bordetella pertussis to human ciliated respiratory epithelial cells. J. Exp. Med. *168*, 267–277.

Uhl, M.A., and Miller, J.F. (1996). Integration of multiple domains in a two-component sensor protein: the Bordetella pertussis BvgAS phosphorelay. Embo J. *15*, 1028–1036.

Urisu, A., Cowell, J.L., and Manclark, C.R. (1986). Filamentous hemagglutinin has a major role in mediating adherence of Bordetella pertussis to human WiDr cells. Infect. Immun. *52*, 695–701.

van Ulsen, P. (2011). Protein folding in bacterial adhesion: secretion and folding of classical monomeric autotransporters. Adv. Exp. Med. Biol. *715*, 125–142.

Voulhoux, R., and Tommassen, J. (2004). Omp85, an evolutionarily conserved bacterial protein involved in outer-membrane-protein assembly. Res. Microbiol. *155*, 129–135.

Voulhoux, R., Bos, M.P., Geurtsen, J., Mols, M., and Tommassen, J. (2003). Role of a highly conserved bacterial protein in outer membrane protein assembly. Science *299*, 262–265.

Ward, C.K., Latimer, J.L., Nika, J., Vakevainen, M., Mock, J.R., Deng, K., Blick, R.J., and Hansen, E.J. (2003). Mutations in the lspA1 and lspA2 genes of Haemophilus ducreyi affect the virulence of this pathogen in an animal model system. Infect. Immun. *71*, 2478–2486.

Ward, C.K., Lumbley, S.R., Latimer, J.L., Cope, L.D., and Hansen, E.J. (1998). Haemophilus ducreyi secretes a filamentous hemagglutinin-like protein. J. Bacteriol. *180*, 6013–6022.

Ward, C.K., Mock, J.R., and Hansen, E.J. (2004). The LspB protein is involved in the secretion of the LspA1 and LspA2 proteins by Haemophilus ducreyi. Infect. Immun. *72*, 1874–1884.

Weiss, A.A., Hewlett, E.L., Myers, G.A., and Falkow, S. (1983). Tn5-induced mutations affecting virulence factors of Bordetella pertussis. Infect. Immun. *42*, 33–41.

Werner, J., and Misra, R. (2005). YaeT (Omp85) affects the assembly of lipid-dependent and lipid-independent outer membrane proteins of Escherichia coli. Mol. Microbiol. *57*, 1450–1459.

Williamson, M.P. (1994). The structure and function of proline-rich regions in proteins. Biochem. J. *297 (Pt 2)*, 249–260.

Yen, M.R., Peabody, C.R., Partovi, S.M., Zhai, Y., Tseng, Y.H., and Saier, M.H. (2002). Protein-translocating outer membrane porins of Gram-negative bacteria. Biochim Biophys Acta *1562*, 6–31.

Yeo, H.-J., Yokoyama, T., Walkiewicz, K., Kim, Y., Grass, S., and Geme, J.W.S. (2007). The structure of the Haemophilus influenzae HMW1 pro-piece reveals a structural domain essential for bacterial two-partner secretion. J. Biol. Chem. *282*, 31076–31084.

Łyskowski, A., Leo, J.C., and Goldman, A. (2011). Structure and biology of trimeric autotransporter adhesins. Adv. Exp. Med. Biol. *715*, 143–158.